Theory of SWAP version 2.0

948903

# Theory of SWAP version 2.0

## Simulation of water flow, solute transport and plant growth in the Soil-Water-Atmosphere-Plant environment

J.C. van Dam
J. Huygen
J.G. Wesseling
R.A. Feddes
P. Kabat
P.E.V. van Walsum
P. Groenendijk
C.A. van Diepen

Report 71
Department Water Resources, Wageningen Agricultural University

Technical Document 45
DLO Winand Staring Centre, Wageningen, 1997

ABSTRACT

Van Dam, J.C., J. Huygen, J.G. Wesseling, R.A. Feddes, P. Kabat, P.E.V. van Walsum, P. Groenendijk and C.A. van Diepen, 1997. *Theory of SWAP version 2.0. Simulation of water flow, solute transport and plant growth in the Soil-Water-Atmosphere-Plant environment.* Wageningen Agricultural University and DLO Winand Staring Centre. Technical Document 45. 168 blz., 12 tab., 35 fig., 196 ref.

SWAP simulates vertical transport of water, solutes and heat in variably saturated, cultivated soils. The program has been developed by DLO Winand Staring Centre and Wageningen Agricultural University, and is designed to simulate transport processes at field scale level and during whole growing seasons. This manual describes the theoretical background and modeling concepts that were used for soil water flow, solute transport, heat flow, evapotranspiration, crop growth, multi-level drainage and interaction between field water balance and surface water management.

Keywords: agrohydrology, drainage, evapotranspiration, irrigation, salinization, simulation model, soil water, surface water management.

ISSN 0928-0944



Projectnummer 461 [TD45.HM/10.97]

## Contents

***Annexes***

## Preface

SWAP has been developed from the agrohydrological models SWATRE and SWACROP and some of its numerous derivations, e.g. SWASALT for salt transport and FLOCR for shrinking and swelling clay soils. For years the need was felt for a new model base version, which took advantage of the experiences gained with the existing SWATRE versions. This model, SWAP, should integrate water flow, solute transport and crop growth according to current modeling concepts and simulation techniques.

Researchers at both the DLO Winand Staring Centre and Wageningen Agricultural University were involved in the SWAP development. Their cooperation started in 1990 and will continue to apply and further improve the performance of SWAP.

The changes with respect to the well known SWATRE and SWACROP version are manifold. They include a more versatile numerical solution of the Richards' equation, incorporation of solute and heat transport, attention for soil heterogeneity, shrinking and swelling of clay soils and water repellency, coupling to the detailed WOFOST crop growth model, extension with regional drainage at various levels, and interaction with surface water management. In this way SWAP offers its users a whole range of new possibilities to address both research and practical applications in the field of agriculture, water management and environmental problems. Examples include design and monitoring of field irrigation and drainage systems, surface water management, soil and groundwater pollution by salts and pesticides and crop water use and crop production studies.

Parallel to SWAP, an extended model version (SWAPS) has been developed to address the exchange processes at the land surface - atmosphere interface (Ashby et al., 1996). SWAPS deals extensively with the evaporation processes and its applications are mainly focused on hydro-meteorological and climate studies.

Current documentation of SWAP and SWAPS includes the following reports:
- SWAP 2.0:Theory (Technical document 51, this issue)
  Input and output (Technical document 85)
  Developers manual (in progress)
- SWAPS 1.0:Technical reference manual (Technical document 42)

These reports, together with the programs, are available through the SWAP-development group. This group is presently working on a book providing the theoretical background of SWAP and SWAPS, and a number of case studies, which will be described in a second book.

## Summary

Knowledge of water flow and solute transport processes in the vadose zone is essential to derive proper management conditions for plant growth and environmental protection in agricultural and environmental systems. SWAP aims to simulate these processes in relation to plant growth at field scale level and for entire growing seasons. SWAP employs the experience gained with the agrohydrological models SWATRE and SWACROP. Main improvements with respect to these models are the incorporation of solute and heat transport, soil heterogeneity, detailed crop growth, regional drainage at various levels and interaction between soil profile and surface water management. This manual describes the theoretical background and modeling concepts that were used in the model.

Chapter 2 describes the calculation of soil water flow. SWAP employs the Richards' equation for soil water movement in the soil matrix. Due to its physical bases, the Richards' equation allows the use of soil hydraulic function data bases and simulation of all kind of scenario analysis. The soil hydraulic functions are described by the analytical expressions of Van Genuchten and Mualem or by tabular values. Hysteresis of the retention function can be taken into account with the scaling model of Scott (1983). Root water extraction at various depths in the root zone are calculated from potential transpiration, root length density and possible reductions due to wet, dry, or saline conditions. The numerical solution of the Richards' equation as described by Belmans (1983) has been adapted such that the solution applies both to the unsaturated and saturated zone, that water balance errors due to non-linearity of the differential water capacity are minimized and that the calculated soil water fluxes at the soil surface are more accurate. The top boundary condition procedure has been extended in order to improve runoff calculations and allow alternating conditions of shallow groundwater table and ponding. At the lower boundary of the soil profile, which may be either in the unsaturated or saturated part of the soil, the user may specify the soil water flux, pressure head, flux as function of groundwater level, free drainage or lysimeter with free drainage.

Chapter 3 focuses on solute transport. In the unsaturated zone SWAP simulates the solute processes convection, diffusion and dispersion, non-linear adsorption, first order decomposition and root uptake. This permits the simulation of ordinary pesticide and salt transport, including the effect of salinity on crop growth. In case of detailed pesticide transport or nitrate leaching, daily water fluxes can be generated as input for the models PESTLA and ANIMO. In the saturated zone two- or three-dimensional flow patterns exist, depending on the existing hydraulic head gradients. It can be shown that the solute residence time distribution of an aquifer with drainage to drains or ditches is similar to that of a mixed reservoir. Using this similarity, SWAP

solves the differential equation for solute amounts in a mixed reservoir, with flux type boundary conditions to the unsaturated zone and the drainage devices. In this way solute transport from the soil surface to the surface water can be calculated.

The heat flow equation (Chapter 4) is solved either analytically or numerically. The analytical solution assumes uniform and constant thermal conductivity and soil heat capacity. At the soil surface a sinusoidal temperature wave is assumed. In the numerical solution the thermal conductivity and soil heat capacity depend are calculated from the soil composition and the volume fractions of water and air as described by De Vries (1975). At the soil surface the daily average temperature is used as boundary condition.

As SWAP is designed to simulate field scale conditions, the inherent spatial soil heterogeneity should be considered (Chapter 5). Spatial variability of the soil hydraulic functions is described with the scaling concept of Miller and Miller (1956). The user may provide the reference curve and a number of scaling factors, and SWAP will generate for each scaling factor the soil hydraulic functions and the corresponding water and solute balance and relative crop yield. The concepts of Bronswijk (1991), including the shrinkage characteristic, are used to calculate crack width and crack depth in shrinking and swelling clay soils. The shrinkage characteristic is described with an analytical function. When the rainfall intensity exceeds the maximum matrix infiltration rate, the runoff water collects in the cracks. In order to calculate runoff, instead of daily rainfall averages, actual rainfall intensities should be provided. Water in the cracks may infiltrate laterally into the soil matrix or flow rapidly to nearby drains or ditches. In the clay matrix the Richards' equation, which includes a source term for the laterally infiltrated water, is solved. Once the water fluxes are known, the transport of solutes can be calculated straightforwardly. Due to water repellency, soil water may bypass large parts of the unsaturated soil domain. The water flow and solute transport in water repellent soils is solved by introducing one extra parameter which is equal to the volume fraction of soil in which the water is mobile. This parameter depends on the soil depth and may also depend on the actual water content in the mobile zone. Solute convection and dispersion only occurs in the mobile zone. Between mobile and immobile zone transfer of solutes occurs due to diffusion and water exchange.

Chapter 6 describes calculation of daily evapotranspiration. SWAP uses a two-step approach. The first step involves calculation of the potential transpiration rate according to Penman-Monteith, using daily values of air temperature, solar radiation, wind speed and air humidity and employing the minimum value of the canopy resistance and the actual air resistance. In the second step the actual evapotranspiration rate is determined using the reduction of root water uptake due to water and/or salinity stress and the reduction due to maximum soil evaporation flux. The calculation procedure for Penman-Monteith is derived from Smith (1991). Instead of data for Penman-

Monteith, also a reference potential evapotranspiration rate may be input, together with a crop factor for full soil cover. Partitioning of potential evapotranspiration rate into potential transpiration rate and potential evaporation rate is based either on the leaf area index or the soil cover fraction. Rainfall interception is based on work of Von Hoyningen-Hüne (1983) and Braden (1985). Potential soil evaporation is restricted to the maximum evaporation flux according to Darcy. In addition the user may choose concepts of Black (1969) or Boesten and Stroosnijder (1986) to restrict soil evaporation.

SWAP contains three crop growth routines: a detailed model (WOFOST), the same model attuned to simulate grass growth, and a simple model (Chapter 7). WOFOST calculates the radiation energy absorbed by the canopy as function of incoming radiation and crop leaf area. Using the absorbed radiation and taking into account photosynthetic leaf characteristics, the potential gross photosynthesis is calculated. The latter is reduced due to water and/or salinity stress, as quantified by the relative transpiration, and yields the actual gross photosynthesis. Part of the carbohydrates ($CH_2O$) produced are used to provide energy for the maintenance of the existing live biomass (maintenance respiration). The remaining carbohydrates are converted into structural matter. In this conversion, some of the weight is lost as growth respiration. The dry matter produced is partitioned among roots, leaves, stems and storage organs, using partitioning factors that are a function of the crop phenological development stage. The fraction partitioned to the leaves, determines leaf area development and hence the dynamics of light interception. The dry weights of the plant organs are obtained by integrating their growth rates over time. During the development of the crop, part of living biomass dies due to senescence. In the simple crop model, the user specifies leaf area index (or soil cover fraction), crop height and rooting depth as function of development stage, which either is controlled by temperature or is linear in time.

Chapter 8 addresses field irrigation and drainage. In SWAP irrigation may be prescribed at fixed times or scheduled according to a number of criteria. The scheduling option allows the evaluation of alternative application strategies. The timing criteria include allowable daily stress, allowable depletion of readily available water in the root zone, allowable depletion of totally available water in the root zone, and critical pressure head or water content at a certain depth. Field drainage can be calculated with a linear flux-groundwater level relationship, with a tabular flux-groundwater relationship, or with drainage equations of Hooghoudt (1940) and Ernst (1956, 1962). The use of drainage equations allows the design or evaluation of drainage systems.

At sub-regional level the interaction between soil water balance, crop growth and surface water management can be simulated (Chapter 9). The surface water system can be partitioned in up to five channel orders, each defined by its bed level, bed width, side-slope and spacing. In each channel, except from

the primary channel, the surface water has the same level, which is either input or calculated from the sub-region water balance. The water level of the primary channel is input. Drainage to each channel order is calculated with the corresponding drainage resistances. Also infiltration from the channels, using the corresponding infiltration resistances, is calculated when the surface water level is higher than the groundwater level. In case of surface water level as output, for each water management period, a fixed or automatic weir can be simulated. The user should provide a water management scheme that specifies the target level for surface water, the maximum mean groundwater level, the maximum soil water pressure head and the minimum air volume in the soil. SWAP will select the highest surface water level for which all criteria are met.

Chapter 10 considers the regional drainage concept. In case the drainage resistance mainly consists of the radial and entrance resistance near the drainage devices, superposition of drainage fluxes to canals at different levels can be applied. The lateral drainage fluxes in the saturated zone are distributed according to the transmissivities of each layer. Once the drainage fluxes are known, the drainage concentrations can be calculated straightforwardly. In case of an homogeneous profile with drainage at one level, it is shown that the solute residence time distribution according to this concept corresponds to the solute residence time distribution of a mixed reservoir as described in Chapter 3.

## List of frequently used symbols

### *Roman alphabet*

| | | |
|---|---|---|
| $A$ | Assimilation rate | kg $m^{-2}$ $d^{-1}$ |
| $A_{reg}$ | Area of subregion surface water management | $cm^2$ |
| $c$ | Solute concentration | g $cm^{-3}$ |
| $c_{m,i}$ | Crop organ maintenance coefficient | g $g^{-1}$ $d^{-1}$ |
| $C$ | Differential soil water capacity ($d\theta/dh$) | $cm^{-1}$ |
| $C_{air}$ | Specific heat capacity of air | J $g^{-1}$ $°C^{-1}$ |
| $C_e$ | Average conversion factor crop organs | g $g^{-1}$ |
| $C_{heat}$ | Soil heat capacity | J $cm^{-3}$ $°C^{-1}$ |
| $d_{aquif}$ | Thickness aquifer | cm |
| $d_{pol}$ | Diameter soil polygon | cm |
| $d_{temp}$ | Damping depth temperature wave | cm |
| $D$ | Total dispersion coefficient | $cm^2$ $d^{-1}$ |
| $D_{dif}$ | Solute diffusion coefficient | $cm^2$ $d^{-1}$ |
| $D_{eq}$ | Equivalent depth Hooghoudt equation | cm |
| $D_i$ | Discharge layer thickness of drainage order $i$ | cm |
| $D_{root}$ | Rooting depth | cm |
| $D_s$ | Crop development stage | - |
| $e$ | Vapour pressure | kPa |
| $e$ | Void ratio | $cm^3$ $cm^{-3}$ |
| $E_p$ | Potential evaporation rate of partly covered soil | cm $d^{-1}$ |
| $E_{p0}$ | Potential evaporation rate of bare soil | cm $d^{-1}$ |
| $ET_{p0}$ | Potential evapotranspiration rate of a dry canopy, completely covering the soil | cm $d^{-1}$ |
| $ET_{w0}$ | Potential evapotranspiration rate of a wet canopy, completely covering the soil | cm $d^{-1}$ |
| $F$ | Fraction soil volume with Darcian flow | - |
| $G$ | Soil heat flux density | J $m^{-2}$ $d^{-1}$ |
| $G_c$ | Solute flux density from mobile to immobile region | g $cm^{-3}$ $d^{-1}$ |
| $G_w$ | Water flux density from mobile to immobile region | $d^{-1}$ |
| $GAI$ | Green area index of crop organs | $m^2$ $m^{-2}$ |
| $h$ | Soil water pressure head | cm |
| $h_{sur}$ | Surface water level | cm |
| $H$ | Soil water hydraulic head | cm |
| $I$ | Irrigation application depth | cm |
| $J$ | Solute flux density | g $cm^{-2}$ $d^{-1}$ |
| $k_c$ | Crop coefficient | - |
| $k_{ads}$ | Linear adsorption coefficient in saturated zone | $cm^3$ $g^{-1}$ |
| $K$ | Hydraulic conductivity | cm $d^{-1}$ |
| $K_f$ | Freundlich coefficient | $cm^3$ $g^{-1}$ |
| $K_r$ | Root uptake preference factor | - |
| $K_y$ | Yield response factor | - |

| | | |
|---|---|---|
| $l_{root}$ | Root length density | cm cm$^{-3}$ |
| $L_{dis}$ | Dispersion length | cm |
| $L_{drain}$ | Distance between drainage canals | cm |
| $L_g$ | Geographic latitude | degree |
| $LAI$ | Leaf area index | m$^2$ m$^{-2}$ |
| $n$ | Shape factor Mualem-Van Genuchten functions | - |
| $N_f$ | Freundlich exponent | - |
| $p$ | Pressure | kPa |
| $P$ | Precipitation depth | cm |
| $P_{age}$ | Crop physiologic age | d |
| $P_i$ | Interception depth | cm |
| $PAR$ | Photosynthetic active radiation flux density | J m$^{-2}$ d$^{-1}$ |
| $q$ | Soil water flux density (positive upward) | cm d$^{-1}$ |
| $q_{heat}$ | Soil heat flux density (positive upward) | J cm$^{-2}$ d$^{-1}$ |
| $Q$ | Solute fraction adsorbed to soil particles | g g$^{-1}$ soil |
| $r$ | Air or crop resistance | s m$^{-1}$ |
| $R$ | Recharge to groundwater | cm d$^{-1}$ |
| $R_n$ | Net radiation flux density | J m$^{-2}$ d$^{-1}$ |
| $R_m$ | Maintenance respiration rate | kg ha$^{-1}$ d$^{-1}$ |
| $R_{ns}$ | Net incoming short wave radiation flux density | J m$^{-2}$ d$^{-1}$ |
| $R_{nl}$ | Net outgoing long wave radiation flux density | J m$^{-2}$ d$^{-1}$ |
| $R_s$ | Incoming short wave radiation flux density | J m$^{-2}$ d$^{-1}$ |
| $s_{c,in}$ | Solute flux density entering the crack reservoir | g cm$^{-2}$ d$^{-1}$ |
| $s_{c,out}$ | Solute flux density leaving the crack reservoir | g cm$^{-2}$ d$^{-1}$ |
| $S$ | Root water extraction rate | cm$^3$ cm$^{-3}$ d$^{-1}$ |
| $S_c$ | Solute storage in cracks | g cm$^{-2}$ |
| $S_e$ | Relative saturation | - |
| $S_{la}$ | Specific leaf area of crop | ha kg$^{-1}$ |
| $S_{sun}$ | Solar constant | J m$^{-2}$ d$^{-1}$ |
| $SC$ | Soil cover fraction | cm$^2$ cm$^{-2}$ |
| $t$ | Time | d |
| $T$ | Temperature | °C |
| $T_{air}$ | Daily average temperature | °C |
| $T_{eff}$ | Daily effective temperature | °C |
| $T_p$ | Potential transpiration rate of actual dry canopy | cm d$^{-1}$ |
| $T_{p0}$ | Potential transpiration rate of full, dry canopy | cm d$^{-1}$ |
| $T_{w0}$ | Potential transpiration rate of full, wet canopy | cm d$^{-1}$ |
| $u$ | Average daytime windspeed | m s$^{-1}$ |
| $u_0$ | Average windspeed over 24 hour | m s$^{-1}$ |
| $U$ | Water storage in the root zone | cm |
| $v$ | Pore water velocity | cm d$^{-1}$ |
| $V_{in}$ | Volume of water external supplied to control unit | cm$^3$ cm$^{-2}$ |
| $V_{out}$ | Volume of water leaving the control unit | cm$^3$ cm$^{-2}$ |
| $V_{sur}$ | Surface water storage | cm$^3$ cm$^{-2}$ |
| $w$ | Crop dry matter growth | kg ha$^{-1}$ d$^{-1}$ |
| $W_i$ | Dry weight of organ $i$ | kg ha$^{-1}$ |
| $W_c$ | Crack water storage | cm |

| | | |
|---|---|---|
| $W_{frac}$ | Fraction day with wet crop | - |
| $X$ | Solute concentration | g $cm^{-3}$ |
| $Y$ | Crop yield | kg $ha^{-1}$ |
| $z$ | Vertical coordinate, positive upward, zero at soil surface | cm |

***Greek alphabet***

| | | |
|---|---|---|
| $\alpha$ | Shape factor Mualem-Van Genuchten functions | $cm^{-1}$ |
| $\alpha_i$ | Scale factor similar media | - |
| $\alpha_r$ | Albedo or reflectance coefficient | - |
| $\alpha_{rs}$ | Reduction factor root water uptake due to salinity stress | - |
| $\alpha_{rw}$ | Reduction factor root water uptake due to water stress | - |
| $\beta_{gwl}$ | Shape factor groundwater level | - |
| $\beta_{sun}$ | Solar elevation | degree |
| $\gamma$ | Drainage or infiltration resistance | d |
| $\gamma_a$ | Psychrometric constant | kPa $°C^{-1}$ |
| $\gamma_a^*$ | Modified psychrometric constant | kPa $°C^{-1}$ |
| $\Delta_v$ | Slope vapour pressure curve | kPa $°C^{-1}$ |
| $\varepsilon_{PAR}$ | Light use efficiency | kg $J^{-1}$ |
| $\zeta$ | Death rate of crop organs | kg $ha^{-1}$ $d^{-1}$ |
| $\theta$ | Volumetric water content | $cm^3$ $cm^{-3}$ |
| $\kappa$ | Radiation extinction coefficient | - |
| $\kappa_{di}$ | Extinction coefficient for direct radiation | - |
| $\kappa_{df}$ | Extinction coefficient for diffuse radiation | - |
| $\kappa_{gr}$ | Extinction coefficient for global radiation | - |
| $\kappa_{vk}$ | Von Karman's constant (0.41) | - |
| $\lambda$ | Shape factor Mualem-Van Genuchten functions | - |
| $\lambda_i$ | Characteristic length similar media | cm |
| $\lambda_{heat}$ | Soil thermal conductivity | J $cm^{-1}$ $°C^{-1}$ $d^{-1}$ |
| $\lambda_w$ | Latent heat of vaporization | J $g^{-1}$ |
| $\mu$ | First order rate coefficient of transformation | $d^{-1}$ |
| $\nu$ | Moisture ratio | - |
| $\xi$ | Crop partitioning factor | - |
| $\rho$ | Density | g $cm^{-3}$ |
| $\rho_b$ | Dry soil bulk density | g $cm^{-3}$ |
| $\rho_{rad}$ | Crop reflection coefficient | - |
| $\sigma_{leaf}$ | Leaf scattering coefficient for visible radiation | - |
| $\sigma_{sb}$ | Stefan Boltzmann constant ($4.9\ 10^{-6}$) | J $m^{-2}$ $K^{-4}$ $d^{-1}$ |
| $\sigma_{sun}$ | Solar declination | degree |
| $\phi$ | Hydraulic head, positive upward, zero at soil surface | cm |
| $\phi_{avg}$ | Average phreatic level | cm |
| $\phi_{gwl}$ | Phreatic level midway between drains or ditches | cm |
| $\phi_{por}$ | Soil porosity | $cm^3$ $cm^{-3}$ |

### *Subscripts and superscripts*

| | |
|---|---|
| a | actual |
| ads | adsorption |
| air | air |
| atm | atmosfeer |
| bot | bottom |
| c | crack |
| con | convection |
| crop | crop |
| dif | diffusion |
| dis | dispersion |
| drain | drain |
| dry | dry |
| entr | entrance |
| eq | equivalent |
| gr | groundwater |
| gross | gross |
| gwl | groundwater level |
| heat | heat |
| hor | horizontal |
| i | index |
| im | immobile |
| imp | impermeable |
| int | interface |
| j | index |
| k | kelvin |
| l | liquid |
| lab | laboratory |
| lat | lateral |
| leaf | leaf |
| m | matrix |
| net | net |
| p | potential |
| pond | ponding layer |
| prec | precipitation |
| rad | radial |
| ref | reference |
| res | residual |
| resis | resistance |
| root | root |
| run | runoff |
| s | solid |
| sat | saturated |
| simp | semi-impermeable |
| sh | shoot |
| stem | stem |
| stor | storage organ |
| sur | surface |
| top | top |
| tot | total |
| ver | vertical |
| w | water |
| weir | weir |
| wet | wet |

# 1 Introduction

Knowledge of water and solute movement in the variably saturated soil near the earth surface is essential to understand man's impact on the environment. Top soils show the largest concentration of biological activity on earth. Water movement in the upper soil determines the rate of plant transpiration, soil evaporation, runoff and recharge to the groundwater. In this way unsaturated soil water flow is a key factor in the hydrological cycle. Due to the high solubility of water, soil water transports large amounts of solutes, ranging from nutrients to all kind of contaminations. Therefore an accurate description of unsaturated soil water movement is essential to derive proper management conditions for vegetation growth and environmental protection in agricultural and natural systems.

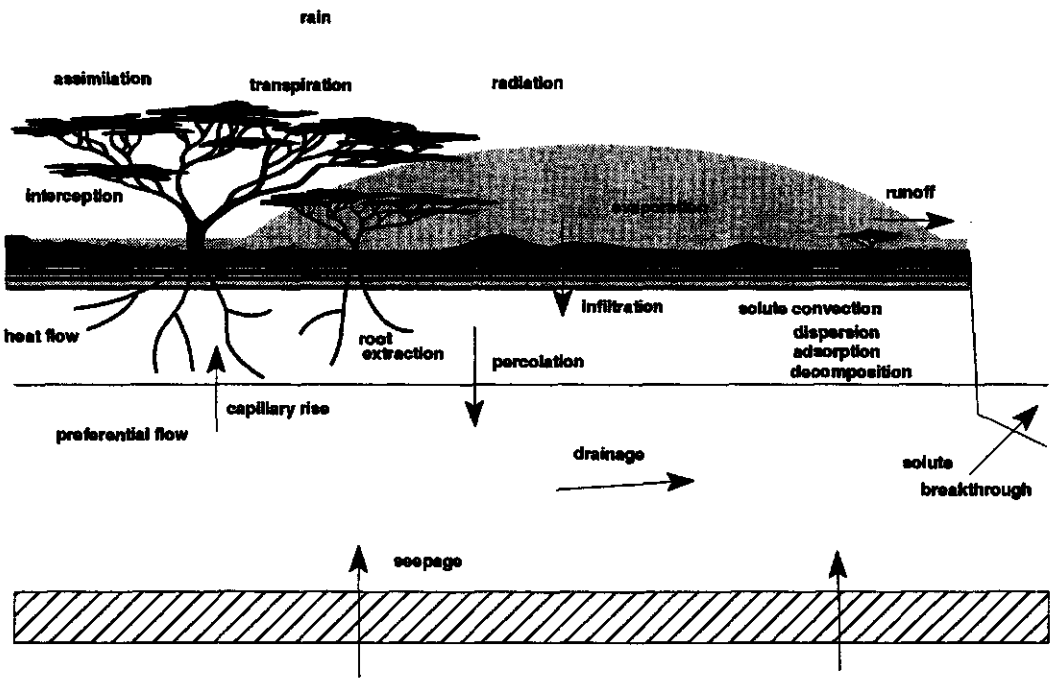


*Fig. 1.1 Water flow, solute transport and crop growth processes at the field scale, as applied in SWAP*

SWAP aims at simulating water, solute and heat transport in the soil-atmosphere-plant environment (Fig. 1.1). The program includes detailed submodels on soil water flow, solute transport, soil heat flow, soil evaporation, plant transpiration and crop growth, all operating from diurnal to seasonal cycles. Earlier version of the program were developed by Feddes et al. (1978), Belmans et al. (1983), Wesseling et al. (1991), Kabat et al. (1992) and Van den Broek et al. (1994). The changes with respect to these programs are manifold. The numerical solution of Richards' flow equation has been adapted

to allow simulation of shallow groundwater tables and infiltration and runoff during short duration rainfall events. Transport of salts, pesticides and heat has been added. The crop growth routine CROPR was replaced by WOFOST 6.0 (Supit et al., 1994), which includes many relevant physical, chemical and biological processes for crop growth. Field scale heterogeneity is addressed by including the scaling concept of similar media, shrinking and swelling of clay soils and preferential flow and transport in water repellent soils. The options to calculate field drainage were extended. An important new feature of SWAP concerns the simulation of groundwater and surface water interactions at sub-regional scales and the possibility to link with regional groundwater flow- and quality models. In order to facilitate data input and analysis of output data, a users friendly shell has been written. Also SWAP may generate input data for current versions of the nutrient model ANIMO (Groenendijk and Kroes, 1997), and the pesticide model PESTLA (Van den Berg, 1997).

SWAP is written in the FORTRAN 77 programming language. The program runs on 486 or higher, IBM compatible PC's and on VAX mainframe computers. The modular program structure and informative texts in the subroutines allow researchers to adapt the program to their own need.

This technical document describes the theoretical background and concepts implemented in SWAP version 2.0. In the following chapters attention is paid successively to soil water flow, solute transport, soil heat flow, soil heterogeneity, daily evapotranspiration, crop growth, field irrigation and drainage, interaction with surface water management and regional drainage. Relevant literature is cited as much as possible, resulting in almost 200 references. The annexes contain information of the soil hydraulic functions, critical pressure head values of the rootwater extraction term, salt tolerance data, the numerical solution of the Richards' equation and heat transport equation, and data of measured shrinkage characteristics.

Detailed information of in- and output of SWAP version 2.0 will be given in Technical document 85.

# 2 Soil water flow

## 2.1 Soil water flow equation

Spatial differences of the soil water potential cause flow of soil water. Darcy's equation is used to quantify these soil water fluxes. For one-dimensional vertical flow, Darcy's equation can be written as:

$$q = - K(h) \frac{\partial (h + z)}{\partial z} \tag{2.1}$$

where $q$ is soil water flux density (positive upward) (cm $d^{-1}$), $K$ is hydraulic conductivity (cm $d^{-1}$), $h$ is soil water pressure head (cm) and $z$ is the vertical coordinate (cm) taken positively upward.

Water balance considerations of an infinitely small soil volume result in the continuity equation for soil water:

$$\frac{\partial \theta}{\partial t} = - \frac{\partial q}{\partial z} - S(h) \tag{2.2}$$

where $\theta$ is volumetric water content ($cm^3$ $cm^{-3}$), $t$ is time (d) and $S$ is soil water extraction rate by plant roots ($cm^3$ $cm^{-3}$ $d^{-1}$).

Combination of Eq. 2.1 and 2.2 results in the well-known Richards' equation:

$$\frac{\partial \theta}{\partial t} = C(h) \frac{\partial h}{\partial t} = \frac{\partial \left[ K(h) \left( \frac{\partial h}{\partial z} + 1 \right) \right]}{\partial z} - S(h) \tag{2.3}$$

where $C$ is the water capacity ($d\theta/dh$) ($cm^{-1}$).

Richards' equation has a clear physical basis at a scale where the soil can be considered to be a continuum of soil, air and water. SWAP solves Eq. 2.3 numerically, subject to specified initial and boundary conditions and with known relations between $\theta$, $h$ and $K$. These relationships can be measured directly in the soil, or might be obtained from basic soil data as discussed in Par. 2.2. Because of its versatility, SWAP applies Richards' equation integrally for the unsaturated-saturated zone, with possible presence of transient and perched groundwater levels.

## 2.2 Soil hydraulic functions

The relationships between the water content $\theta$, the pressure head $h$ and the hydraulic conductivity $K$ are generally summarized in the retention function

$\theta(h)$ and the unsaturated hydraulic conductivity function $K(\theta)$. These soil hydraulic functions need to be specified for each distinct soil layer. In this section we will briefly discuss measurement methods, analytical expressions and hysteresis of the soil hydraulic functions. Special attention is paid to measurement methods because of the importance of accurate soil hydraulic data for both the water and solute balance.

### 2.2.1 Measurement methods

We may distinguish between laboratory and field methods. Table 2.1 and 2.2 show commonly applied laboratory methods for measurement of $\theta(h)$ and $K(\theta)$, including the $h$-ranges for which the methods are suitable. Stolte et al. (1994) measured $K(\theta)$ with six of these methods in case of a sand, a sandy loam and two silt loam soils. They compared the results and discussed the limitations of each method.

*Tabel 2.1 Laboratory measurement methods of the retention function*

| Method | Range (cm) | Reference |
|---|---|---|
| Sandbox apparatus | $-200 < h < 0$ | Klute (1986) |
| Pressure cell | $-1000 < h < 0$ | Kool et al., (1985) |
| Pressure membrane | $-20.000 < h < -1000$ | Klute (1986) |
| Vapour equilibration | $h < -100.000$ | Koorevaar et al. (1983) |

*Tabel 2.2. Laboratory measurement methods of the unsaturated hydraulic conductivity function.*

| Method | Range (cm) | Reference |
|---|---|---|
| Suction cell | $-100 < h < 0$ | Klute and Dirksen (1986) |
| Crust method | $-100 < h < 0$ | Bouma et al. (1983) |
| Drip Infiltrometer | $-100 < h < 0$ | Dirksen (1991) |
| Evaporation method | $-800 < h < 0$ | Wendroth et al. (1993) |
| Pressure cell | $-1000 < h < 0$ | Van Dam et al. (1994) |
| Sorptivity method | $-1000 < h < 0$ | Dirksen (1979) |
| Hot air method | $-10000 < h < -100$ | Van Grinsven et al. (1985) |
| Centrifuge method | $-1000 < h < 0$ | Nimmo et al., 1987 |
| Spray method | $-250 < h < 0$ | Dirksen and Matula (1994) |

In the field, simultaneous measurement of $\theta$ and $h$ directly provides the retention function. The $K(\theta)$ might be derived form these data by application of

the instantaneous profile method (Hillel, 1980) or one of its modifications. In general irrigation-drainage events are used in order to achieve wet and dry conditions and a range of soil water fluxes. The $h$-range of the determined functions is limited to the actual drainage conditions (in general -300 cm $< h < 0$).

Near saturation, $K(\theta)$ may change very rapidly. To determine $K$ in the very wet range more accurately at field conditions, the suction infiltrometer has been developed (Elrick and Reynolds, 1992). In only a few years, this device has become widely used.

In a review of $K(\theta)$ measurements, Dirksen (1991) provided criteria to select the appropriate measurement method for field and laboratory. These criteria include the theoretical basis, control of initial and boundary conditions, error propagation in data analysis, range of application, equipment, operator skill and time, check on measurements and results obtained.

All these methods are so-called direct measurement methods. Also indirect and inverse methods can be used to determine the soil hydraulic functions. At indirect methods, $\theta(h)$ and $K(\theta)$ are derived from more easily obtained soil data as soil texture, bulk density and organic matter content (Van Genuchten and Leij, 1992). At inverse methods, non-linear parameter estimation is used to derive the soil hydraulic functions from a measured flow event, either in the laboratory or in the field (Carrera and Neuman, 1986; Kool et al., 1987; Russo et al., 1991; Feddes et al., 1993; Hopmans et al., 1994).

Data sets on soil hydraulic functions are reported by Mualem (1976), Carsel and Parrish (1988), Yates et al. (1992), Wösten et al. (1994), and Leij et al. (1996).

### 2.2.2 Analytical functions

Although tabular forms of $\theta(h)$ and $K(\theta)$ have been used for many years, currently analytical expressions are generally applied for a number of reasons. Analytical expressions are more convenient as model input and a rapid comparison between horizons is possible by comparing parameter sets. In case of hysteresis, scanning curves can be derived by some modification of the analytical function. Also scaling, which is used to describe spatial variability of $\theta(h)$ and $K(\theta)$, requires an analytical expression of the reference curve. Another reason is that extrapolation of the functions beyond the measured data range is possible. Last but not least, analytical functions allow for calibration and estimation of the soil hydraulic functions by inverse modeling.

Brooks and Corey (1964) proposed an analytical function of $\theta(h)$ which has been used for a number of years. Mualem (1976) derived a predictive model

of the $K(\theta)$ relation based on the retention function. Van Genuchten (1980) proposed a more flexible $\theta(h)$ function than the Brooks and Corey relation and combined it with Mualem's predictive model to derive $K(\theta)$. This model has been used in numerous studies, forms the basis of several national and international data-banks (e.g. Carsel and Parrish, 1988; Yates et al., 1992; Wösten et al., 1994; Leij et al, 1996), and is implemented in SWAP.

The analytical $\theta(h)$ function proposed by Van Genuchten (1980) reads:

$$\theta = \theta_{res} + \frac{\theta_{sat} - \theta_{res}}{(1 + |\alpha h|^n)^m} \tag{2.4}$$

where $\theta_{sat}$ is the saturated water content ($cm^3\ cm^{-3}$), $\theta_{res}$ is the residual water content in the very dry range ($cm^3\ cm^{-3}$) and $\alpha$ ($cm^{-1}$), $n$ (-) and $m$ (-) are empirical shape factors. Without loosing much flexibility, $m$ can be taken equal to :

$$m = 1 - \frac{1}{n} \tag{2.5}$$

Using the above $\theta(h)$ relation and applying the theory on unsaturated hydraulic conductivity by Mualem ((1976), the following $K(\theta)$ function results:

$$K = K_{sat}\, S_e^{\lambda} \left[1 - (1 - S_e^{\frac{1}{m}})^m\right]^2 \tag{2.6}$$

where $K_{sat}$ is the saturated conductivity ($cm\ d^{-1}$), $\lambda$ is a shape parameter (-) depending on $\partial K/\partial h$, and $S_e$ is the relative saturation defined as:

$$S_e = \frac{\theta - \theta_{res}}{\theta_{sat} - \theta_{res}} \tag{2.7}$$

Van Genuchten et al. (1991) developed the program RETC to estimate the parameter values of this model from measured $\theta(h)$ and $K(\theta)$ data. Annex A lists model parameters derived from a data base of more than 600 soil samples in the Netherlands, known as the Staring series (Wösten et al., 1994). Annex B lists model parameters for the USDA textural classes as derived by Carsel and Parrish (1988). The Staring series correspond to the legend of the Dutch soil map 1:50 000. The data are meant to be applied in regional studies. The units of the Staring series were obtained by recognizing a number of soil texture classes, with a separation between top- and sublayers. The average relationships per texture class are calculated by taking the geometric mean of every separate soil hydraulic function per unit. The geometric mean was used because of the log-normal distribution of the data. The Staring series may serve as a class-pedotransfer function, by which averaged soil hydraulic functions are assigned to a certain texture class.

However, the user should be aware of the limitations of the Staring series:
- the definition of the units has been based on texture and organic matter content only, differences of geologic sediment or bulk density are not taken into account;
- geometric averaging may result in properties different from the real average;
- the units of the Staring series are developed for regional applications, for local applications measurements are indispensable;
- the Staring series apply to Dutch circumstances, in other countries different soil hydraulic functions may apply.

### 2.2.3 Hysteresis

Hysteresis refers to non-uniqueness of the $\theta(h)$ relation and is caused by variations of the pore diameter (inkbottle effect), differences in radii of advancing and receding meniscus, entrapped air, thermal gradients and swelling/shrinking processes (Hillel, 1980; Feddes et al., 1988). Gradual desorption of an initially saturated soil sample gives the main drying curve, while slow absorption of an initially dry sample results in the main wetting curve. In the field partly wetting and drying occurs in numerous cycles, resulting in so-called drying and wetting scanning curves lying between the main drying and the main wetting curves.

Several researchers used domain models to predict these scanning curves. Although domain models are physically based, they require accurate measurements of the complete soil water characteristic and additional assumptions concerning the pore geometry. To circumvent the tedious laboratory analysis, empirical hysteresis models have been developed that use a limited number of parameters. Scott et al. (1983) derived scanning curves by rescaling the main wetting or the main drying curve to the actual water content. This method requires measurement of only the main wetting and drying curves. Among others, Kool and Parker (1987) obtained acceptable results with Scotts' concept in the case of eight soils. This method is implemented in SWAP. It employs the Mualem-Van Genuchten model (Eq. 2.4 to 2.7) to describe the main and scanning curves. Four parameters ($\alpha$, $n$, $\theta_{res}$ and $\theta_{sat}$) describe the $\theta(h)$ relation. In case of the main wetting and main drying curve some of these parameters are related. We will assume $\theta_{res}$ and $\theta_{sat}$ to be equal for both curves. In general $\theta_{sat}$ will be somewhat less than porosity due to air entrapment under field conditions with intensive rainfall. Usually the $K(\theta)$ function shows only minor hysteresis effects and we will assume $K(\theta)$ to be uniquely defined. As Eq. 2.6 shows, this can only be achieved by choosing for the main wetting and main drying curve a common value for $m$ and thus for $n$. This means that the main wetting and main drying retention function, as described by Eq. 2.4, only differ in the parameter $\alpha$.

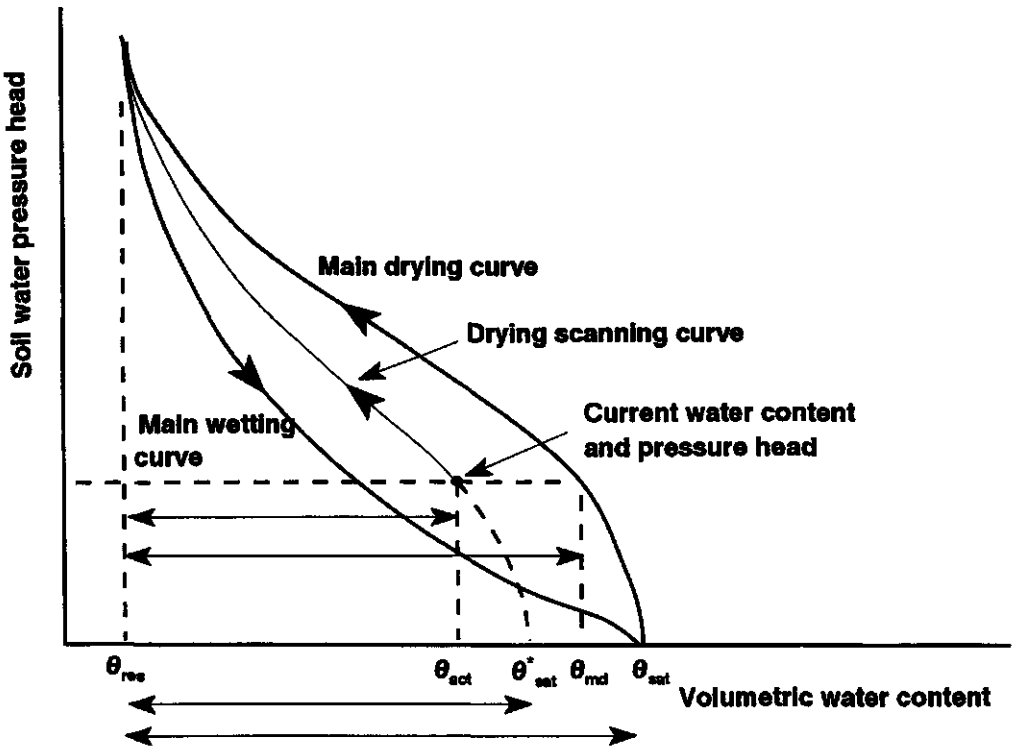


*Fig. 2.1 Linear scaling of the main drying curve in order to derive a drying scanning curve. The retention function is described by the van Genuchten analytical function*

The scanning curves are derived by linear scaling of the main curves. Figure 2.1 shows this in case of a drying scanning curve. Linear scaling of the main drying curve to the current water content is achieved by defining the adapted saturated water content $\theta_{sat}^*$ (Fig. 2.1):

$$\frac{\theta^*_{sat} - \theta_{res}}{\theta_{sat} - \theta_{res}} = \frac{\theta_{act} - \theta_{res}}{\theta_{md} - \theta_{res}} \qquad (2.8)$$

where $\theta_{act}$ is the actual water content and $\theta_{md}$ is the water content of the main drying curve at the actual soil water pressure head. In case of transition from wetting to drying, $\theta_{sat}^*$ can be solved directly from Eq. 2.8. Applying the same principle of linear scaling in case of a wetting scanning curve results in:

$$\theta^*_{res} = \theta_{sat} - \frac{\theta_{sat} - \theta_{act}}{\theta_{sat} - \theta_{mw}} (\theta_{sat} - \theta_{res}) \qquad (2.9)$$

with $\theta_{res}^*$ the adapted residual water content and $\theta_{mw}$ the water content of the main wetting curve at the actual soil water pressure head. The drying scanning curve is accordingly described by the parameter set ($\alpha_d$,$n$,$\theta_{res}$,$\theta_{sat}^*$) and the wetting scanning curve by ($\alpha_w$,$n$,$\theta_{res}^*$,$\theta_{sat}$). The unique $K(\theta)$ relation follows from the parameter set ($n$, $\theta_{res}$, $\theta_{sat}$, $K_{sat}$, $\lambda$).

Hysteresis will affect soil water movement when frequent changes occur from wetting to drying conditions. The effects are most pronounced if at the soil surface a pressure head boundary condition applies, e.g. at events with a large precipitation/irrigation flux in relatively dry soils (Hopmans and Dane, 1986).

## 2.3 Soil water extraction by roots

The maximum possible root water extraction rate, integrated over the rooting depth, is equal to the potential transpiration rate, $T_p$ (cm $d^{-1}$), which is governed by atmospheric conditions (Chapter 6). The potential root water extraction rate at a certain depth, $S_p(z)$ ($d^{-1}$), may be determined by the root length density, $l_{root}(z)$ (cm $cm^{-3}$), at this depth as fraction of the integrated root length density (e.g. Bouten, 1992):

$$S_p(z) = \frac{l_{root}(z)}{\int_{-D_{root}}^{0} l_{root}(z)\, dz}\, T_p \qquad (2.10)$$

where $D_{root}$ is the root layer thickness (cm).

SWAP can handle every distribution of $l_{root}(z)$. In practice this distribution is often not available. Therefore in many applications of SWAP, a uniform root length density distribution is assumed, i.e.:

$$\frac{l_{root}(z)}{\int_{-D_{root}}^{0} l_{root}(z)\, dz} = \frac{1}{D_{root}} \qquad (2.11)$$

which leads to simplified form of Eq. 2.10 (Feddes et al., 1978):

$$S_p(z) = \frac{T_p}{D_{root}} \qquad (2.12)$$

Stresses due to dry or wet conditions and/or high salinity concentrations may reduce $S_p(z)$. The water stress in SWAP is described by the function proposed by Feddes et al. (1978), which is depicted in Fig. 2.2. Critical pressure head values of this sink term function are given in Annex C (Wesseling et al., 1991) and Annex D (Taylor and Ashcroft, 1972). For salinity stress the response function of Maas and Hoffman (1977) is used (Fig. 2.3), as this function has been calibrated for many crops (Maas, 1990). Annex E lists salt tolerance data for a number of crops. It is still not clear if under the conditions where both stresses apply, the stresses are *additive* or *multiplicative* (Van Genuchten, 1987; Dirksen, 1993; Shalhevet, 1994). In order to simplify parameter calibration and data retrieval, we assume in SWAP the water and salinity stress to be multiplicative. This means that the actual root water flux, $S_a(z)$ ($d^{-1}$), is calculated from:

$$S_a(z) = \alpha_{rw}\alpha_{rs}S_p(z) \qquad (2.13)$$

where $\alpha_{rw}$ (-) and $\alpha_{rd}$ (-) are the reduction factors due to water and salinity stresses, respectively (Fig. 2.2 and 2.3). Integration of $S_a(z)$ over the root layer yields the actual transpiration rate $T_a$ (cm $d^{-1}$).

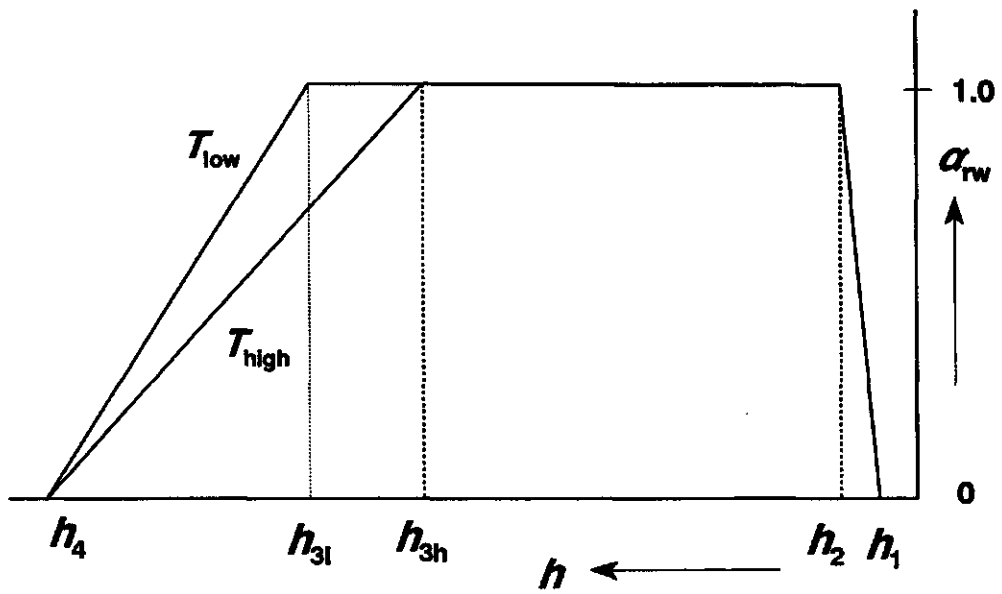


*Fig. 2.2 Reduction coefficient for root water uptake, $\alpha_{rw}$, as function of soil water pressure head h and potential transpiration rate $T_p$ (after Feddes et al., 1978)*

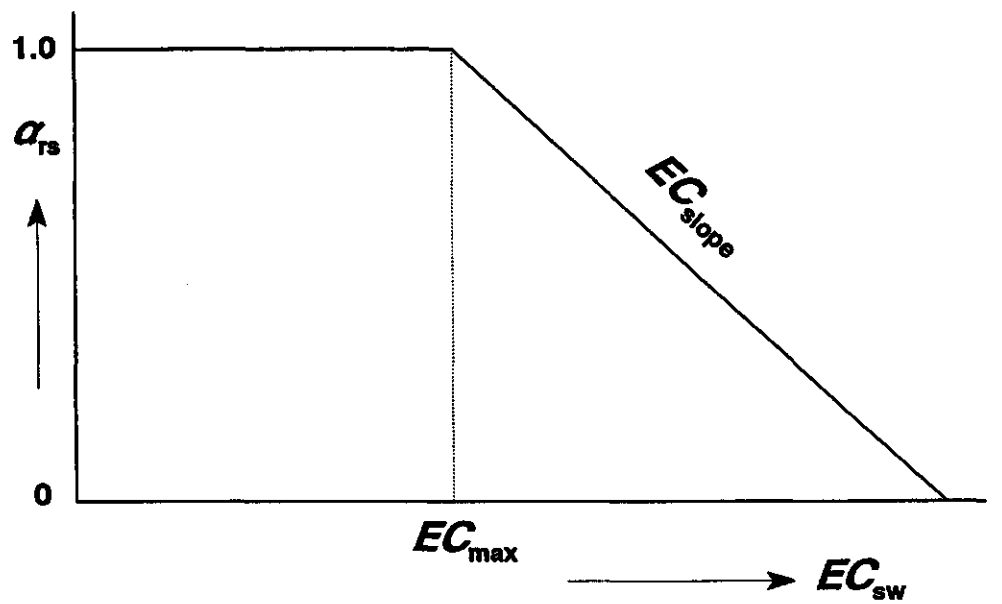


*Fig. 2.3 Reduction coefficient for root water uptake, $\alpha_{rs}$, as function of soil water electrical conductivity $EC_{sw}$ (after Maas and Hoffman, 1977)*

## 2.4 Numerical discretization of soil water flow equation

Accurate numerical solution of Richards' partial differential equation is difficult due to its hyperbolic nature and due to the strong non-linearity of the soil hydraulic functions. The calculated soil water fluxes may to a large extend be affected by the structure of the numerical scheme and the applied time and space discretizations (Van Genuchten, 1982; Milly, 1985; Celia et al., 1990; Warrick, 1991; Zaidel and Russo, 1992). In SWAP a numerical scheme has been chosen which solves the one-dimensional Richards' equation with an accurate mass balance and which converges rapidly. This scheme has been shown to handle short duration infiltration and runoff events during intensive rain showers accurately and simulations of whole growing seasons within reasonable time.

### 2.4.1 Numerical discretization

A common method to solve Richards' equation has been the implicit, backward, finite difference scheme with explicit linearization as described by Haverkamp et al. (1977) and Belmans et al. (1983). Three adaptations to this scheme were made to arrive at the numerical scheme currently applied in SWAP. The first adaptation concerns the handling of the differential water capacity $C$. The old scheme was limited to the unsaturated zone only. The saturated zone and fluctuations of the groundwater table had to be modelled separately (Belmans et al., 1983). The new numerical scheme enables us to solve the flow equation in the unsaturated and saturated zone simultaneously. In order to do so, in the numerical discretization of Richards' equation, the $C$-term only occurs as numerator, not as denominator (see Eq. 2.16).

The second adaptation concerns the numerical evaluation of the $C$-term. Because of the high non-linearity of $C$, averaging during a time step results in serious mass balance errors when simulating highly transient conditions. A simple but effective adaptation was suggested by Milly (1985) and further analysed by Celia et al. (1990). Instead of applying during a *time* step

$$\theta_i^{j+1} - \theta_i^j = C_i^{j+\frac{1}{2}} \left( h_i^{j+1} - h_i^j \right) \tag{2.14}$$

where $C_i^{j+\frac{1}{2}}$ denotes the average water capacity during the time step, subscript $i$ is the node number (increasing downward) and superscript $j$ is the time level, they applied at each *iteration* step:

$$\theta_i^{j+1} - \theta_i^j = C_i^{j+1,p-1} \left( h_i^{j+1,p} - h_i^{j+1,p-1} \right) + \theta_i^{j+1,p-1} - \theta_i^j \tag{2.15}$$

where superscript $p$ is the iteration level and $C_i^{j+1,p-1}$ is the water capacity evaluated at the $h$ value of the last iteration. At convergence $(h_i^{j+1,p} - h_i^{j+1,p-1})$ will be small, which eliminates effectively remaining inaccuracies in the evaluation of $C$.

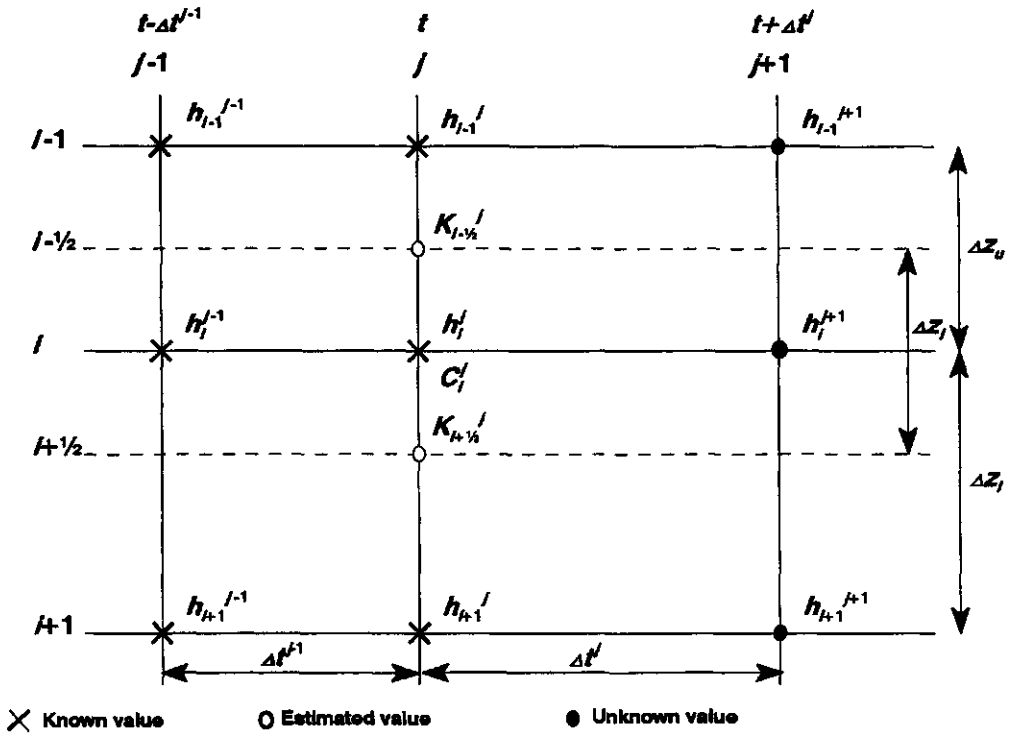


*Fig. 2.4 Known, estimated, and unknown values of soil water pressure head h, hydraulic conductivity K, differential water capcaity C, in the discretized time-space domain.*

The third adaptation concerns the averaging of $K$ between the nodes. Haverkamp and Vauclin (1979), Belmans et al. (1983) and Hornung and Messing (1983) proposed to use the geometric mean. In their simulations the geometric mean increased the accuracy of calculated fluxes and caused the fluxes to be less sensitive to changes in nodal distance. However, the geometric mean has serious disadvantages too (Warrick, 1991). When simulating infiltration in dry soils or high evaporation from wet soils, the geometric mean severely underestimates the water fluxes. Other researchers proposed to use the harmonic mean of $K$ or various kind of weighted averages (Ross, 1990; Warrick, 1991; Zaidel and Russo, 1992; Desbarats, 1995). Van Dam and Feddes (1997) show that, although arithmetic averages at larger nodal distances overestimate the soil water fluxes in case of infiltration and evaporation events, at nodal distances in the order of 1 cm arithmetic averages are more close to the theoretically correct solution than geometric averages. Also they show that the remaining inaccuracy between calculated and theoretically correct fluxes, is relatively small compared to effects of soil spatial variability and hysteresis. Therefore SWAP applies arithmetic averages of $K$, which is in line with commonly applied finite element models (Kool and Van Genuchten, 1991; Šimůnek et al., 1992).

The implicit, backward, finite difference scheme with explicit linearization, including the three adaptations, yields the following discretization of Richards' equation:

$$C_i^{j+1,p-1}\left(h_i^{j+1,p} - h_i^{j+1,p-1}\right) + \left(\theta_i^{j+1,p-1} - \theta_i^j\right) =$$

$$\frac{\Delta t^j}{\Delta z_i}\left[K_{i-\frac{1}{2}}^j\left(\frac{h_{i-1}^{j+1,p} - h_i^{j+1,p}}{\Delta z_u}\right) + K_{i-\frac{1}{2}}^j - K_{i+\frac{1}{2}}^j\left(\frac{h_i^{j+1,p} - h_{i+1}^{j+1,p}}{\Delta z_\ell}\right) - K_{i+\frac{1}{2}}^j\right] - \Delta t^j S_i^j \qquad (2.16)$$

where $\Delta t^j = t^{j+1} - t^j$, $\Delta z_u = z_{i-1} - z_i$, $\Delta z_\ell = z_i - z_{i+1}$, $\Delta z_i = (\Delta z_u + \Delta z_\ell)/2$. Figure 2.4 showes the symbols in the space-time domain. $K$ and $S$ are evaluated at the old time level $j$ (explicit linearization), which can be shown to give a good approximation at the time steps used. This numerical scheme applies both to the saturated and unsaturated zone. Starting in the saturated zone, the groundwater table is simply found at $h = 0$. Also perched water tables may occur above dense layers in the soil profile. Calculations show that in order to simulate infiltration and evaporation accurately, near the soil surface the nodal distance should be in the order of centimetres. For this reason the nodal distance in SWAP is made variable. Application of Eq. 2.16 to each node, subject to the prevailing boundary conditions, results in a tri-diagonal system of equations (see Annex F) which can be solved efficiently (Press et al., 1989).

Until recently the pressure head difference $|h_i^{j+1,p} - h_i^{j+1,p-1}|$ in the iterative solution of Eq. 2.16 has been used as convergence criterium. Instead Huang et al. (1996) proposed to use the water content difference $|(\theta_i^{j+1,p} - \theta_i^{j+1,p-1})|$. The advantage of a criterium based on $\theta$ is that it is automatically more sensitive in pressure head ranges with a large differential soil water capacity, $C = (d\theta/dh)$, while it allows less iterations at low $h$-values where $\theta$ hardly changes. Huang et al. (1996) show the higher efficiency of the $\theta$-criterium for a large number of infiltration problems. Moreover the $\theta$-criterium was found to be more robust when the soil hydraulic characteristics were extremely non-linear. Also our experiences with the $\theta$-criterium in SWAP are positive. If the soil gets saturated at the node considered, $\theta$ becomes constant and the convergence criterium is switched to maximum differences of $h$.

The optimal time step should minimize the computational effort of a simulation while the numerical solution still meets the convergence criterium for solving Richards' equation. The number of iterations needed to reach convergence, $N_{it}$, can effectively be used for this purpose (Kool and Van Genuchten, 1991). We apply in SWAP the following criteria:

$N_{it} < 2$ : multiply time step with a factor 1.25
$2 \leq N_{it} \leq 4$ : keep time step the same
$N_{it} > 4$ : divide time step by a factor 1.25

In the SWAP input file a minimum and a maximum time step, $\Delta t_{min}$ and $\Delta t_{max}$ (d), are defined. For the initial time step, SWAP will take $\Delta t = \sqrt{\Delta t_{min} \Delta t_{max}}$. Depending on $N_{it}$, the time step will be decreased, maintained or increased for the following timesteps. If during an iteration $N_{it}$ exceeds 6, SWAP will divide $\Delta t$ by a factor 3, and start iterating again. The timestep is always confined to the range $\Delta t_{min} \leq \Delta t \leq \Delta t_{max}$. Exceptions to above procedure occur, when the upper boundary flux changes from evaporation to intensive rainfall (> 1.0 cm $d^{-1}$), in which case $\Delta t$ is reset to $\Delta t_{min}$, and at the end of a day, in which case $\Delta t$ is set equal to the remaining time in the day.

### 2.4.2 Top boundary condition

Appropriate criteria for the procedure with respect to the top boundary condition are important for accurate simulation of rapidly changing soil water fluxes near the soil surface. This is e.g. the case at infiltration/runoff events during intensive rain showers or when the soil occasionally gets flooded in areas with shallow groundwater tables.

At moderate weather and soil wetness conditions the soil top boundary condition will be flux-controlled. In either very wet or very dry conditions the prevailing water pressure head at the soil surface starts to govern the boundary condition. Figure 2.5 shows the applied procedure in SWAP to select between flux- and pressure head controlled top boundary. A prescribed flux at the soil surface is denoted as $q_{sur}$ (cm $d^{-1}$), and a prescribed pressure head as $h_{sur}$ (cm). Soil water fluxes are defined positive when they are directed upward.

In Fig. 2.5 criterium <1> considers if the soil is saturated. If so, criterium <2> determines whether the soil is still saturated at the next time level $t^{i+1}$ (head is prescribed) or becomes unsaturated. The inflow $Q_{in}$ (cm) is defined as:

$$Q_{in} = (q_{bot} - q_{top} - q_{drain})\ \Delta t^{i} \tag{2.17}$$

where $q_{bot}$ is the flux at the soil profile bottom (cm $d^{-1}$), $q_{top}$ the potential flux at the soil surface (cm $d^{-1}$), and $q_{drain}$ the flux to drains or ditches (cm $d^{-1}$). The potential flux at the soil surface $q_{top}$ follows from:

$$q_{top} = q_{eva} - q_{prec} - \frac{h_{pond}}{\Delta t^{i}} \tag{2.18}$$

where $q_{eva}$ is the potential soil evaporation (cm $d^{-1}$), $q_{prec}$ is the precipitation at the soil surface (cm $d^{-1}$) and $h_{pond}$ is the height of water ponding on the soil surface (cm).

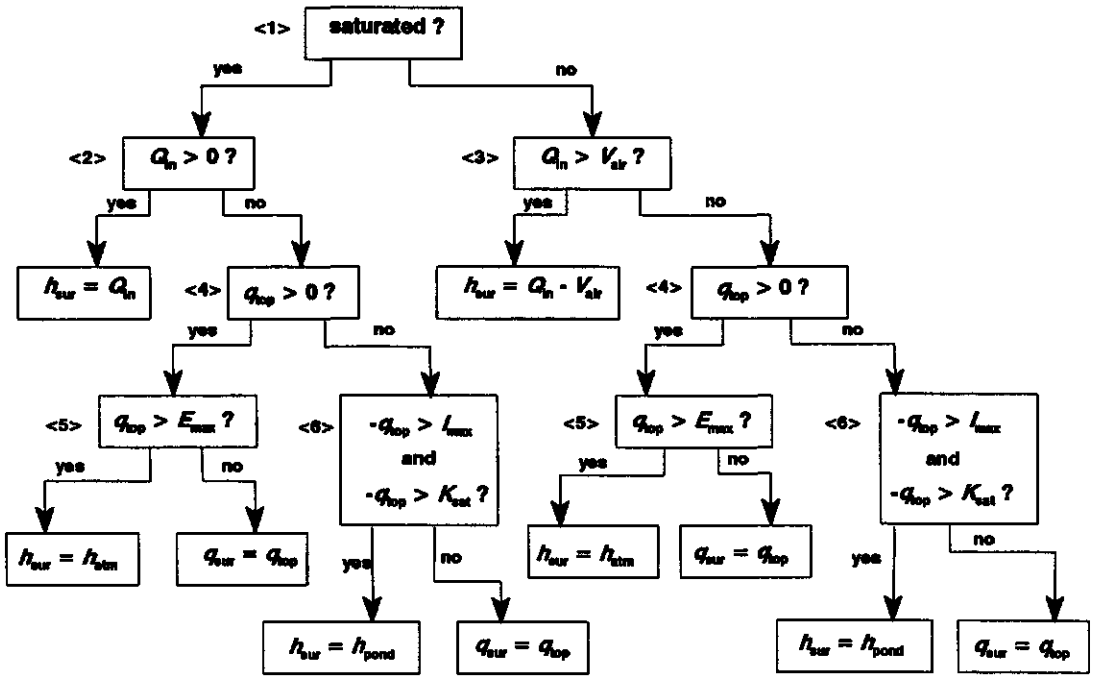


*Fig. 2.5 SWAP procedure to select the top boundary condition, which can be either flux controlled ($q_{sur}$ prescribed) or head controlled ($h_{sur}$ prescribed).*

When the soil is unsaturated, criterium <3> determines whether the soil will be saturated at the next time level $t^{j+1}$ (head is prescribed) or the soil remains unsaturated. The symbol $V_{air}$ (cm) denotes the pore volume in the soil profile being filled with air at time level $t^j$. If the soil remains unsaturated, criterium <4> distinguishes between evaporation and infiltration. In case of evaporation, the maximum flux is limited to the maximum flux according to Darcy, $E_{max}$ (cm d$^{-1}$):

$$E_{max} = -2\ K_{½} \left( \frac{h_{atm} - h_1^j - z_1}{\Delta z_1} \right) \tag{2.19}$$

with $h_{atm}$ (cm) the soil water pressure head in equilibrium with the prevailing air relative humidity:

$$h_{atm} = 13.3\ 10^5 \ln \frac{\theta_{act}}{\theta_{sat}} \tag{2.20}$$

with $e_{act}$ and $e_{sat}$ the actual and saturated vapour pressure, respectively (kPa).

In case of infiltration, a head-controlled condition applies, if the potential flux $q_{top}$ exceeds the maximum infiltration rate $I_{max}$ as well as the saturated hydraulic conductivity $K_{sat}$ (criterium <6>). $I_{max}$ (cm d$^{-1}$) is calculated as:

$$I_{max} = 2\ K_{½} \left( \frac{h_{pond} - h_1^j - z_1}{\Delta z_1} \right) \qquad (2.21)$$

During the iterative procedure of calculating $h_1^{j+1,p}$ from the tri-diagonal system of equations (Annex F), the top boundary condition is updated at each iteration $p$.

### 2.4.3 Bottom boundary condition

In the unsaturated zone water flow and solute transport occur mainly in the vertical direction. Once in the saturated zone, water starts to move in a three dimensional pattern, following the prevailing pressure gradients. The bottom boundary of the one-dimensional SWAP is either the unsaturated zone or in the upper part of the saturated zone where the transition takes place to three-dimensional groundwater flow.

At the lower boundary we can define three types of conditions:
- Dirichlet condition, the pressure head $h$ is specified;
- Neumann condition, the flux $q$ is specified;
- Cauchy condition, the flux depends on the groundwater level.

The main advantage of the *Dirichlet condition* is the easy recording of the phreatic surface in case of a present groundwater table. A drawback is that at shallow groundwater tables the simulated phreatic surface fluctuations are very sensitive to the soil hydraulic functions. The *Neumann condition* is usually applied when a no-flow boundary (e.g. an impermeable layer) can be identified, or in case of a deep groundwater table, resulting in free drainage. The *Cauchy condition* is used when unsaturated flow models are combined with models for regional groundwater flow or when effects of surface water management are to be simulated (see Chapter 10). The relation between flux and groundwater level can be obtained from drainage formulae (see Chapter 8 and 9) and/or from regional groundwater flow models (e.g. Van Bakel, 1986).

SWAP makes a distinction between the local drainage flux to ditches and drains $q_{drain}$ (cm $d^{-1}$), as calculated according to Chapter 8 and 9, and the seepage flux due to regional groundwater flow, $q_{bot}$ (cm $d^{-1}$). Figure 2.6 shows a soil profile which is drained by ditches and which receives seepage from a semi-confined aquifer. The Cauchy condition applies to the bottom boundary. The drainage flux to the ditches depends on the simulated groundwater level $\phi_{gwl}$ midway between the ditches, as is described in Chapter 8 and 9. In order to distinguish between the (local) drainage flux and (regional) bottom flux, SWAP assumes that the drainage flux is extracted laterally in the saturated zone of the soil profile. So the bottom flux $q_{bot}$, as defined by the user or

calculated by the program, excludes the drainage flux. In case of Fig. 2.6, $q_{bot}$ solely depends on the average groundwater level, $\phi_{avg}$, the hydraulic head in the semi-confined aquifer, $\phi_{aquif}$, and the resistance of the semi-confining layer, $c_{conf}$ (see Eq. 2.23).

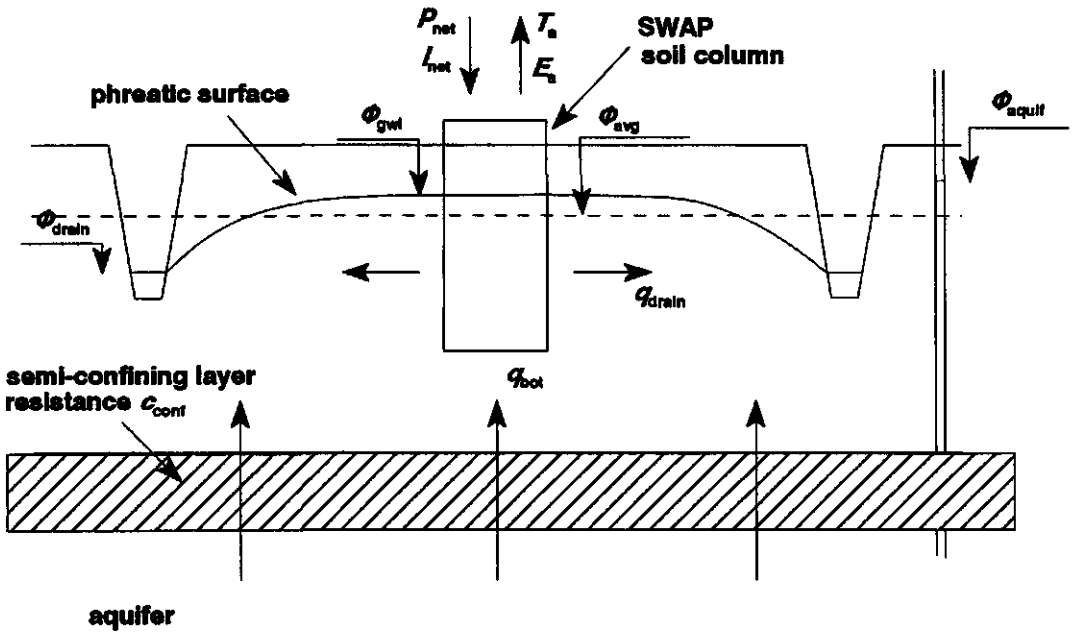


*Fig. 2.6 Pseudo two-dimensional Cauchy lower boundary condition, in case of drainage to ditches and seepage from a deep aquifer.*

SWAP offers eight options to prescribe the lower boundary condition:

1) Specify groundwater level, $\phi_{gwl}$ (cm), as function of time.

2) Specify bottom flux, $q_{bot}$ (cm $d^{-1}$), as function of time.

3) Calculate $q_{bot}$ from an aquifer below an aquitard, see Fig. 2.6. The average phreatic head, $\phi_{avg}$ (cm), is calculated as:

$$\phi_{avg} = \phi_{drain} + \beta_{gwl} (\phi_{gwl} - \phi_{drain}) \qquad (2.22)$$

with $\phi_{drain}$ the hydraulic head of the drain (cm) and $\beta_{gwl}$ the groundwater shape factor (-). Possible values for $\beta_{gwl}$ are 0.66 (parabolic), 0.64 (sinusoidal), 0.79 (elliptic) and 1.00 (no drains). The bottom flux $q_{bot}$ is calculated by:

$$q_{bot} = \frac{\phi_{aquif} - \phi_{avg}}{c_{conf}} \qquad (2.23)$$

where $\phi_{aquif}$ is the hydraulic head in the semi-confined aquifer (cm), and $c_{conf}$ is the semi-confining layer resistance (d). In the aquifer a sinusoidal wave is assumed:

$$\phi_{aquif} = \phi_{aquif,m} + \phi_{aquif,a}\cos\left(\frac{2\pi}{\phi_{aquif,p}}(t - t_{max})\right) \qquad (2.24)$$

where $\phi_{aquif,m}$, $\phi_{aquif,a}$, and $\phi_{aquif,p}$ are the mean (cm), amplitude (cm) and period (d) of the hydraulic head sinus wave in the semi-confined aquifer, and $t_{max}$ is a time (d) at which $\phi_{aquif}$ reaches its maximum.

4) Calculate $q_{bot}$ from an exponential flux - average groundwater relationship, which is valid for deep sandy areas:

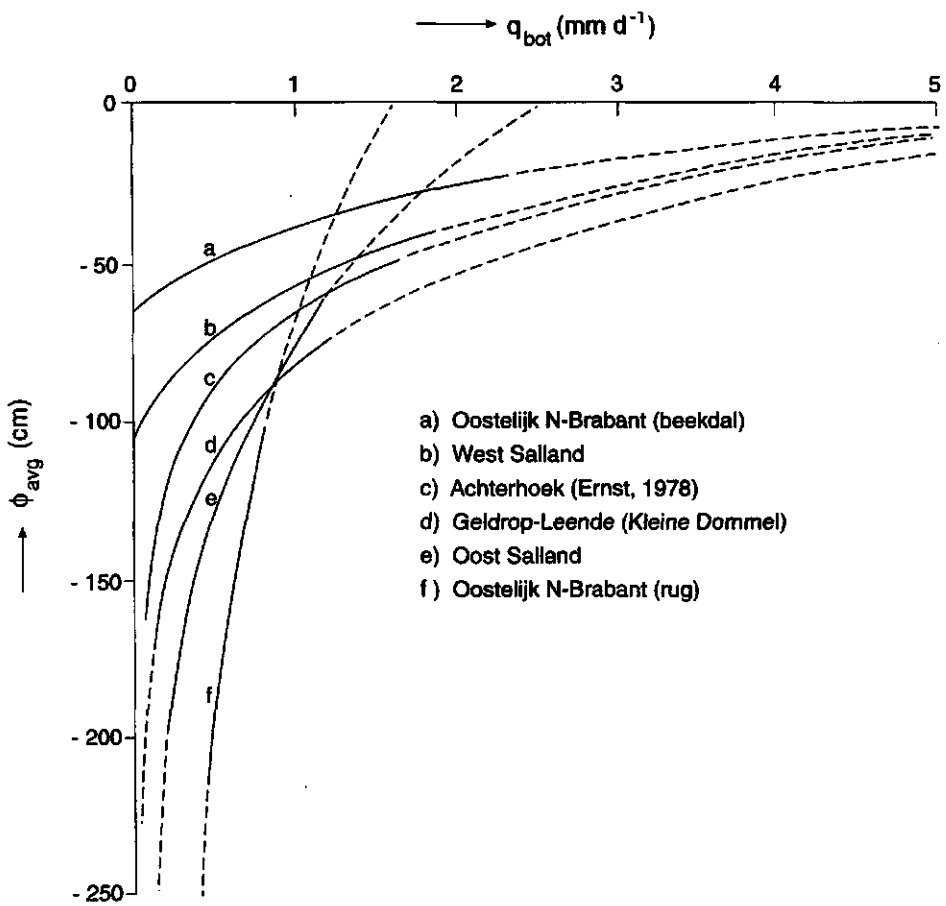


*Fig. 2.7 Bottom flux $q_{bot}$ as function of average groundwater level $\phi_{avg}$, as measured in six sandy regions in the Netherlands (Ernst and Feddes, 1979).*

$$q_{bot} = a_{qbot}\, e^{b_{qbot}|\phi_{avg}|} \qquad (2.25)$$

where $a_{qbot}$ (cm $d^{-1}$) and $b_{qbot}$ ($cm^{-1}$) are empirical coefficients. Examples of this relationship are given in Fig. 2.7. For additional data of $q_{bot}$ - $\phi_{avg}$ relationships, see Massop and De Wit (1994).

5) Specify pressure head of bottom compartment, $h_n$ (cm), as function of time.

6) Prescribe zero flux at bottom of the soil profile, $q_{bot} = 0$.

7) Prescribe free drainage of soil profile. In that case, unit gradient is assumed at the bottom boundary:

$$\frac{\partial H}{\partial z} = 1 \qquad ==> \qquad q_{bot} = -k_{numnod} \qquad (2.26)$$

8) Prescribe free outflow at soil-air interface. Drainage will only occur if the pressure head in the bottom compartment $h_n$ increases until above zero. During drainage, $h_n$ is set equal to zero and $q_{bot}$ calculated by solving the Richards' equation. After a drainage event, $q_{bot}$ is set to zero and $h_n$ calculated by solving the Richards' equation.

In case of options 1, 2, 3, 5 and 6, in addition to $q_{bot}$ the drainage flux $q_{drain}$ can be defined (Chapter 8 and 9). In case of option 4, Eq. 2.25 includes drainage to local ditches or drains, so $q_{drain}$ should not be defined separately. In case of options 7 and 8, the simulated soil profile is unsaturated, so lateral drainage will not occur.

# 3 Solute transport

## 3.1 Introduction

Many solutes enter the natural system at the soil surface. The solute residence time in the unsaturated zone is important for soil- and groundwater pollution management. For instance organic compounds are mainly decomposed in the unsaturated zone, where the biological activity is concentrated. Most plants are able to extract water and nutrients from the soil only in the unsaturated zone. In irrigated areas, the long term salinity in the root zone will depend on the amount of percolation from the unsaturated zone. Whereas in the unsaturated zone the transport of solutes is predominantly vertical, once being in the groundwater solutes may diverge in any direction, threatening surface waters, nature reserves and drinking wells. Using an analytical model, Beltman et al. (1995) show the importance of the transport processes in the unsaturated zone as compared to the transport processes in the saturated zone. It is clear that a thorough understanding is needed of the processes that govern the transport, adsorption, root uptake and decomposition of the solutes in the unsaturated zone, in order to analyse and manage soil and water related environmental problems.

SWAP is designed to simulate transport processes at field scale level. Although for management purposes most farmers try to have more or less the same soil and drainage condition per field, still the existing soil spatial heterogeneity within a field may cause a large variation of solute fluxes (Biggar and Nielsen, 1976; Van de Pol et al., 1977; Van der Zee and Van Riemsdijk, 1987). Most of this variation is caused by variation of the soil hydraulic functions (Par. 5.1), preferential flow due to macropores in structured soils (Par. 5.2) or unstable wetting fronts in unstructured soils (Par. 5.3). In many cases it will not be possible to determine the variation (including the correlations) of all the physical parameters. One approach is to measure for a period of time the solute concentrations in the soil profile and drainage water and apply calibration or inverse modelling to determine 'effective' transport parameters (Groen, 1997). Another approach is the use of Monte Carlo simulations, where the variation of the transport parameters is derived from comparable fields (Boesten and Van der Linden, 1991). Jury (1982) proposed to use transfer functions, which don't explicitly describe the transport processes within the soil, but just describe the relation between solutes that enter and that leave a soil profile. Some limitations of the transfer function approach are that it requires a field experiment for calibration and that extrapolation to other circumstances is risky because of its stochastic rather than physical basis. SWAP confines to the physical processes in order to be flexible in parameter input and allow the simulation of all kind of design and management scenario's. The spatial variability can be taken into account by calibration, inverse modelling or Monte Carlo simulation.

SWAP is focused on the transport of salts, pesticides and other solutes that can be described with relatively simple kinetics. Processes that are not considered in SWAP are:
- volatilization and gas transport
- transport of non-mixing or immiscible fluids (e.g. oil and water)
- chemical equilibria of various solutes (e.g. between $Na^+$, $Ca^{2+}$ and $Mg^{2+}$)
- chemical and biological chain reactions (e.g. mineralization, nitrification)

First we describe the transport processes that are considered in SWAP. Next we discuss conservation of mass, which in combination with the transport processes provides the solute transport equation. Finally we consider solute transport in the saturated zone. The program is designed to simulate the solute concentrations entering drains and surface waters from the combined unsaturated - saturated soil system.

## 3.2 Transport processes

The three main solute transport mechanisms in soil water are diffusion, convection and dispersion. *Diffusion* is solute transport which is caused by the solute gradient. Thermal motion of the solute molecules within the soil solution cause a net transport of molecules from high to low concentrations. The solute flux $J_{dif}$ (g cm$^{-2}$ d$^{-1}$) is generally described by Fick's first law:

$$J_{dif} = -\theta D_{dif} \frac{\partial c}{\partial z} \tag{3.1}$$

with $D_{dif}$ the diffusion coefficient (cm$^2$ d$^{-1}$) and $c$ the solute concentration in soil water (g cm$^{-3}$). $D_{dif}$ is very sensitive to the actual water content, as it strongly affects the solute transport path and the effective cross-sectional transport area. In SWAP we employ the relation proposed by Millington and Quirk (1961):

$$D_{dif} = D_w \frac{\theta^{7/3}}{\phi_{por}^2} \tag{3.2}$$

with $D_w$ the solute diffusion coefficient in free water (cm$^2$ d$^{-1}$) and $\phi_{por}$ the soil porosity (cm$^3$ cm$^{-3}$).

The bulk transport of solutes occurs when solutes are carried along with the moving soil water. The mean flux of this transport is called the *convective* flux, $J_{con}$ (g cm$^{-2}$ d$^{-1}$), and can be calculated from the average soil water flux:

$$J_{con} = qc \tag{3.3}$$

When describing water flow, we usually consider the Darcy flux $q$ (cm d$^{-1}$), which is averaged over a certain cross section. In case of solute transport, we

need to consider the water velocity variation between pores of different size and geometry and also the water velocity variation inside a pore itself. The variety of water velocities cause some solutes to advance faster than the average solute front, and other solutes to advance slower. The overall effect will be that steep solute fronts tends to smoothen or to disperse. Solutes seem to flow from high to low concentrations. If the time required for solutes to mix in the transverse direction is small, compared to the time required for solutes to move in the flow direction by mean convection, the *dispersion* flux $J_{dis}$ (g cm$^{-2}$ d$^{-1}$) is proportional to the solute gradient (Bear, 1972):

$$J_{dis} = -\theta D_{dis} \frac{\partial c}{\partial z} \tag{3.4}$$

with $D_{dis}$ the dispersion coefficient (cm$^2$ d$^{-1}$). Under laminar flow conditions $D_{dis}$ itself is proportional to the pore water velocity $v$ (Bolt, 1979):

$$D_{dis} = L_{dis} v \tag{3.5}$$

with $L_{dis}$ the dispersion length (cm). Dispersion length depends on the scale over which the water flux and solute convection are averaged. Typical values of $L_{dis}$ are 0.5 - 2.0 cm in packed laboratory columns and 5-20 cm in the field, although they can be considerably larger in regional groundwater transport (Jury et al., 1991). Unless water is flowing very slowly through repacked soil, the dispersion flux is usually much larger than the diffusion flux.

The total solute flux $J$ (g cm$^{-2}$ d$^{-1}$) is therefore described by:

$$J = J_{dif} + J_{con} + J_{dis} = qc - \theta(D_{dif} + D_{dis})\frac{\partial c}{\partial z} \tag{3.6}$$

Figure 3.1 shows the effect of various processes on the breakthrough curve. Piston flow refers to the situation where only transport due to convection is considered. Dispersion smoothens the solute front. Adsorption will delay the solute breakthrough, in contrast to exclusion, e.g. in case of mobile/immobile flow, which causes a more early breakthrough (see Par. 5.3).

## 3.3 Continuity and transport equation

By considering conservation of mass in an elementary volume, we may derive the continuity equation for solute transport:

$$\frac{\partial X}{\partial t} = -\frac{\partial J}{\partial z} - S_s \tag{3.7}$$

with $X$ being the total solute concentration in the soil system (g cm$^{-3}$) and $S_s$ the solute sink term (g cm$^{-3}$ d$^{-1}$) accounting for decomposition and uptake by roots.

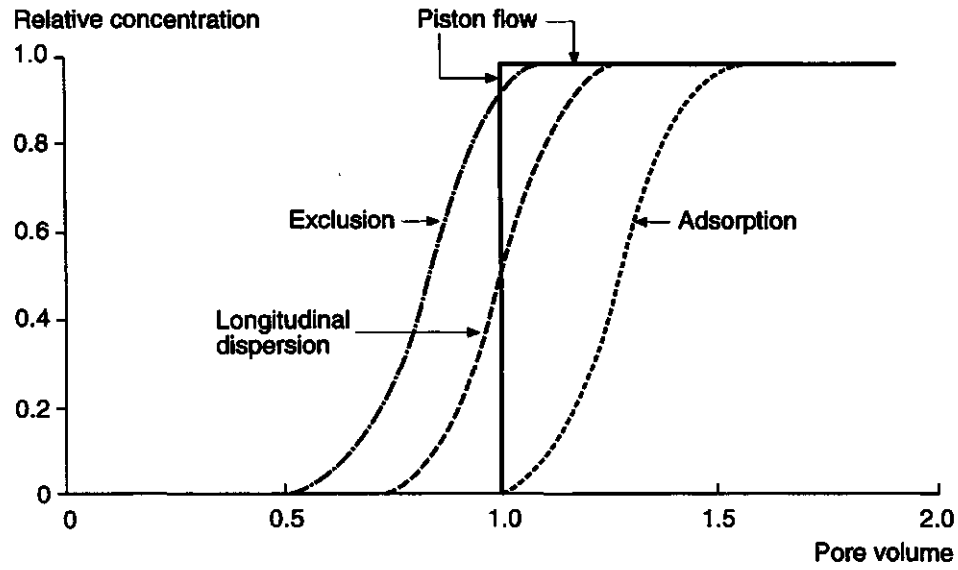


*Fig. 3.1 Schematic breakthrough curves in case of piston flow and in case of adsorption, longitudinal dispersion or ion exclusion (Bresler et al., 1982).*

The solutes may be dissolved in the soil water and/or may be adsorbed to organic matter or to clay minerals:

$$X = \theta c + \rho_b Q \tag{3.8}$$

with $\rho_b$ being the dry soil bulk density (g $cm^{-3}$) and $Q$ the amount adsorbed (g $g^{-1}$). The adsorption isotherm describes the amount of solutes adsorbed in equilibrium with the dissolved concentration. At this stage we will assume instantaneous equilibrium between $c$ and $Q$ and use the non-linear Freundlich equation, which is a flexible function for many organic and inorganic solutes. In Par. 5.3 it will be shown that the mobile-immobile concept, as applied in SWAP, also allows the transfer of solutes from the dissolved state to the adsorbed state and vice versa at a certain rate.
Freundlich adsorption can be written as:

$$Q = K_f \, c_{ref} \left(\frac{c}{c_{ref}}\right)^{N_f} \tag{3.9}$$

with $K_f$ the Freundlich coefficient ($cm^3 \, g^{-1}$), $N_f$ is the Freundlich exponent (-) and $c_{ref}$ is a reference value of the solute concentration (g $cm^{-3}$) which is used to make $N_f$ dimensionless.

The solute sink term $S_s$ can be written as:

$$S_s = \mu(\theta c + \rho_b Q) + K_r S c \tag{3.10}$$

where $\mu$ is the first order rate coefficient of transformation ($d^{-1}$), $K_r$ is the root uptake preference factor (-) and $S$ the root water extraction rate ($d^{-1}$). At the

right hand side of Eq. 3.10, the first term accounts for linear decomposition and the second term for root uptake proportional to water uptake. $K_r$ accounts for positive or negative selection of solute ions relative to the amount of soil water that is extracted.

The coefficient $\mu$ is affected by soil temperature, water content and depth. Analogous to Boesten and Van der Linden (1991), SWAP calculates $\mu$ from:

$$\mu = f_T \, f_\theta \, f_z \, \mu_{ref} \tag{3.11}$$

in which $f_T$ is a soil temperature factor (-), $f_\theta$ and $f_z$ are reduction factors (-) accounting for the effect of soil water content and soil depth, and $\mu_{ref}$ ($d^{-1}$) is $\mu$ at reference conditions (e.g. soil from the plough layer at 20 °C and at suction $h$ = -100 cm).

The factor $f_T$ is described according to Boesten (1986) as:

$$f_T = e^{\gamma_T (T - 20)} \tag{3.12}$$

where $\gamma_T$ is a parameter ($°C^{-1}$), and $T$ is the soil temperature in °C.

Wolfe et al. (1990) describe the importance of the water content in transformation processes. Realizing that it is a large simplification, in SWAP we adopt the relation as proposed by Walker (1974) :

$$f_\theta = \left( \frac{\theta}{\theta_{ref}} \right)^B \qquad \text{with} \qquad f_\theta \leq 1 \tag{3.13}$$

where $\theta_{ref}$ is $\theta$ at $h$ = -100 cm and $B$ is a constant (-).

The transformation reduction factor for soil depth, $f_z$, should be derived from in situ measurements. The user may specify $f_z$ as function of soil depth in the input file.

Combination of Eq. 3.6, 3.7, 3.8, and 3.10, yields the transport equation applied in SWAP which is valid for dynamic, one-dimensional, convective-dispersive mass transport, including non-linear adsorption, linear decay and proportional root uptake in unsaturated/saturated soil (Van Genuchten and Cleary, 1979; Nielsen et al., 1986; Boesten and Van der Linden, 1991):

$$\frac{\partial(\theta c + \rho_b Q)}{\partial t} = - \frac{\partial qc}{\partial z} + \frac{\partial}{\partial z}\left(\theta(D_{dif} + D_{dis}) \frac{\partial c}{\partial z}\right) - \mu(\theta c + \rho_b Q) - K_r S c \tag{3.14}$$

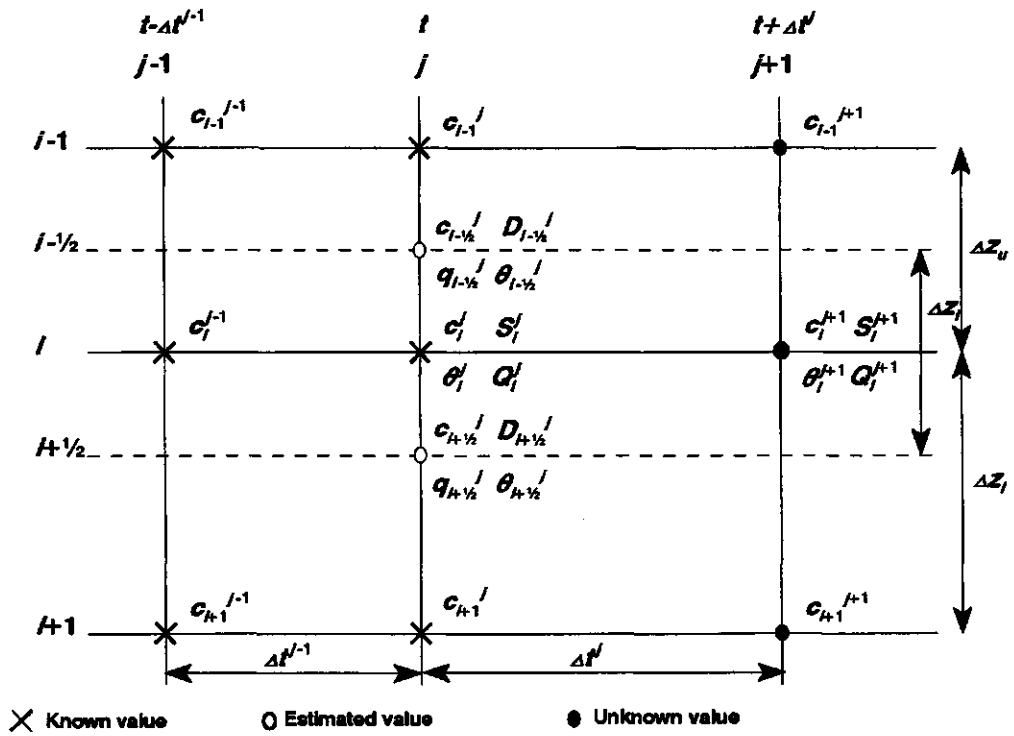


*Fig. 3.2 Known, estimated, and unknown variables in the discretized time-space domain, used to solve numerically the solute transport equation*

An explicit, central finite difference scheme is used to solve Eq. 3.14 (see Fig. 3.2):

$$\frac{\theta_i^{j+1} c_i^{j+1} + \rho_b Q_i^{j+1} - \theta_i^j c_i^j - \rho_b Q_i^j}{\Delta t^j} = \frac{q_{i-½}^j c_{i-½}^j - q_{i+½}^j c_{i+½}^j}{\Delta z_i} +$$

$$\frac{1}{\Delta z_i}\left[\frac{\theta_{i-½}^j D_{i-½}^j \left(c_{i-1}^j - c_i^j\right)}{\Delta z_u} - \frac{\theta_{i+½}^j D_{i+½}^j \left(c_i^j - c_{i+1}^j\right)}{\Delta z_l}\right] - \tag{3.15}$$

$$\mu_i^j \left(\theta_i^j c_i^j + \rho_b Q_i^j\right) - K_r S_i^j c_i^j$$

where $D$ (= $D_{dif}$ + $D_{dis}$) is the overall dispersion coefficient (cm$^2$ d$^{-1}$); the superscript $j$ denotes the time level, subscript $i$ the node number and subscripts $i$-1/2 and $i$+1/2 refer to linearly interpolated values at the upper and lower compartment boundary, respectively. Compared to an implicit, iterative scheme, above explicit scheme has the advantage that incorporation of non-linear adsorption, mobile/immobile concepts, and other non-linear processes is relatively easy. In order to ensure stability of the explicit scheme, the time

step $\Delta t^j$ should meet the criterium (Van Genuchten and Wierenga, 1974):

$$\Delta t^j \leq \frac{\Delta z_i^2 \, \theta_i^j}{2D_i^j} \tag{3.16}$$

This stability criterium applies to non-sorbing substances and is therefore also safe for sorbing substances.

## 3.4 Boundary conditions

As *initial condition*, the user needs to specify the solute concentrations, $c_i$ (g cm$^{-3}$), in the soil water and the average solute concentration, $c_{gr}$ (g cm$^{-3}$), in the groundwater.

For the *top boundary condition*, the solute concentrations in irrigation and rain water, $c_{irr}$ and $c_{prec}$ (g cm$^{-3}$), need to be specified. During evaporation no solutes enter the soil profile at the surface. During infiltration, the solute concentration of water that enters the soil profile at the top, $c_{pond}$ (g cm$^{-3}$), is affected by the ponding layer and its concentration at the former time step, the solute amounts coming in by rain and irrigation, and the solute amounts transported laterally to cracks:

$$c_{pond}^j = \frac{(P_{net}^j \, c_{prec} + I_{net}^j \, c_{irr}) \, \Delta t^j + h_{pond}^{j-1} \, c_{pond}^{j-1}}{h_{pond}^j - (q_{top} + q_{lat}) \, \Delta t^j} \tag{3.17}$$

where $P_{net}$ is the net precipitation rate (cm d$^{-1}$, see Par. 6.7), $I_{net}$ is the net irrigation rate (cm d$^{-1}$, see Par. 6.7), $h_{pond}$ is the height of water ponding on the soil surface, $q_{top}$ is the water flux at the soil surface (cm d$^{-1}$, positive upward) and $q_{lat}$ is the water flux flowing to cracks (cm d$^{-1}$, see Par. 5.2). The solute flux $J_{top}$ (g cm$^{-2}$) entering the soil at the surface, equals:

$$J_{top} = q_{top} \, c_{pond} \, (1.0 - A_c) \tag{3.18}$$

where $A_c$ is the relative crack area (cm$^2$ cm$^{-2}$). The solute flux that enters the cracks is described in Par. 5.2.

For the *drainage boundary condition*, SWAP assumes that the lateral drainage flux leaves the soil profile laterally at the lowest compartment. During drainage ($q_{drain} > 0$), the solute flux $J_{drain}$ (g cm$^{-2}$) that leaves the one-dimensional soil profile is calculated as:

$$J_{drain} = q_{drain} \, c_n \tag{3.19}$$

where $c_n$ is the solute concentration in the lowest compartment. During infiltration ($q_{drain} < 0$), $J_{drain}$ follows from:

$$J_{drain} = q_{drain}\ c_{gr} \tag{3.20}$$

where $c_{gr}$ is the average solute concentration in the groundwater (g cm$^{-3}$, see Par. 3.5).

For the *bottom boundary condition*, SWAP uses the flux through the bottom of the soil profile $q_{bot}$ (cm d$^{-1}$, see Par. 9.2). In case of upward flow ($q_{bot} > 0$), the solute flux $J_{bot}$ (g cm$^{-2}$, positive is upwards) equals:

$$J_{bot} = q_{bot}\ c_{gr} \tag{3.21}$$

If $q_{bot}$ is directed downwards ($q_{bot} < 0$), the solute flux $J_{bot}$ (g cm$^{-2}$) equals:

$$J_{bot} = q_{bot}\ c_n \tag{3.22}$$

## 3.5 Residence time in the saturated zone

In the saturated zone, prevailing soil water pressure gradients will induce a three-dimensional flow and transport pattern. A strict deterministic approach would require a coupling of the one-dimensional agrohydrological model with a two- or three-dimensional model for the saturated zone. In many situations this is not feasible due to limitations of data, time, computer resources or experience. Also the required accuracy of the analysis might not justify such a detailed approach. Therefore in SWAP a simplified approach is followed to calculate the transport of solutes to drains or ditches.

Ernst (1973) and Van Ommen (1985) showed that the breakthrough curve of a field with fully penetrating drainage canals, is identical to the breakthrough curve of a reservoir with complete mixing (Fig. 3.3). This is also valid if linear adsorption and transformation at first order rate take place (Van Ommen, 1985). Linear adsorption might be described by:

$$Q = k_{ads}\ c_{gr} \tag{3.23}$$

where $k_{ads}$ is the linear adsorption coefficient in the saturated zone (cm$^3$ g$^{-1}$) and $c_{gr}$ is the average solute concentration in the groundwater (g cm$^{-3}$). Numerical analysis by Duffy and Lee (1992) showed that dispersion in the saturated zone has only a minor effect for $L_{drain}/d_{aquif} \geq 10$, where $L_{drain}$ is the distance between the drainage canals (cm) and $d_{aquif}$ the thickness of the aquifer (cm). Generally $L_{drain}/d_{aquif}$ will be around 10 or larger, therefore dispersion might be ignored.

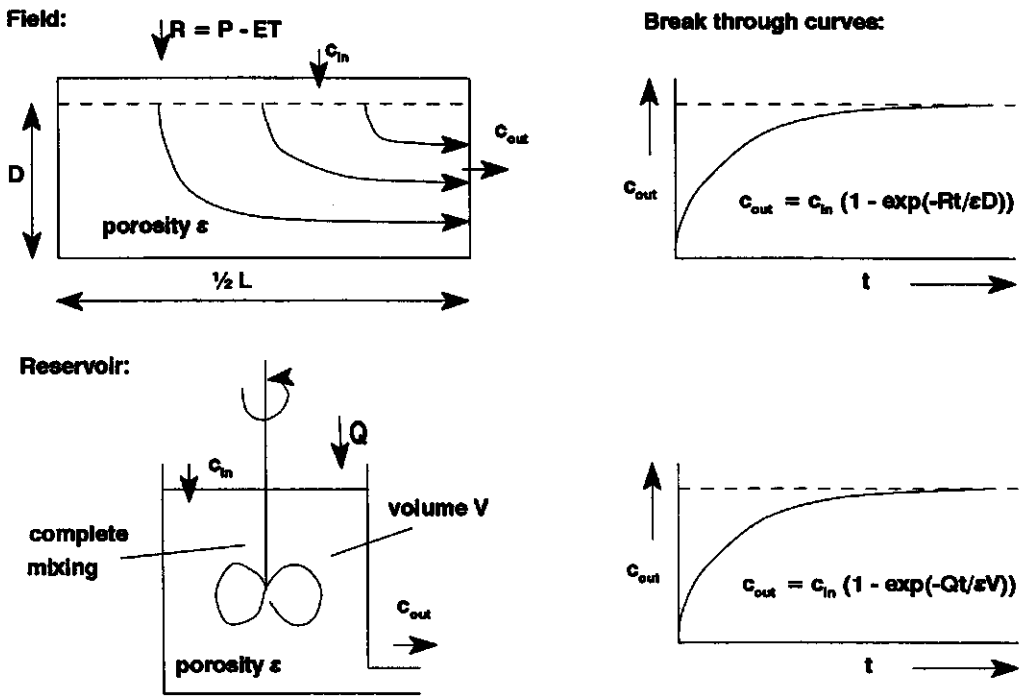


*Fig. 3.3 Breakthrough curves of fields with fully penetrating drains and reservoirs with complete mixing, have a similar exponential shape.*

In order to derive the breakthrough curve, we will use the similarity between breakthrough curves of drained fields and mixed reservoirs. Starting point is the solute transport equation of the unsaturated zone, Eq. 3.14. Replacement of non-linear adsorption by linear adsorption, and omittance of dispersion and root water uptake, results in the mass balance equation of the saturated zone:

$$\frac{\partial\,(\theta_s c_{gr} + \rho_b k_{ads} c_{gr})}{\partial\, t} = \frac{q_{drain}}{d_{aquif}}\,(c_{in} - c_{gr}) - \mu_{gr}(\theta_s c_{gr} + \rho_b k_{ads} c_{gr}) \qquad (3.24)$$

where $\theta_s$ is the saturated water content ($cm^3\ cm^{-3}$), $q_{drain}$ is the drainage flux ($cm\ d^{-1}$), $c_{in}$ is the solute concentration of water percolating from the unsaturated zone ($g\ cm^{-3}$) and $\mu_{gr}$ is the first order rate coefficient for transformation in the saturated zone ($d^{-1}$). Eq. 3.24 applies to a drainage situation ($q_{drain} > 0$). In case of infiltration ($q_{drain} < 0$), SWAP assumes the infiltrating water from the drainage system to be solute free, and Eq. 3.24 transforms to:

$$\frac{\partial\,(\theta_s c_{gr} + \rho_b k_{ads} c_{gr})}{\partial\, t} = \frac{q_{drain}}{d_{aquif}}\,c_{in} - \mu_{gr}(\theta_s c_{gr} + \rho_b k_{ads} c_{gr}) \qquad (3.25)$$

Eq. 3.24 and 3.25 are discretized as an explicit, forward difference scheme.

For instance, SWAP discretizes Eq. 3.24 as follows:

$$\frac{c_{gr}^{j+1} - c_{gr}^{j}}{\Delta t^{j}} (\theta_s + \rho_b k_{ads}) = \frac{q_{drain}^{j}}{d_{aquif}} (c_{in}^{j} - c_{gr}^{j}) - \mu_{gr}(\theta_s c_{gr}^{j} + \rho_b k_{ads} c_{gr}^{j}) \qquad (3.26)$$

The stability of Eq. 3.26 depends on the size of the time step. In SWAP, the time step will be limited by the soil water dynamics and solute transport near the soil surface, and no stability problems are expected. The boundary conditions that apply to the saturated zone, are included in Eq. 3.24 and 3.25.

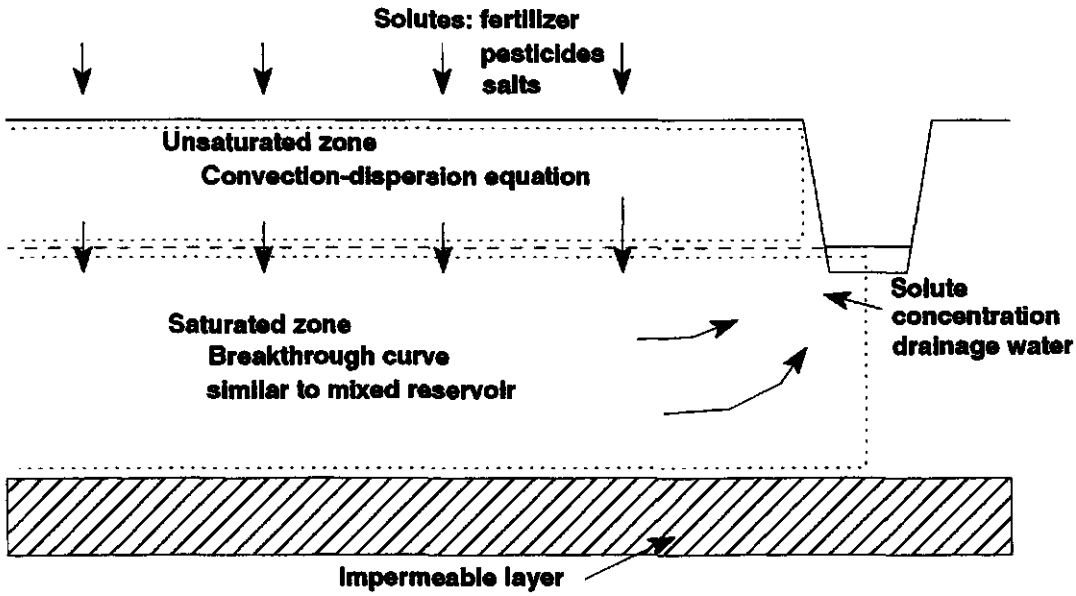


*Fig. 3.4 Combination of one-dimensional transport in the unsaturated zone and two-dimensional transport in the saturated zone, in order to calculate solute amounts leached to drains or ditches.*

Figure 3.4 shows the overall concept for solute breakthrough. In the unsaturated zone the convection dispersion equation (Eq. 3.14) is used, while in the saturated zone the solute leaching is calculated similar to a completely mixed reservoir (Eq. 3.24 or 3.25). The concept assumes a homogeneous aquifer and field drainage at one level. In case of heterogeneous groundwater flow or multi-level drainage, the off-line connection with other regional transport models (e.g. ANIMO, see Chapter 10) can be used.

# 4 Soil heat flow

Soil temperature may affect the surface energy balance, soil hydraulic properties, decomposition rate of solutes and growth rate of roots. SWAP version 2.0 uses the soil temperatures only to adjust the solute decomposition rate. The program calculates the soil temperatures either analytically or numerically. In the following sections the heat flow equations and the applied analytical and numerical solutions are discussed.

## 4.1 Soil heat flow equation

Commonly, heat flow by radiation, convection and conduction is modeled by the conduction equation alone. According to De Vries (1975), the rate of heat transfer by water vapour diffusion is small and proportional to the temperature gradient. Therefore, such diffusion might be taken into account by slightly increasing the soil thermal diffusivity. This approach is followed in SWAP as well. Apparent thermal properties rather than real thermal properties are assumed to account for both conductive and non-conductive heat flow.

The one-dimensional soil heat flux, $q_{heat}$ (J cm$^{-2}$ d$^{-1}$), is described as:

$$q_{heat} = -\lambda_{heat}\frac{\partial T}{\partial z} \tag{4.1}$$

where $\lambda_{heat}$ is the thermal conductivity (J cm$^{-1}$ °C$^{-1}$ d$^{-1}$) and $T$ is the soil temperature (°C).

Conservation of energy results in:

$$C_{heat}\frac{\partial T}{\partial t} = -\frac{\partial q_{heat}}{\partial z} \tag{4.2}$$

where $C_{heat}$ is the soil heat capacity (J cm$^{-3}$ °C$^{-1}$).

Combination of Eq. 4.1 and 4.2 yields the differential equation for soil heat flow:

$$C_{heat}\frac{\partial T}{\partial t} = \frac{\partial}{\partial z}\left(\lambda_{heat}\frac{\partial T}{\partial z}\right) \tag{4.3}$$

## 4.2 Analytical solution

If the values of $\lambda$ and $C_h$ are considered constants, the soil thermal diffusivity $D_{heat}$ ($cm^2\ d^{-1}$) can be defined:

$$D_{heat} = \frac{\lambda_{heat}}{C_{heat}} \tag{4.4}$$

and Eq. 4.3 simplifies to:

$$\frac{\partial T}{\partial t} = D_{heat}\frac{\partial^2 T}{\partial z^2} \tag{4.5}$$

This partial differential equation can be solved for simple boundary conditions, assuming $D_{heat}$ constant or very simple functions for $D_{heat}$ (Van Wijk, 1966; Feddes, 1971; Wesseling, 1987). We might assume that the soil surface temperature varies sinusoidally during the year:

$$T(0,t) = T_{mean} + T_{ampl}\sin\left(\frac{2\pi t}{365}\right) \tag{4.6}$$

where $T_{mean}$ is the mean yearly temperature (°C), $T_{ampl}$ is the wave amplitude (°C), and $t$ is time (d) starting January 1st. In case of a semi-infinite soil profile with constant $D_{heat}$ and subject to the top boundary condition according to Eq. 4.6, the solution to Eq. 4.5 is:

$$T(z,t) = T_{mean} + T_{ampl}e^{\frac{z}{d_{temp}}}\sin\left(\frac{2\pi t}{365} + \frac{z}{d_{temp}}\right) \tag{4.7}$$

where $d_{temp}$ is the damping depth (cm), which is calculated as:

$$d_{temp} = \sqrt{\frac{365\ D_{heat}}{\pi}} \tag{4.8}$$

## 4.3 Numerical solution

In reality, $\lambda_{heat}$ and $C_{heat}$ depend on the soil moisture content and vary with time and depth. Also the soil surface temperature will deviate from a sinus wave. Therefore higher accuracy can be reached by numerical solution of the heat flow equation. Numerical discretization of Eq. 4.3 is achieved in a similar way as the discretization of the water flow equation (Eq. 2.3). SWAP employs

a fully implicit finite difference scheme as described by Wesseling (1998). The soil heat flow equation is written as:

$$C_i^{j+½}(T_i^{j+1} - T_i^j) = \frac{\Delta t^j}{\Delta z_i}\left[\lambda_{i-½}^{j+½}\frac{T_{i-1}^{j+1} - T_i^{j+1}}{\Delta z_u} - \lambda_{i+½}^{j+½}\frac{T_i^{j+1} - T_{i+1}^{j+1}}{\Delta z_l}\right] \quad (4.9)$$

where superscript $j$ denotes the time level, subscript $i$ is the node number, $\Delta z_u = z_{i+1} - z_i$ and $\Delta z_l = z_i - z_{i+1}$ (see Fig. 2.4). The coefficients $C_{heat}$ and $\lambda_{heat}$ are not affected by the temperature, which makes Eq. 4.9 linear.

Both volumetric heat capacity and thermal conductivity depend on the soil composition. The volumetric heat capacity is calculated as weighted mean of the heat capacities of the individual components (De Vries, 1963):

$$C_{heat} = f_{sand}C_{sand} + f_{clay}C_{clay} + f_{organic}C_{organic} + \theta C_{water} + f_{air}C_{air} \quad (4.10)$$

where $f$ and $C$ on the right hand side of Eq. 4.10 are respectively the volume fraction ($cm^3\ cm^{-3}$) and volumetric heat capacity ($J\ cm^{-3}\ °C^{-1}$) of each component. Table 4.1 gives values of the volumetric heat capacity for the different soil components.

*Tabel 4.1 Volumetric heat capacity and thermal conductivity of the soil components.*

| Component | Volumetric heat capacity ($J\ cm^{-3}\ °C^{-1}$) | Thermal conductivity ($J\ cm^{-1}\ °C^{-1}\ d^{-1}$) |
|---|---|---|
| Sand | 2.128 | 7603 |
| Clay | 2.385 | 2523 |
| Organic | 2.496 | 216 |
| Water | 4.180 | 492 |
| Air (20 °C) | 1.212 | 22 |

In order to calculate $C_{heat}$ (and $\lambda_{heat}$) in De Vries model, we need to input the percentage (by volume) of sand and clay, denoted $VP_{sand}$ and $VP_{clay}$ respectively. $VP_{sand}$ and $VP_{clay}$ are taken as percentages of the total *solid* soil matter and may differ for each soil layer. The total volume fraction of solid matter is given by:

$$\theta_{solid} = 1 - \theta_{sat} \quad (4.11)$$

where $\theta_{sat}$ is the saturated volumetric water content. The volume fraction of air is equal to the saturated minus the actual water content:

$$f_{air} = \theta_{sat} - \theta \tag{4.12}$$

$f_{sand}$, $f_{clay}$ and $f_{organic}$ are then calculated by:

$$f_{sand} = \frac{VP_{sand}}{100}\,\theta_{solid} \tag{4.13}$$

$$f_{clay} = \frac{VP_{clay}}{100}\,\theta_{solid} \tag{4.14}$$

$$f_{organic} = \theta_{solid} - f_{sand} - f_{clay} \tag{4.15}$$

where Eq. 4.15 assumes that solid matter that is not sand or clay, is organic.

As shown in Table 4.1, the thermal conductivities of the various soil components differ very markedly. Hence the space-average thermal conductivity of a soil depends upon its mineral composition and organic matter content, as well as the volume fractions of water and air. Since the thermal conductivity of air is very much smaller than that of water or solid matter, a high air content (or low water content) corresponds to a low thermal conductivity. The components which affect thermal conductivity $\lambda_{heat}$ are the same as those which affect the volumetric heat capacity $C_{heat}$, but the measure of their effect is different so that the variation in $\lambda_{heat}$ is much greater than of $C_{heat}$. In the normal range of soil wetness experienced in the field, $C_{heat}$ may undergo a threefold or fourfold change, whereas the corresponding change in $\lambda_{heat}$ may be hundredfold or more. One complicating factor is that, unlike heat capacity, thermal conductivity is sensitive not merely to the volume composition of a soil but also to the sizes, shapes, and spatial arrangements of the soil particles (Hillel, 1980). SWAP employs the method of De Vries (1975) as applied by Ten Berge (1986) to calculate the thermal conductivity. A clear description of the method is given in Ashby et al. (1996). The method requires no extra input data.

At the soil surface the daily average air temperature $T_{avg}$ is used as boundary condition. At the bottom of the soil profile SWAP assumes $q_{heat} = 0.0$.

Application of Eq. 4.9 to each node and including the boundary conditions at the top and bottom of the soil profile, results in a tri-diagonal system of equations, as shown in Annex G. SWAP solves the equations with *LU*-decomposition for tridiagonal systems (Press et al., 1989).

# 5 Soil heterogeneity

## 5.1 Spatial variability of soil hydraulic functions

### 5.1.1 Introduction

In most hydrological and drainage problems we deal with fields soils, which show inherent spatial variability of soil, vegetation and lower boundary condition. We may analyse the spatial variability effect by running the model at various locations. In general this is not feasible due to the huge amount of data required for an area. Especially the collection of soil physical data would require a too high investment. A practical approach is to differentiate between subareas with different sequences of soil horizons, and find an equivalent uniform porous medium for either each horizon or the total soil profile. Depending on the chosen scale of the fields, certain amount of the natural heterogeneity will be lost (Wösten, 1990).

As the flow and transport processes in the unsaturated zone are strongly non-linear, the mean input of soil hydraulic functions in general will deviate from the areal mean water and solute balance. Therefore non-linear scaling techniques need to be used to derive 'effective' soil hydraulic properties, which can be used to simulate the area-average water balance. For example, in case of the Hupsel catchment (650 ha), the average water regime could closely be simulated with 'effective' soil hydraulic functions (Hopmans and Stricker, 1989; Feddes et al., 1993). As shown by Kim (1995), in semi-humid climates effective soil hydraulic functions may give a good approximation of the area-average water balance. However in arid climates, runoff and fast percolation complicate the use of equivalent soil hydraulic functions (Kim, 1995).

Another way to quantify the effect of spatial heterogeneity, is to determine the stochastic distribution of the soil hydraulic functions in an area, and next performing a large number of simulations with input data derived from this stochastic distribution. These so-called Monte Carlo simulations will result in a stochastic distribution of water and solute balance components. Alternatively, the stochastic distribution of soil hydraulic properties may be dealt with by writing Richards' equation (Eq. 2.3) in a perturbated form (e.g. Mishra et al., 1990). Miller and Miller (1956) proposed the similar media scaling method to investigate the effect of field spatial heterogeneity of soil hydraulic properties. The similar media scaling method is used in SWAP.

### 5.1.2 Similar media scaling

Assuming geometrically similar media, Miller and Miller (1956) showed that the variability in both the $\theta(h)$ and $K(\theta)$ relation can be described by just one

dimensionless scale factor $\alpha$. The scale factor $\alpha_i$ at a certain location $i$ is equal to:

$$\alpha_i = \frac{\lambda_i}{\lambda_{ref}} \tag{5.1}$$

where $\lambda_i$ is the characteristic length at location $i$ and $\lambda_{ref}$ is the characteristic length of a reference soil (Fig. 5.1). Then, applying the theory of capillary retention, the pressure head $h_i$ at a given water content at any location $i$ is related to the pressure head $h_{ref}$ according to:

$$h_i = \frac{h_{ref}}{\alpha_i} \tag{5.2}$$

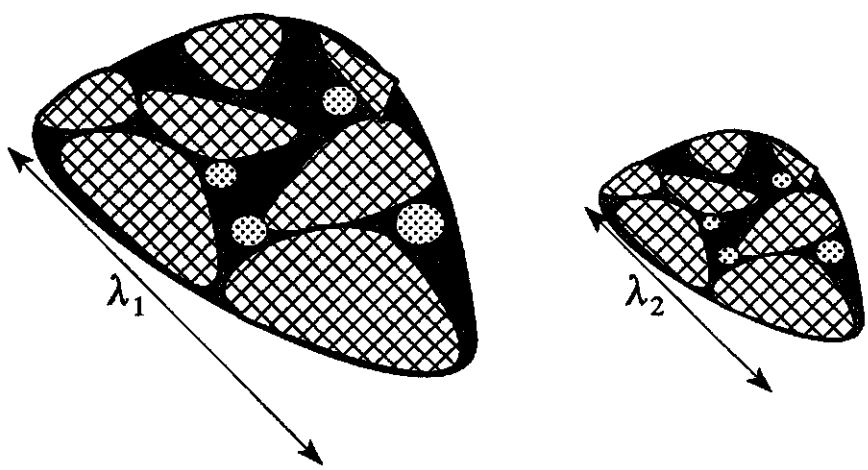


*Fig. 5.1 Characteristic lenghts $\lambda_i$ in geometrically similar media (Miller and Miller, 1956).*

Using Poiseuille's law, the hydraulic conductivity $K_i$ at any location $i$ at the given water content is related to the hydraulic conductivity $K_{ref}$ as:

$$K_i = \alpha_i^2 K_{ref} \tag{5.3}$$

Natural soils will to some degree deviate from geometrically similar media. This is clear from e.g. the saturated water content, which should be uniform if the similar media concept would apply strictly. Jury et al. (1987) point out that due to dissimilarity, scaling of different soil properties, e.g. $h$ and $K$, might result in different statistical properties of each scaling factor distribution. Youngs and Price (1981) measured microscopic characteristic lengths for porous materials ranging from glass beads and washed sands to sieved arable soils. They concluded that even for dissimilar soils the scaling concept is a good approximation.

In order to derive scaling factors $\alpha_i$ and their statistical distribution, we should have $\theta(h)$ and $K(\theta)$ data of a series of soil samples. Clausnitzer et al. (1992) developed an effective program for scaling of $\theta(h)$ and $K(\theta)$ data of a series of soil samples. In their scaling approach, first a mean curve is fit to all the data available. Because natural soils don't have identical porosities, $h$ and $K$ are written as functions of the relative saturation rather than as functions of the volumetric water content $\theta$. In the second step, the corresponding set of scaling factors is calculated for each soil sample. Next a new mean curve is fitted through the scaled hydraulic data ($h_i\ \alpha_i$ and $K_i / \alpha_i^2$, respectively). These steps are repeated, until both the mean curve and the scaling factors converge. Finally the stochastic distribution of the scaling factors (in general log-normal) and its mean and standard deviation are calculated. The program of Clausnitzer et al. (1992) allows for separate as well as simultaneous scaling of $\theta(h)$ and $K(\theta)$.

In order to apply the scaling method with SWAP, the user should give as input the Mualem - Van Genuchten parameters that describe the reference curve, and a set of scaling factors. For each scaling factor, SWAP will generate the soil hydraulic functions and calculate the water and solute balance.

## 5.2 Water flow and solute transport in cracked clay soils

### 5.2.1 Water flow

Detailed simulation of the physical transport processes in cracked clay soils is not feasible as this requires to much soil data. On the other hand, calibrated empirical models may show large errors when used for predictive purposes. The concept implemented in SWAP compromises between a physical and an empirical approach. The concept is physically based, as it employs Richards' and the convection-dispersion equation, as well as a *shrinkage characteristic.* Overland flow to the cracks and lateral adsorption of crack water into the soil matrix (see Fig. 5.4) don't require extra soil parameters, as they are solved with ordinary soil physics and an accurate numerical solution of Richards' equation. On the other hand, the lateral diffusion of solutes from the soil matrix to the cracks and vice-versa, requires calibration of an empirical parameter. In this way a parsimonious, generally applicable concept for flow and transport through cracks has been derived.

Additionally to the soil hydraulic functions $\theta(h)$ and $K(\theta)$, we need to specify the shrinkage characteristic which describes the relation between the void ratio $e$ and the moisture ratio v (Bronswijk, 1991). The void ratio $e$ ($cm^3\ cm^{-3}$) is defined as

$$e = \frac{V_p}{V_s} \tag{5.4}$$

and the moisture ratio v ($cm^3$ $cm^{-3}$) as

$$v = \frac{V_w}{V_s} \tag{5.5}$$

where $V_p$ is the total pore volume ($cm^3$), either filled with air or water, $V_w$ the water volume ($cm^3$) and $V_s$ the solid volume ($cm^3$). Figure 5.2 shows a typical shrinkage characteristic. To facilitate input and data analysis we might use an exponential relationship for the residual shrinkage stage (Kim, 1992):

$$e = \alpha_{sh}\, e^{-\beta_{sh} v} + \gamma_{sh} v \tag{5.6}$$

with $\alpha_{sh}$, $\beta_{sh}$, and $\gamma_{sh}$ dimensionless fitting parameters. The SWAP user needs to specify the void ratio $e_0$ at $v = 0$, the moisture ratio $v_1$ at the transition of residual to normal shrinkage, and the structural shrinkage, $v_s$ (Fig. 5.2). With these three input data, SWAP generates the parameters $\alpha_{sh}$, $\beta_{sh}$, and $\gamma_{sh}$, and describes the $e(v)$ relationship. Measured shrinkage characteristics of seven soil profiles in the Netherlands, as described by Bronswijk and Evers-Vermeer (1990), are listed in Annex H. The shrinkage characteristic allows the calculation of the relative cross sectional area of the cracks at the soil surface, $A_c$ ($cm^0$), and the level of the crack bottom, $Z_c$ (cm).

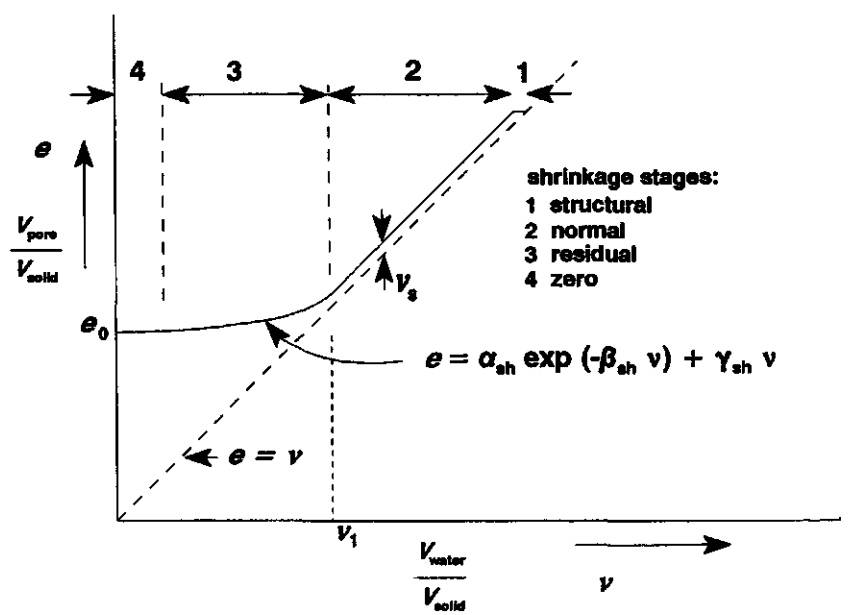


*Fig. 5.2 Void ratio e as function of moisture ratio v for a typical clay soil, showing the four stages of the shrinkage characteristic (after Bronswijk, 1991)*

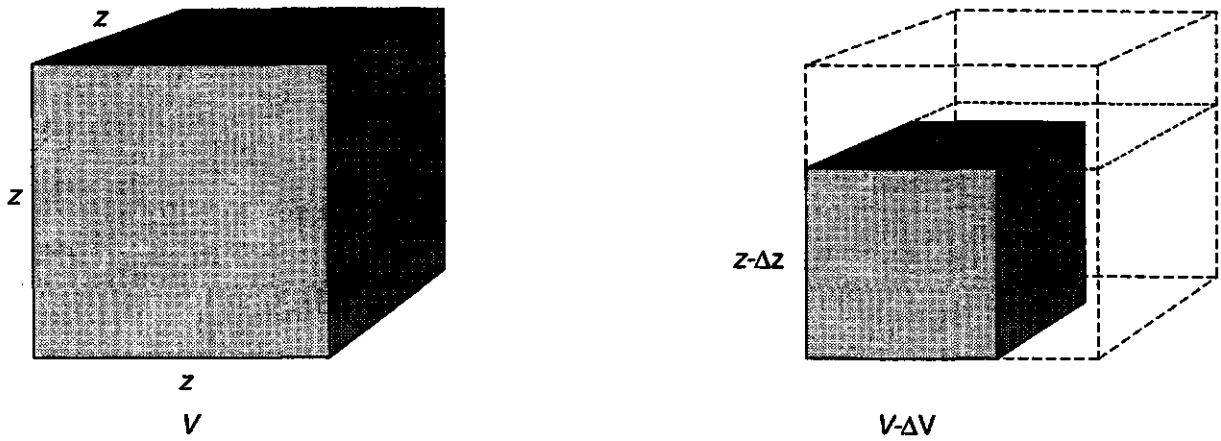


*Fig. 5.3 Isotropic shrinkage of a soil cube (Bronswijk, 1991)*

Soil shrinkage can be described as follows. Figure 5.3 shows a soil cube before and after *isotropic* shrinkage. From this figure, it can be derived that:

$$V = z^3, \quad V - \Delta V = (z - \Delta z)^3 \quad \text{and} \quad \Delta V = z^3 - (z - \Delta z)^3 \tag{5.7}$$

Therefore:

$$1 - \frac{\Delta V}{V} = \left(1 - \frac{\Delta z}{z}\right)^3 \tag{5.8}$$

in which $V$ is the original volume of the soil cube ($cm^3$), $\Delta V$ is the volume change upon shrinkage ($cm^3$), $z$ is the original height of the soil cube (cm) and $\Delta z$ is surface subsidence upon shrinkage (cm).

In the case of one-dimensional subsidence without cracking, it can easily be shown that:

$$1 - \frac{\Delta V}{V} = \left(1 - \frac{\Delta z}{z}\right)^1 \tag{5.9}$$

In a study on pedogenetically unripened soils, Rijniersce (1983) called the exponent in Eq. 5.8 and 5.9 the geometry factor $r_s$. Following Bronswijk (1991), we adopt in SWAP this terminology for clay soils as well, and arrive at a general relation between volume change and subsidence of a soil volume:

$$1 - \frac{\Delta V}{V} = \left(1 - \frac{\Delta z}{z}\right)^{r_s} \tag{5.10}$$

For three-dimensional isotropic shrinkage: $r_s = 3$. When cracking dominates subsidence: $r_s > 3$. In case of subsidence only: $r_s = 1$. Shrinkage geometry as described above, is affected by soil material, depth (e.g. depth in soil profile), soil strength (clay pastes often show only subsidence) and water content. In many cases volume changes in clay soils may considered to be isotropic.

The matrix and crack infiltration at a given rainfall intensity are calculated as (Bronswijk, 1988):

$$P < I_{max}: I_m = A_m\, P$$
$$I_c = A_c\, P$$

$$P > I_{max}: I_m = A_m\, I_{max}$$
$$I_c = A_m\, (P - I_{max}) + A_c\, P$$

with $P$ the rainfall intensity (cm $d^{-1}$), $I_{max}$ the maximum infiltration rate of the soil matrix (cm $d^{-1}$), $I_m$ the infiltration rate into the soil matrix (cm $d^{-1}$), $I_c$ infiltration rate into the cracks (cm $d^{-1}$), and $A_m$ and $A_c$ relative areas of soil matrix and cracks, respectively ($cm^2$ $cm^{-2}$). $I_{max}$ follows directly from Eq. 2.21.

Water collected in the cracks, will either infiltrate laterally to the soil matrix, or flow rapidly to nearby drains and/or ditches, as depicted in Fig. 5.4. In order to calculate the total infiltration flux, we need to derive the lateral crack surface area. Consider a crack pattern of polygons with diameter $d_{pol}$ (Fig. 5.5).

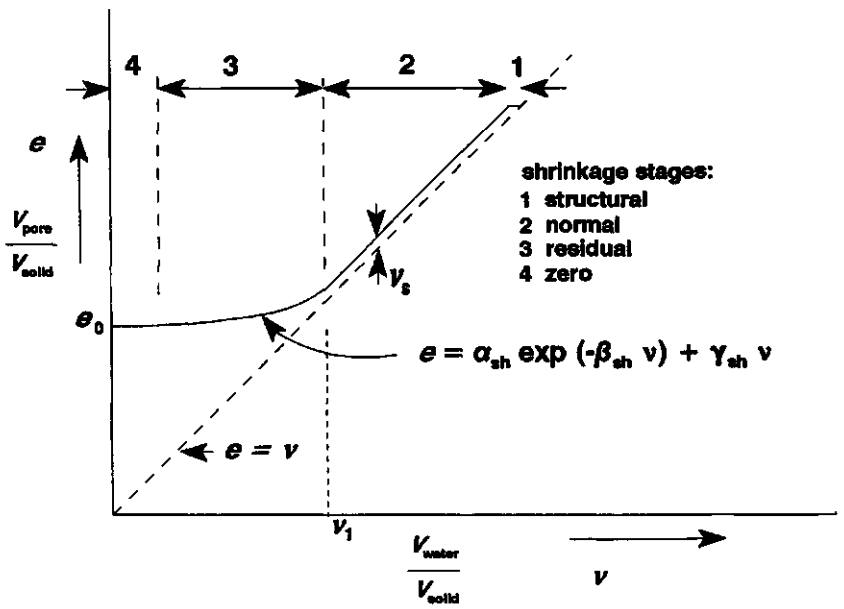


*Fig. 5.4 Concept of water flow in a cracked clay soil as applied in SWAP*

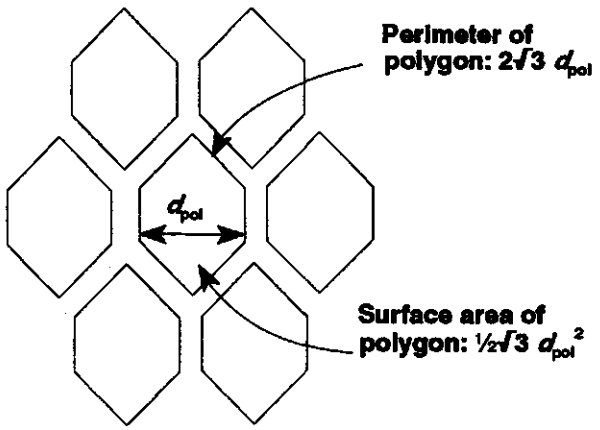


*Fig. 5.5 Assumed geometry of the soil matrix polygons of a cracked clay soil (Bronswijk, 1991)*

It can be derived that the relative area of the crack walls with respect to the surface area, $A_{wall,rel}$ (cm$^2$ cm$^{-2}$), equals:

$$A_{wall,rel} = \frac{4\ \Delta z_i}{d_{pol}} \tag{5.11}$$

with $\Delta z_i$ the soil compartment height (cm). The infiltration flux $q_{c,i}$ (cm d$^{-1}$) at compartment $i$ can derived straight from Darcy, if we assume a linear lateral pressure gradient into the soil matrix:

$$q_{c,i} = -K(h_i)\ \frac{\partial H}{\partial x} = -K(h_i)\ \frac{h_i}{¼\ d_{pol}} \tag{5.12}$$

where $K$ is the unsaturated hydraulic conductivity (cm d$^{-1}$), $h_i$ is the nodal soil water pressure head (cm) in the soil matrix, $H$ the soil water potential (cm) and $x$ the horizontal distance (cm). Next SWAP calculates the water level in the cracks, $GW_c$ (cm), from the crack volume as function of depth and the actual crack water storage. The total lateral infiltration flux, $q_{c,m}$ (cm d$^{-1}$), follows from (Fig. 5.4):

$$q_{c,m} = \sum_{z=Z_c}^{z=GW_c} q_{c,i}\ \frac{4\ \Delta z_i}{d_{pol}} \tag{5.13}$$

The lateral infiltrated water is added as a source term in the Richards' equation for the water movement in the soil matrix, in a similar way as the sink term for root water extraction (Eq. 2.3).

Bypass flow rate to drains or ditches, $q_{c,d}$ (cm d$^{-1}$), is calculated similarly to linear reservoirs:

$$q_{c,d} = f_{c,d}\ W_c \tag{5.14}$$

where $f_{c,d}$ is an exponential rate coefficient ($d^{-1}$) and $W_c$ is the crack water storage (cm).

Finally the change of water storage in the cracks, $\Delta W_c$ (cm), follows from:

$$\Delta W_c = (I_c - q_{c,m} - q_{c,d})\ \Delta t \tag{5.15}$$

### 5.2.2 Solute transport

The solutes that enter the cracks may originate from the precipitation directly falling into the cracks, or from runoff water when the infiltration capacity at the soil surface is exceeded ($P > I_{max}$). The solute concentration of the water entering the cracks, $c_{in}$ (g $cm^{-3}$), equals:

$$c_{in} = \frac{A_m\ (P - I_{max})\ c_{pond} + A_c\ P\ c_{prec}}{I_c} \tag{5.16}$$

with $c_{pond}$ and $c_{prec}$ solute concentrations (g $cm^3$) of water ponding on the soil surface and of the precipitation, respectively.

When water flows down the cracks during intensive rain showers, solutes are leached out of the crack walls and transported quickly to the subsoil (e.g. Bronswijk et al., 1995). Therefore, lateral solute diffusion between the soil matrix and water flowing down the cracks should be taken into account. The lateral solute diffusion, $c_{lat,i}$ (g $cm^{-3}$ $d^{-1}$), for the nodes $GW_c < z < 0$ is calculated by:

$$c_{lat,i} = D_{lat}\ I_c\ (c_{in} - c_i) \tag{5.17}$$

where $D_{lat}$ is the effective lateral diffusion coefficient ($cm^{-1}$ $d^{-1}$) and $c_i$ the solute concentration in the soil matrix (g $cm^{-3}$). $D_{lat}$ is a function of the crack structure and transmitting properties of the crack wall and has to be derived from field or laboratory measurements. The amount of solutes that enter the water reservoir in the cracks, $s_{c,in}$ (g $cm^{-2}$ $d^{-1}$), equals:

$$s_{c,in} = I_c\ c_{in} + \sum_{z = GW_c}^{z = 0} (c_{lat,i}\ \Delta z_i) \tag{5.18}$$

In the crack water reservoir the solutes are mixed. Part of the solutes will enter the soil matrix along the crack wall in contact with the water. Another part is transported with the bypass flow directly to the drains and/or ditches (Fig. 5.4):

$$s_{c,out} = c_c\ (q_{c,m} + q_{c,d}) \tag{5.19}$$

with $s_{c,out}$ the total flux of solutes leaving the crack reservoir (g $cm^{-2}$ $d^{-1}$) and $c_c$ the solute concentration in the crack reservoir (g $cm^{-3}$).

Change of solute storage in the cracks $S_c$ (g cm$^{-2}$) is straightforwardly calculated as:

$$\Delta S_c = (s_{c,in} - s_{c,out})\ \Delta t \tag{5.20}$$

In the soil matrix the convection-dispersion equation is applied, as described in Par. 3.3. The lateral diffused solute amounts due to water flowing down the cracks, $c_{lat,i}$, and the adsorbed solutes from the water reservoir in the cracks, $q_{c,i}c_c$, are added as a source term to Eq. 3.14.

## 5.3 Water flow and solute transport in water repellent soils

### 5.3.1 Introduction

In field soils soil water may bypass large parts of the unsaturated soil domain. This phenomenon is generally called preferential flow and has a large effect on the leaching of nutrients, salts and pesticides to the saturated zone. Preferential flow can be caused by macropores in structured soils (Par. 5.2) or by unstable wetting fronts in unstructured soils that originate from soil layering, air entrapment and water repellency (Raats, 1973; Ritsema et al., 1993). In SWAP attention is paid to water repellency, which is attributed to organic coatings of soil particles, to organic matter and to specific micro flora. Water repellency is widespread in dry top soils and can be quantified by water drop penetration time tests (Krammes and DeBano, 1965; Dekker and Jungerius, 1990). More than 75 % of the cropland and grassland top soils in the Netherlands are slightly to extremely water repellent, whereas more than 95 % of the top soils in nature reserves are strongly to extremely water repellent (Dekker and Ritsema, 1994).

De Rooij (1996) provides an overview of theories and experiments with respect to preferential flow due to water repellency. The same author performed an extensive lysimeter experiment which showed the large heterogeneity of water and solute fluxes at the 5 cm scale. De Rooij (1996) developed an analytical three region model, which could be applied to the collected lysimeter data, but which is less suitable for fields with transient flow and fluctuating groundwater levels.

Numerically, flow in water repellent soil might be simulated with a dual-porosity model as has been used for macropores in structured soils (Gerke and Van Genuchten, 1993; Saxena et al., 1994). However, the water exchange between the mobile and immobile domains in the case of water repellent soils is difficult to simulate. Also field observations show a time dependent preferential flow path volume (Ritsema and Dekker, 1994) while dual-porosity models assume a constant volume of the preferential flow path.

Another limitation of dual-porosity models is that they require twice as many soil physical parameters as single porosity models.

Another approach is the *mobile-immobile concept*. This concept has been used to explain accelerated breakthrough in the case of steady state solute transport (De Smedt and Wierenga, 1979; Van Genuchten and Wagenet, 1989). Van Dam et al. (1990, 1996) extended the mobile-immobile concept to both water flow and solute transport and to transient flow conditions. Their concept of preferential flow is easy to conceive, uses a limited number of physically based and easy to measure parameters (e.g. the soil volume fraction in which water is mobile), is applicable to transient flow conditions and can relatively easily be implemented in current one-dimensional soil water flow and solute transport codes. The concept has been applied to bromide tracer experiments in water repellent soils in lysimeters (Saxena et al., 1994) and in field soils (Van Dam et al. 1990, 1996). In the next paragraphs we elaborate on the mobile-immobile concept for soil water fluxes and solute transport as implemented in SWAP.

### 5.3.2 Water flow

Usually in the laboratory, when measuring the retention function and the hydraulic conductivity curve, soil samples are first brought to saturation and during the experiment relatively long equilibrium times are allowed. These conditions suppress effects of water repellency. The soil hydraulic functions measured in the laboratory will be denoted as $\theta_{lab}(h)$ and $K_{lab}(h)$.

In the field, immobile soil domains may occur either as large, separate volumes (Fig. 5.6) or as numerous small volumes corresponding to less accessible pores. We will assume that the soil hydraulic functions as measured in the laboratory are valid in the preferential flow domains. A second assumption is that the degree of saturation in the immobile region, $S_{d,im}$ (-) is constant. Then the bulk field water retention function $\theta_{bulk}(h)$ can be calculated as (Fig. 5.6):

$$\theta_{bulk}(h) = F\,\theta_{lab}(h) + (1 - F)\,\theta_{sat}\,S_{d,im} \qquad (5.21)$$

where $F$ equals the mobile fraction of the soil volume (-), and $\theta_{sat}$ the saturated water content ($cm^3\ cm^{-3}$).

Richards' equation only applies to the mobile region. Therefore the effective retention function, which is used to solve Richards' equation, follows from:

$$\theta(h) = F\,\theta_{lab}(h) \qquad (5.22)$$

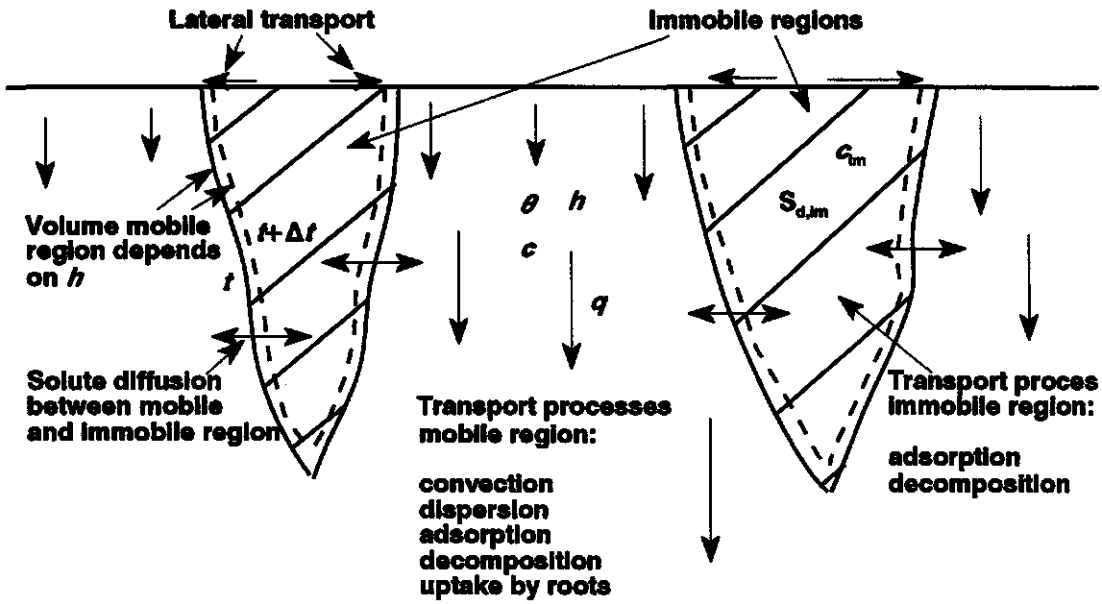


*Fig. 5.6 Mobile/immobile regions, state variables and solute transport processes in a water repellent soil. The symbols are explained in the text*

Note that θ is defined with respect to the total soil volume (mobile + immobile region), while $\theta_{lab}$ and $S_{d,im}$ are defined with respect to the mobile and immobile soil volume, respectively. The factor $F$ can roughly be estimated by visual observation of dry and wet spots in the field shortly after precipitation, and more accurately with tracer colour tests, e.g. with iodide (Van Ommen et al., 1989b) or Brilliant Blue (Flury and Flühler, 1995), with a disc permeameter in combination with a tracer (Clothier et al., 1992), or by model calibration (Van Dam et al., 1990).

The field conductivity function $K(h)$, which accounts for the immobile soil volumes, can be derived straight from Darcy (Eq. 2.1). We assume that the texture and unsaturated hydraulic conductivity curve of the immobile and mobile soil fractions are the same. In that case $q$ at a certain gradient $\partial H/\partial z$ will be reduced by the factor $F$ due to the reduction in flow domain. Thus, the effective field conductivity curve $K(h)$ which should be used in the solution of Richards' equation, is related to $K_{lab}(h)$ measured in the laboratory as:

$$K(h) = F\,K_{lab}(h) \tag{5.23}$$

Equation 5.23 neglects the effect of divergence of flow when the factor $F$ changes with depth. Also it assumes at a given soil depth the same hydraulic conductivity curve in the mobile and immobile parts.

Field studies (Ritsema and Dekker, 1994) show that the mobile fraction $F$ varies in time. In general, when the soil becomes wetter, $F$ increases. We

might approximate this by a linear relationship between log $h$ and $F$. Notice that when the immobile regions contain water, variation of $F$ with $h$ induces exchange of water between the mobile and immobile soil volumes. This exchange can be included as an extra loss term $G_w$ in the Richards' equation:

$$\frac{\partial \theta}{\partial t} = \frac{\partial \left[ K \left( \frac{\partial h}{\partial z} + 1 \right) \right]}{\partial z} - S - G_w \tag{5.24}$$

where $S$ the rootwater extraction rate ($d^{-1}$) and $G_w$ the amount of water ($d^{-1}$) transferred from the mobile to the immobile region.

$G_w$ follows from (Fig. 5.6):

$$G_w = \frac{[\, F(t) - F(t + \Delta t) \,]\, \theta_{sat}\, S_{d,im}}{\Delta t} \tag{5.25}$$

### 5.3.3 Solute transport

In the mobile region the transport of solutes is affected by convection, dispersion, adsorption, decomposition and root water uptake (Fig. 5.6). These processes are included in the solute transport equation (Eq. 3.14), but corrections are needed as only the soil volume fraction $F$ is mobile:

$$\frac{\partial \left( \theta c + F \rho_b K_f c_{ref} \left( \frac{c}{c_{ref}} \right)^{N_f} \right)}{\partial t} = - \frac{\partial qc}{\partial z} + \frac{\partial \left( \theta D \frac{\partial c}{\partial z} \right)}{\partial z} - \mu \left( \theta c + F \rho_b K_f c_{ref} \left( \frac{c}{c_{ref}} \right)^{N_f} \right) - K_r S c - G_c \tag{5.26}$$

with $c$ the solute concentration in the mobile soil water (g $cm^{-3}$), $\rho_b$ the soil dry bulk density (g $cm^{-3}$), $K_f$ the Freundlich coefficient ($cm^3$ $g^{-1}$), $c_{ref}$ the reference concentration for adsorption (g $cm^{-3}$), $N_f$ the Freundlich exponent (-), $t$ the time (d), $D$ the overall dispersion coefficient ($cm^2$ $d^{-1}$), $\mu$ the first order rate coefficient for decomposition ($d^{-1}$), $K_r$ the root uptake preference factor (-), and $G_c$ the transfer rate of solutes from the mobile to the immobile region (g $cm^{-3}$ $d^{-1}$). $G_c$ contains a diffusion term and a term that accounts for solute transfer due to variation of $F$:

$$G_c = K_{dif} (c - c_{im}) + G_w c_x \tag{5.27}$$

with $K_{dif}$ an effective diffusion coefficient ($d^{-1}$) between the mobile and immobile region, $c_{im}$ is the solute concentration in the immobile region and $c_x$

equals $c$ if $G_w$ is positive (mobile region decreases) and equals $c_{im}$ if $G_w$ is negative (mobile region increases) .

In the immobile region, water flow is absent and transport of solutes will occur by diffusion only. The roots are assumed to avoid largely the immobile regions. Hence rootwater uptake in the immobile region is small and can be neglected. The change of solute amounts in the immobile region is therefore governed by solute transfer between mobile and immobile regions and by solute decomposition:

$$\frac{\partial (1 - F) \left( \theta_{sat} S_{d,im} c_{im} + \rho_b K_f c_{ref} \left( \frac{c_{im}}{c_{ref}} \right)^{N_f} \right)}{\partial t} = \tag{5.28}$$

$$- \mu (1 - F) \left( \theta_{sat} S_{d,im} c_{im} + \rho_b K_f c_{ref} \left( \frac{c_{im}}{c_{ref}} \right)^{N_f} \right) + G_c$$

Equations 5.26 and 5.28 are solved with an explicit central finite difference scheme, as described in Par. 3.3.

# 6 Daily evapotranspiration

## 6.1 Introduction

Evapotranspiration covers both transpiration of the plants and evaporation of the soil or of ponding water. In the past, many empirical equations have been derived to calculate potential evapotranspiration which refers to evapotranspiration of cropped soils with an optimum water supply. These empirical equations are valid for the local conditions under which they were derived; they are hardly transferable to other areas. Nowadays, therefore, the focus is mainly on physically-based approaches, which have a wider applicability (Feddes and Lenselink, 1994).

For the process of evapotranspiration, three conditions in the soil-plant-atmosphere continuum must be met:
(a) A continuous supply of water;
(b) Energy available to change liquid water into vapour;
(c) A vapour pressure gradient to maintain a flux from the evaporating surface to the atmosphere.

The various methods of determining evapotranspiration are based on one or more of these requirements. For example, the soil water balance approach is based on (a), the energy balance approach on (b), and the combination method (energy balance plus heat and mass transfer) on parts of (b) and (c). Penman (1948) was the first to introduce the combination method. He estimated the evaporation from an open water surface, and then used that as a reference evaporation. Multiplied by a crop factor (Feddes, 1987), this provided an estimate of the potential evapotranspiration from a cropped surface.

The combination method requires measured climatic data on temperature, humidity, solar radiation and wind speed. Since the combination method retains a number of empirical relationships, numerous modifications to adjust it to local conditions have been proposed.

Analyzing a range of lysimeter data worldwide, Doorenbos and Pruitt (1977) proposed the FAO Modified Penman method, which has found worldwide application in irrigation and drainage projects. These authors adopted the same two-step approach as Penman to estimate crop water requirements (i.e. estimating a reference evapotranspiration, selecting crop coefficients per crop and per growth stage, and then multiplying the two to find the crop water requirements, in this way accounting for incomplete soil cover and different surface roughness). They replaced Penman's open water evaporation by the evapotranspiration from a reference crop. The reference crop of Doorenbos and Pruitt was defined as 'an extended surface of a tall green grass cover of

uniform height (8 - 15 cm), actively growing, completely shading the ground, and not short of water'. There was evidence, however, that the method sometimes over-predicted the crop water requirements (Allen, 1991).

Using similar physics as Penman, Monteith (1965) derived an equation that describes the evapotranspiration from a dry, extensive, horizontally-uniform vegetated surface, which is optimally supplied with water. This equation is known as the Penman-Monteith equation. Recent comparative studies (e.g. those by Jensen et al. 1990, who analyzed various methods of estimating potential evapotranspiration) have shown the supreme performance of the Penman-Monteith approach under varying climatic conditions, thereby confirming the results of many individual studies reported over the past years. An expert consultation (Smith, 1991) agreed to recommend the Penman-Monteith approach as the currently best-performing combination equation. Potential and even actual evapotranspiration estimates are possible with the Penman-Monteith equation, through the introduction of canopy and air resistances to water vapour diffusion. This direct, or one-step, approach is increasingly being followed nowadays, especially in research environments. Nevertheless, since accepted canopy and air resistances may not yet be available for many crops, a two-step approach is still recommended under field conditions. The first step is the calculation of the potential evapotranspiration, using the minimum value of the canopy resistance and the actual air resistance. In the second step the actual evapotranspiration is calculated using the root water uptake reduction due to water and/or salinity stress (Par. 2.3). This two-step approach is adopted in SWAP.

## 6.2 Penman-Monteith equation

The original form of the Penman-Monteith equation can be written as (Monteith, 1965, 1981):

$$\lambda_w ET_p = \frac{10^{-4}\,\Delta_v(R_n - G) + 8.64\,10^6\,\rho_{air} C_{air}(e_{sat} - e_{act})\,\frac{1}{r_{air}}}{\Delta_v + \gamma_{air}\left(1 + \frac{r_{crop}}{r_{air}}\right)} \qquad (6.1)$$

where $\lambda_w$ is the latent heat of vaporization (J g$^{-1}$), $ET_p$ is the potential transpiration rate of the canopy (cm d$^{-1}$), $R_n$ is the net radiation flux at the canopy surface (J m$^{-2}$ d$^{-1}$), $G$ is the soil heat flux (J m$^{-2}$ d$^{-1}$), $\rho_{air}$ is the air density (g cm$^{-3}$), $C_{air}$ is the heat capacity of moist air (J g$^{-1}$ °C$^{-1}$), $e_{sat}$ is the saturation vapour pressure (kPa), $e_{act}$ is the actual vapour pressure (kPa), $r_{crop}$ is the crop resistance (s m$^{-1}$), $r_{air}$ is the aerodynamic resistance (s m$^{-1}$), $\Delta_v$ is the slope of the vapour pressure curve (kPa °C$^{-1}$), and $\gamma_{air}$ is the psychrometric constant (kPa °C$^{-1}$).

To facilitate analysis of the combination equation, an aerodynamic and radiation term are defined:

$$ET_p = ET_{rad} + ET_{aero} \tag{6.2}$$

where $ET_p$ is potential transpiration rate of crop canopy (cm $d^{-1}$), $ET_{rad}$ is the radiation term (cm $d^{-1}$) and $ET_{aero}$ is the aerodynamic term (cm $d^{-1}$).

The radiation term equals:

$$ET_{rad} = \frac{10^{-4}\ \Delta_v\ (R_n - G)}{\lambda_w\ (\Delta_v + \gamma^*_{air})} \tag{6.3}$$

where $\gamma_{air}^*$ is the modified psychrometric constant (kPa $°C^{-1}$):

$$\gamma^*_{air} = \gamma_{air}\left(1 + \frac{r_{crop}}{r_{air}}\right) \tag{6.4}$$

The aerodynamic term equals:

$$ET_{aero} = \frac{8.64\ 10^6\ \rho_{air} C_{air}\ (e_{sat} - e_{act})}{\lambda_w\ (\Delta_v + \gamma^*_{air})\ r_{air}} \tag{6.5}$$

Many meteorological stations provide mean daily values of air temperature $T_{air}$ (°C), solar radiation $R_s$ (J $m^{-2}$ $d^{-1}$), wind speed $u_0$ (m $s^{-1}$) and air humidity $e_{act}$ (kPa). As a result of the FAO expert consultation, a calculation procedure for the Penman-Monteith equation was proposed using daily values of $T_{air}$, $R_s$, $u_0$ and $e_{act}$ (Smith, 1991; Verhoef and Feddes, 1991; Feddes and Lenselink, 1994). This procedure is applied in SWAP and is explained in the next paragraphs.

## 6.3 Radiation term

The net radiation flux $R_n$ is the difference between net incoming short wave radiation flux $R_{ns}$ (J $m^{-2}$ $d^{-1}$) and net outgoing long wave radiation flux $R_{nl}$ (J $m^{-2}$ $d^{-1}$):

$$R_n = R_{ns} - R_{nl} \tag{6.6}$$

$R_{ns}$ depends on the albedo or canopy reflection coefficient $\alpha_r$ (-):

$$R_{ns} = (1.0 - \alpha_r) R_s \tag{6.7}$$

In case of a bare soil SWAP assumes $\alpha_r = 0.15$, in case of a crop $\alpha_r = 0.23$.

$R_{nl}$ is the difference between thermal radiation from vegetation and soil to the atmosphere and the reflected radiation from atmosphere and clouds. Radiation laws provide the relation (Smith, 1991):

$$R_{nl} = \sigma_{sb} T_{air,k}^4 \, (0.34 - 0.14\sqrt{e_{act}}) \, (0.1 + 0.9 \, N_{rel}) \tag{6.8}$$

where $\sigma_{sb}$ is Stefan Boltzmann constant = 4.90 $10^{-6}$ (J $m^{-2}$ $K^{-4}$ $d^{-1}$), $T_{air,K}$ is absolute air temperature (= $T_{air}$ + 273 K), and $N_{rel}$ is relative sunshine duration (-), which is calculated as:

$$N_{rel} = \frac{T_{atm} - a}{b} \tag{6.9}$$

where $T_{atm}$ is atmospheric transmission (-) and $a$ and $b$ are empirical constants (-). The calculation of the atmospheric transmission will be explained in Par 7.3. The empirical constants $a$ and $b$ are calculated by:

$$\begin{aligned} a &= 0.4885 - 0.0052 L_g \\ b &= 0.1563 + 0.0074 L_g \end{aligned} \tag{6.10}$$

where $L_g$ is geographical latitude (degrees, N = +),

Since the magnitude of daily soil heat flux is relatively small at longer time intervals, SWAP assumes $G$ = 0.

## 6.4 Aerodynamic term

Latent heat of vaporization, $\lambda_w$ (J $g^{-1}$), depends on the air temperature $T_{air}$ (°C) (Harrison, 1963):

$$\lambda_w = 2.501 - 2.361 \times 10^{-3} \, T_{air} \tag{6.11}$$

Saturation vapour pressure, $e_{sat}$ (kPa), also can be calculated from air temperature (Tetens, 1930):

$$e_{sat} = 0.611 \, \exp\left(\frac{17.27 \, T_{air}}{T_{air} + 237.3}\right) \tag{6.12}$$

The slope of the vapour pressure curve, $\Delta_v$ (kPa °$C^{-1}$), is calculated as (Murray, 1967):

$$\Delta_v = \frac{4098 \, e_{sat}}{(T_{air} + 237.3)^2} \tag{6.13}$$

The psychrometric constant, $\gamma_{air}$ (kPa °$C^{-1}$), follows from (Brunt, 1952):

$$\gamma_{air} = 0.00163 \frac{p_{air}}{\lambda_w} \quad (6.14)$$

with $p_{air}$ the atmospheric pressure (kPa) at elevation $z_0$ (m), which is calculated from (Burman et al., 1987):

$$p_{air} = 101.3 \left( \frac{T_{air,K} - 0.0065 z_0}{T_{air,K}} \right)^{5.256} \quad (6.15)$$

Employing the ideal gas law, the atmospheric density, $\rho_a$ (g cm$^{-3}$), can be shown to depend on $p$ and the virtual temperature $T_{vir}$ (K):

$$\rho_{air} = 3.486\ 10^{-3} \frac{p_{air}}{T_{vir}} \quad (6.16)$$

where the virtual temperature is derived from:

$$T_{vir} = \frac{T_{air,K}}{1 - 0.378 \frac{e_{act}}{p_{air}}} \quad (6.17)$$

The heat capacity of moist air, $C_{air}$ (J g$^{-1}$ °C$^{-1}$), follows from:

$$C_{air} = 622 \frac{\gamma_{air} \lambda_w}{p_{air}} \quad (6.18)$$

The aerodynamic resistance $r_{air}$ depends on the wind speed profile and the crop height $h_{crop}$ (m) in following way (Allen et al., 1989):

$$r_{air} = \frac{\ln\left(\frac{z_m - d}{z_{om}}\right) \ln\left(\frac{z_h - d}{z_{oh}}\right)}{\kappa_{vk}^2 u} \quad (6.19)$$

where $z_m$ is height wind speed measurements (m), $z_h$ is height temperature and humidity measurements (m), $\kappa_{vk}$ is von Karman constant = 0.41 (-), $u$ is wind speed measurement at height $z_m$ (m s$^{-1}$), $d$ is zero plane displacement of wind profile (m), $z_{om}$ is roughness parameter for momentum (m) and $z_{oh}$ is roughness parameter for heat and vapour (m).

The parameters $d$, $z_{om}$ and $z_{oh}$ are defined as:

$$d = \frac{2}{3} h_{crop} \tag{6.20}$$

$$z_{om} = 0.123\ h_{crop} \tag{6.21}$$

$$z_{oh} = 0.1\ z_{om} = 0.0123\ h_{crop} \tag{6.22}$$

with $h_{crop}$ the crop height.

Generally meteorological stations provide 24 hour averages of wind speed measurements. To calculate $r_{air}$, the average daytime wind (7.00 - 19.00 h) should be used. For ordinary conditions we may assume (Smith, 1991):

$$u = 1.33\ u_0 \tag{6.23}$$

where $u_0$ is the average wind speed over 24 hours (m $s^{-1}$).

## 6.5 Potential transpiration rate of a fully covered soil and potential evaporation rate of a bare soil

SWAP calculates three quantities with the Penman-Monteith equation (Eq. 6.1):

- $ET_{w0}$ (cm $d^{-1}$), potential evapotranspiration rate of a *wet canopy, completely covering the soil*;
- $ET_{p0}$ (cm $d^{-1}$), potential evapotranspiration rate of a *dry canopy, completely covering the soil*;
- $E_{p0}$ (cm $d^{-1}$), potential evaporation rate of a *wet, bare soil.*

These quantities are obtained by varying the values for crop resistance, crop height and the reflection coefficient. In case of a wet canopy, the crop resistance $r_{crop}$ is set to zero. In case of a dry crop with optimal water supply in the soil, $r_{crop}$ is minimal and varies between 30 s $m^{-1}$ for arable crops to 150 s $m^{-1}$ for trees in a forest (Allen et al., 1986, 1989). In case of the bare wet soil, the program takes $r_{crop}$ = 0 and 'crop height' $h_{crop}$ = 0.1 cm. Reflection coefficient $\alpha_r$ in case of a (wet or dry) crop equals 0.23, while for a bare soil $\alpha_r$ = 0.15 is assumed.

***Alternative to Penman-Monteith***

Application of the Penman-Monteith equation requires daily values of air temperature, net radiation, wind speed and air humidity, which data might not be available. Therefore SWAP allows the use of a reference potential evapotranspiration rate $ET_{ref}$ (cm $d^{-1}$). In that case $ET_{p0}$ is calculated by: where $k_c$ is the so called crop factor, which depends on the crop type and the

$$ET_{p0} = k_c\, ET_{ref} \qquad (6.24)$$

method employed to obtain $ET_{ref}$. The crop factor converts the reference evapotranspiration rate into the potential evapotranspiration rate of a dry canopy that completely covers the soil: $k_c$ is thus taken to be constant from crop emergence up to maturity.

This approach, however, does not allow differentiation between a dry crop, wet crop and wet soil. Therefore SWAP assumes: $ET_{w0} = ET_{p0}$ and $E_{p0} = ET_{p0}$.

The reference evapotranspiration rate can be determined in several ways, such as pan evaporation, the Penman open water evaporation (Penman, 1948), the FAO modified Penman equation (Doorenbos and Pruitt, 1977) or even the Penman-Monteith equation applied for a (different) reference crop (Bos et al., 1996). All these authors give corresponding crop factors. Note that in general crop factors take into account incomplete soil cover and thus depend on development stage. As SWAP treats reductions in soil evaporation and plant transpiration in a different way (see Par 6.6), *the program only requires as input the crop factor for full soil cover.*

## 6.6 Potential transpiration and evaporation rate of a partly covered soil

Programs like CROPWAT (Smith, 1992) and CRIWAR (Bos et al., 1996) use crop factors that are a function of the crop development stage. After multiplication with a reference *potential* evapotranspiration rate, a kind of evapotranspiration rate is obtained that is representative for a potentially transpiring crop that is well supplied with water in the root zone and that partly covers the soil. Because the soil has generally a dry top layer, soil evaporation is usually below the potential evaporation rate. Hence, the crop factor combines the effect of an incomplete soil cover and reduced soil evaporation. It enables effective extraction of the potential crop transpiration rate from the reference potential evapotranspiration rate, under the assumption that soil evaporation is constant and relatively small. Significant errors however may be expected when the soil is regularly rewetted and the soil cover fraction is low.

Different from the above mentioned approach, SWAP firstly separates potential plant transpiration rate $T_p$ (cm $d^{-1}$) and potential soil evaporation rate $E_p$ (cm $d^{-1}$) and subsequently calculates the reduction of potential plant transpiration rate (Par. 2.3) and potential soil evaporation rate (Par. 6.8) according to a more physically based approach. In order to partition potential evapotranspiration rate into potential transpiration rate and potential soil evaporation rate, either the leaf area index, *LAI* ($m^2$ $m^{-2}$) or the soil cover fraction, *SC* (-), both as a function of crop development, are used.

***Use of leaf area index***

In case the detailed crop model is used, *LAI* is calculated. When the simple crop model is used, *LAI* as a function of crop development stage should be provided by the user.

The potential evaporation rate of a soil under a standing crop is derived from the Penman Monteith equation by neglecting the aerodynamic term. The aerodynamic term will be small because the wind velocity near the soil surface is relatively small, which makes the aerodynamic resistance $r_{air}$ very large (Ritchie, 1972). Thus, the only source for soil evaporation is net radiation that reaches the soil surface. Assuming that the net radiation inside the canopy decreases according to an exponential function, and that the soil heat flux can be neglected, we can derive (Goudriaan, 1977; Belmans, 1983):

$$E_p = E_{p0}\, e^{-\kappa_{gb} LAI} \tag{6.25}$$

where $\kappa_{gb}$ (-) is the extinction coefficient for global solar radiation. Ritchie (1972) and Feddes (1978) used $\kappa_{gr} = 0.39$ for common crops. More recent approaches estimate $\kappa_{gr}$ as the product of the extinction coefficient for diffuse visible light, $\kappa_{df}$ (-), which varies with crop type from 0.4 to 1.1, and the extinction coefficient for direct visible light, $\kappa_{dir}$ (-):

$$\kappa_{gr} = \kappa_{df}\, \kappa_{dir} \tag{6.26}$$

Both $\kappa_{df}$ and $\kappa_{dir}$ are input at the crop data section.

SWAP assumes that the evaporation rate of the water intercepted by the vegetation is equal to $ET_{w0}$, independent of the soil cover fraction. The ratio of the daily amount of intercepted precipitation $P_i$ (see Par. 6.7) and $ET_{w0}$, indicates the fraction of the day that the crop is wet, $W_{frac}$ (-):

$$W_{frac} = \frac{P_i}{ET_{w0}} \qquad \text{with} \qquad 0 < W_{frac} < 1 \tag{6.27}$$

While the crop is wet, the intercepted water evaporates and the transpiration rate through the leaf stomata is taken to be negligible. After the canopy has become dry, the transpiration through the leaf stomata starts again. SWAP calculates a daily average of the potential transpiration rate, $T_p$ (cm $d^{-1}$), taking into account the fraction of the day $W_{frac}$ during which the intercepted water evaporates as well as reduction of the potential soil evaporation rate $E_p$ in case of partly soil cover:

$$T_p = (1.0 - W_{frac})\, T_{p0} - E_p \qquad \text{with} \quad T_p \geq 0 \tag{6.28}$$

***Use of soil cover fraction***

This option can only be used in SWAP when the simple crop model is used. The soil cover fraction, *SC* (-), should be specified as a function of crop development stage.

Potential soil evaporation rate is calculated as:

$$E_p = (1 - SC)\ ET_{p0} \tag{6.29}$$

Taking into account the fraction of the day that the crop is wet, which is calculated similarly to Eq. 6.27, $T_p$ follows from:

$$T_p = (1 - W_{frac})\ SC\ ET_p \qquad \text{with} \qquad T_p \geq 0 \tag{6.30}$$

## 6.7 Interception of rainfall

Von Hoyningen-Hüne (1983) and Braden (1985) measured interception of precipitation for various crops. They proposed the following general formula for canopy interception:

$$P_i = a\ LAI \left( 1 - \frac{1}{1 + \frac{b\ P_{gross}}{a\ LAI}} \right) \tag{6.31}$$

where $P_i$ is intercepted precipitation (cm), $P_{gross}$ is gross precipitation (cm), $a$ is an empirical coefficient (cm) and $b$ is the soil cover fraction (≈ LAI/3.0) (-). For increasing precipitation amounts, the amount of intercepted precipitation asymptotically reaches the saturation amount $a\ LAI$. In principle $a$ must be determined experimentally and should be specified in the input file. In case of ordinary agricultural crops we may assume $a$ = 0.25.

In case irrigation water is applied through sprinklers, total intercepted precipitation must subsequently be divided into a rain part and an irrigation part, as the solute concentration of both water sources may be different. Observed rainfall $P_{gross}$ minus intercepted rainfall $P_i$ is called net rainfall $P_{net}$. Likewise, applied irrigation depth $I_{gross}$ minus intercepted irrigation water is called net irrigation depth $I_{net}$.

The method of Von Hoyningen-Hüne and Braden is based on daily precipitation values, so daily rainfall must always be specified in the meteo input file. Additionally, rainfall may be specified in SWAP in smaller time steps. In this case the daily fraction $P_{net}/P_{gross}$ is used to correct small time step rainfall for interception losses.

## 6.8 Actual soil evaporation

In case of a wet soil, soil evaporation is determined by the atmospheric demand and equals potential soil evaporation rate $E_p$ (cm $d^{-1}$). When the soil dries out, the soil hydraulic conductivity decreases, which reduces $E_p$ to an

actual evaporation rate $E_a$ (cm $d^{-1}$). In SWAP we calculate the maximum evaporation rate, $E_{max}$ (cm $d^{-1}$), according to Darcy's law as discussed at the top boundary procedure (Eq. 2.19) and set $E_a$ equal to the minimum of $E_p$ and $E_{max}$. Note that due to discretization the value of $E_{max}$ depends on the thickness of the top soil compartments. Increase of compartment thickness, generally results in smaller values for $E_{max}$. For accurate simulations at extreme hydrological conditions, the thickness of the top compartments should be not more than 1 cm. A further refinement of the spatial discretization hardly affects $E_{max}$ (Van Dam and Feddes, 1997).

There is one serious limitation of the $E_{max}$ procedure as described above. $E_{max}$ is governed by the soil hydraulic functions $\theta(h)$ and $K(\theta)$. It still is not clear whether the soil hydraulic functions, that usually represent a top layer of a few decimeter, are valid for the top few cm's of a soil, which are subject to splashing rain, dry crust formation, root extension and all kind of cultivation practices.

Alternatively empirical evaporation functions may be used, which require calibration of their parameters for the soil and local situation considered. SWAP has the options to choose the empirical evaporation functions of Black (1969) or Boesten and Stroosnijder (1986).

Black calculated the cumulative actual evaporation during a drying cycle, $\Sigma E_a$ (cm) as:

$$\sum E_a = \beta_1 \, t_{dry}^{1/2} \tag{6.32}$$

where $\beta_1$ is a soil specific parameter (cm $d^{-0.5}$), characterizing the evaporation process and $t_{dry}$ is the time (d) after a significant amount of rainfall, $P_{min}$. The user should specify $\beta_1$ and $P_{min}$ in the input file. SWAP resets $t_{dry}$ to zero if the net precipitation $P_{net}$ exceeds $P_{min}$.

The parameter $\beta_1$ has been shown to be affected by $E_p$ itself. In order to avoid this effect, Boesten and Stroosnijder (1986) proposed to use the sum of potential evaporation, $\Sigma E_p$ (cm), as time variable:

$$\begin{aligned} \sum E_a &= \sum E_p \quad \text{for} \quad \sum E_p \le \beta_2^2 \\ \sum E_a &= \beta_2 \left(\sum E_{pot}\right)^{1/2} \quad \text{for} \quad \sum E_p > \beta_2^2 \end{aligned} \tag{6.33}$$

where $\beta_2$ is a soil parameter ($cm^{1/2}$), which should be determined experimentally. The parameter $\beta_2$ determines the length of the potential evaporation period, as well as the slope of the $\Sigma E_a$ versus $(\Sigma E_p)^{1/2}$ relationship in the soil limiting stage. Also here the user should specify a minimum amount of rainfall $P_{min}$ (cm) at which the time counter $\Sigma E_p$ in Eq. 6.33 is reset to zero.

For days with $P_{net} < P_{min}$, Boesten and Stroosnijder suggest the following procedure with respect to updates of $\Sigma E_p$. On days of no excess in rainfall ($P_{net} < E_p$), $\Sigma E_p$ follows from Eq. 6.33, that is:

$$(\sum E_p)^j = (\sum E_p)^{j-1} + (E_p - P_{net})^j \tag{6.34}$$

in which superscript $j$ is the day number. $(\Sigma E_a)^j$ is calculated from $(\Sigma E_p)^j$ with Eq. 6.33 and $E_a$ is calculated with

$$E_a^j = P_{net}^j + (\sum E_a)^j - (\sum E_a)^{j-1} \tag{6.35}$$

On days of excess in rainfall ($P_{net} > E_p$)

$$E_a^j = E_p^j \tag{6.36}$$

and the excess rainfall is subtracted from $\Sigma E_a$

$$(\sum E_a)^j = (\sum E_a)^{j-1} - (P_{net} - E_p)^j \tag{6.37}$$

Next $(\Sigma E_a)^j$ is calculated from $(\Sigma E_p)^j$ with Eq. 6.33. If the daily rainfall excess is larger than $(\Sigma E_p)^{j-1}$, then both $(\Sigma E_a)^j$ and $(\Sigma E_p)^j$ are set at zero.

SWAP will determine $E_a$ by taking the minimum value of $E_p$, $E_{max}$ and, if selected by the user, the actual evaporation rates $E_a$ according to the empirical functions of Black or Boesten and Stroosnijder.

# 7 Crop growth

SWAP contains three crop growth routines: a detailed model (WOFOST), the same model attuned to simulate grass growth, and a simple model. The main part of this chapter describes the WOFOST model, the simple crop growth model is clarified in Par. 7.12.

WOFOST (WOrld FOod STudies) originated in the framework of an interdisciplinary study on the potential world food production by the Centre for World Food Studies (CWFS) in cooperation with the Wageningen Agricultural University, Department of Theoretical Production Ecology (WAU-TPE) and the DLO-Centre for Agrobiological Research (CABO-DLO, currently AB-DLO), Wageningen, the Netherlands. After cessation of the CWFS in 1988, the model was further developed at the DLO-Winand Staring Centre (SC-DLO) in cooperation with AB-DLO and WAU-TPE. Related models to WOFOST are the successive SUCROS (Simple and Universal Crop Simulator) models (Spitters et al., 1989; Van Laar et al., 1992), Arid Crop (Van Keulen, 1975; Van Keulen et al., 1981), Spring wheat (Van Keulen and Seligman, 1987), MACROS (Penning de Vries et al., 1989) and ORYZA1 (Kropff et al., 1993). All these Wageningen models follow the hierarchical distinction between potential and actual production, and share similar crop growth submodels, with light interception and $CO_2$ assimilation as growth driving processes, and crop phenological development as growth controlling process.

In SWAP, WOFOST 6.0 has been implemented. The description in Par. 7.1 to 7.11 is based on Spitters et al. (1989), Supit et al. (1994) and the program source code. A user's guide of WOFOST 6.0 was written by Hijmans et al. (1994). Boons-Prins et al. (1993) documented specific parameters for the crops winter wheat, grain maize, spring barley, rice, sugar beet, potato, field bean, soy bean, winter oilseed rape and sunflower. WOFOST input files for these crops will be provided with the SWAP program.

## 7.1 Overview of the detailed crop growth model

Figure 7.1 shows the processes and relations incorporated in WOFOST. The radiation energy absorbed by the canopy is a function of incoming radiation and crop leaf area. Using the absorbed radiation and taking into account photosynthetic leaf characteristics the potential gross photosynthesis is calculated. The latter is reduced due to water and/or salinity stress, as quantified by the relative transpiration, and yields the actual gross photosynthesis.

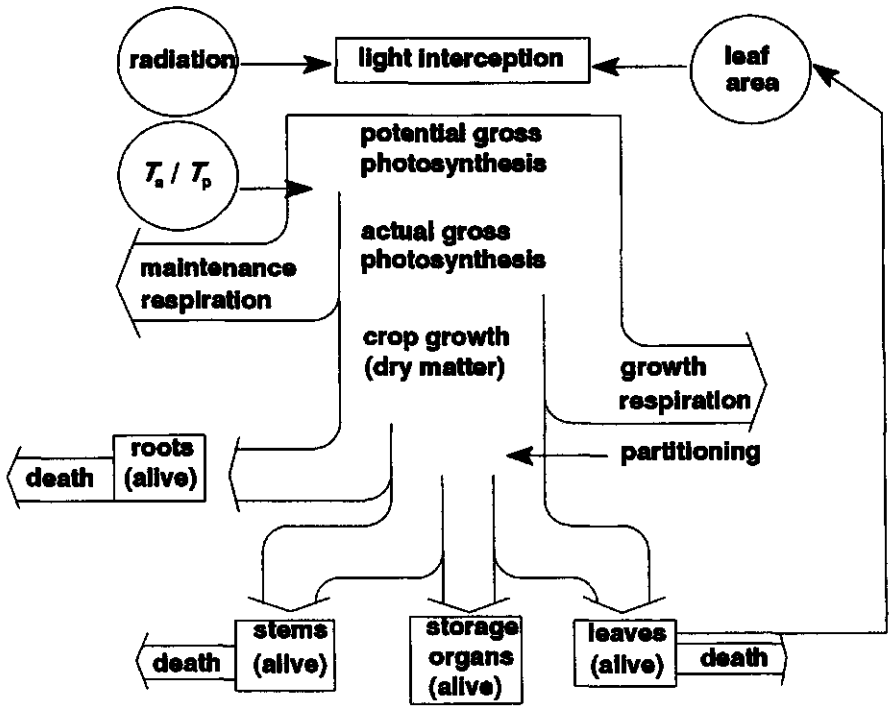


*Fig. 7.1 Overview of crop growth processes as simulated by WOFOST*

Part of the carbohydrates ($CH_2O$) produced are used to provide energy for the maintenance of the existing live biomass (maintenance respiration). The remaining carbohydrates are converted into structural matter. In this conversion, some of the weight is lost as growth respiration. The dry matter produced is partitioned among roots, leaves, stems and storage organs, using partitioning factors that are a function of the phenological development stage of the crop (Spitters et al., 1989). The fraction partitioned to the leaves, determines leaf area development and hence the dynamics of light interception. The dry weights of the plant organs are obtained by integrating their growth rates over time. During the development of the crop, part of living biomass dies due to senescence.

Some simulated crop growth processes are influenced by temperature, like for example the maximum rate of photosynthesis and the maintenance respiration. Other processes, like the partitioning of assimilates or decay of crop tissue, are steered by the phenological development stage.

## 7.2 Phenological development stage

As many physiological and morphological processes change with the phenological stage of the plant, quantification of phenological development is essential in any crop growth simulation model. For many annual crops, the

phenological development can conveniently be expressed in development stage $D_s$ (-), having the value 0 at seedling emergence, 1 at flowering and 2 at maturity (Van Heemst, 1986a; 1986b). The most important phenological change is the one from vegetative ($0 < D_s < 1$) to reproductive stage ($1 < D_s < 2$) , which changes drastically the dry matter allocation to organs.

WOFOST starts crop growth simulation at emergence, which date should be specified by the user. A crop passes through successive phenological development stages from 0 to 2. The length of these stages depends on the development rate. Development rates before and after floral initiation or anthesis ($D_s = 1$) are controlled by day length and/or temperature. In the model, before anthesis both factors can be active. After anthesis only temperature will affect development rate.

Higher temperatures accelerate the development rate, leading to shorter growing periods. This rate responds to temperature according to a curvilinear relationship. However, it has often been demonstrated, that over a wide range of temperatures, the development rate increases more or less linearly with temperature (Van Dobben, 1962; Van Keulen and Seligman, 1987). WOFOST uses the temperature sum to determine the development stage. An effective temperature $T_{eff}$ (°C) is calculated as:

$$T_{eff} = T_{air} - T_{emin} \quad \text{with} \quad 0 < T_{eff} < T_{emax} - T_{emin} \tag{7.1}$$

where $T_{air}$ (°C) is the daily average temperature and $T_{emin}$ (°C) and $T_{emax}$ (°C) are the minimum and maximum effective temperature, respectively. For species originating from temperate regions $T_{emin}$ = 0 to 3 °C, while for species of subtropical and tropical origins $T_{emin}$ = 9 to 14 °C (Angus et al., 1981). Within a species, cultivars may vary substantially in their temperature requirements. The temperature sum, therefore, is characteristic for each cultivar. Accordingly, the development stage, $D_s$ (-), is calculated as:

$$D_s^{j+1} = D_s^j + \frac{T_{eff}}{T_{sum,i}} \tag{7.2}$$

where superscript $j$ is the day number and $T_{sum,i}$ is the temperature sum required to complete either the vegetative or the reproductive stage.

For certain species or cultivars, during the vegetative stage, the effect of day length should be taken into account. Approaches that describe such effects quantitatively are given, amongst others, by Weir et al. (1984), Hadley et al. (1984) and Reinink et al. (1986). In the model, a reduction factor for the development rate as function of day length $f_{lday}$ (-) is introduced:

$$f_{lday} = \frac{L_{day} - L_{oday}}{L_{oday} - L_{oday}} \quad \text{with} \quad 0 < f_{lday} < 1 \tag{7.3}$$

with $L_{day}$ the actual day length (d), $L_{cday}$ the shortest day length for any development (d), and $L_{oday}$ the minimum day length for optimum development (d).

The user should provide information whether the development rate depends on temperature, on day length or on both. Note that in modern cultivars, photosensitivity is much less pronounced than in traditional cultivars, and that for the purpose of modelling the day length influence can be ignored by choosing an appropriate temperature sum, which leads to an equivalent crop life cycle.

The simulation of crop growth stops when the development stage reaches the stage at which the crop will be harvested. The development stage at harvest time should be provided by the user.

## 7.3 Radiation fluxes above the canopy

Measured or estimated daily global solar radiation (wavelength 300-3000 nm) is input for the model. Incoming radiation is partly direct, with the angle of incidence equal to the angle of the sun, and partly diffuse, with incidence under various angles. The sine of solar elevation as a function of the day hour, can be calculated with:

$$\sin\beta_{sun} = \sin L_g \sin\sigma_{sun} + \cos L_g \cos\sigma_{sun} \cos\left(\frac{2\pi\,(t_h + 12)}{24}\right) \qquad (7.4)$$

with $\beta_{sun}$ the solar elevation (degrees), $\sigma_{sun}$ is solar declination (degrees), $L_g$ is geographic latitude (degrees) and $t_h$ is hour of the day.

Only 50 percent of the global solar radiation (wavelength 300-3000 nm) is photosynthetically active (PAR, Photosynthetically Active Radiation, wavelength 400-700 nm). This fraction, is generally called 'light' or 'visible radiation.

The instantaneous incoming photosynthetically active radiation *PAR* (J $m^{-2}$ $d^{-1}$) is calculated by multiplying half of the daily global radiation with the ratio of the actual effective solar elevation and the integral of the effective solar height, taking into account reduced atmospheric transmission at low solar elevations:

$$PAR = 0.5\ R_s \frac{\sin\beta_{sun}\ (1 + 0.4\sin\beta_{sun})}{\int \sin\beta_{mod,sun}} \qquad (7.5)$$

where $R_s$ is global radiation flux density (J $m^{-2}$ $d^{-1}$) and $\int\sin\beta_{mod,sun}$ the integral of $\sin\beta_{sun}$ over the day (-) which is corrected for reduced atmospheric transmission at low solar elevations.

A diffuse radiation flux results from scattering of sun rays by clouds, gases and dust in the atmosphere. To quantify the degree of scattering, the measured daily total radiation is compared with the amount that would have reached the earth's surface in the absence of an atmosphere, $S_{sun}$, which can be calculated from theoretical considerations:

$$S_{sun} = 1.18\ 10^{8}\left(1 + 0.033 \cos\left(\frac{2j\pi}{365}\right)\right) \quad (7.6)$$

where $S_{sun}$ is the solar constant (J $m^{-2}$ $d^{-1}$) and $j$ the Julian day number. The ratio of potential and measured daily total radiation is called atmospheric transmission $A_t$ (-). The proportion of diffuse radiation, $I_{fdif}$ (-), is derived from the atmospheric transmission by an empirical relationship (Spitter et al., 1986). Taking also into account that only 50 percent of the solar radiation is photosynthetically active, the diffuse photosynthetic active radiation $PAR_{dif}$ (J $m^{-2}$ $d^{-1}$) can thus be calculated by:

$$PAR_{dif} = 0.5\ I_{fdif}\ A_t\ S_{sun} \sin\beta_{sun} \quad (7.7)$$

The direct radiation flux, $PAR_{dir}$ (J $m^{-2}$ $d^{-1}$), is obtained by subtracting the diffuse part from the photosynthetically active radiation flux:

$$PAR_{dir} = PAR - PAR_{dif} \quad (7.8)$$

## 7.4 Radiation profiles within the canopy

The total incoming photosynthetically active radiation flux is partly reflected by the canopy. The reflection coefficient is defined as the fraction of the downward radiation flux that is reflected by the whole canopy. According to Goudriaan (1977), the reflection coefficient of a green leaf canopy with a random spherical leaf angle, $\rho_{rad}$ (-), equals:

$$\rho_{rad} = \left(\frac{1 - \sqrt{1 - \sigma_{leaf}}}{1 + \sqrt{1 - \sigma_{leaf}}}\right)\left(\frac{2}{1 + 1.6 \sin \beta_{sun}}\right) \quad (7.9)$$

with $\sigma_{leaf}$ the scattering coefficient of single leaves for visible radiation (-), which is taken to be 0.2. The first term of Eq. 7.9 denotes the reflection of a canopy of horizontal leaves and the second term is the approximate correction factor for a spherical leaf angle distribution. The fraction $(1-\rho_{rad})$ of the incoming visible radiation is potentially available for absorption by the canopy.

Light intensity, adjusted for crop reflection, decreases approximately exponentially with leaf area index when going deeper into the canopy:

$$PAR_L = (1 - \rho_{rad})\ PAR\ e^{-\kappa L} \quad (7.10)$$

where $PAR_L$ is the net light intensity (J $m^{-2}$ $d^{-1}$) at depth $L$, $\kappa$ is the radiation extinction coefficient (-) and $L$ is the cumulative leaf area index, $\Sigma LAI$ ($m^2$ leaf $m^{-2}$ ground), counted from the top of the canopy downwards.

The profiles of the net diffuse flux and the net flux caused by direct irradiance can be characterized analogously (Goudriaan, 1982). Diffuse and direct fluxes each attenuate at a different rate. For a spherical leaf angle distribution with leaves distributed randomly within the canopy volume, the extinction coefficients of the direct component of the direct flux, $\kappa_{di}$ (-), is approximated by (Goudriaan, 1977, 1982):

$$\kappa_{di} = \frac{0.5}{\sin\beta_{sun}} \quad (7.11)$$

and the extinction coefficient of the diffuse flux, $\kappa_{df}$ (-), is calculated as:

$$\kappa_{df} = \kappa_{di}\sqrt{1 - \sigma_{rad}} \quad (7.12)$$

In Eq. 7.11, the factor 0.5 represents the average projection on the ground surface of leaves showing a spherical angle distribution. Averaging $0.5/\sin\beta$ during a day with an overcast sky, gives a value of $\kappa_{di} = 0.8$ (-). In SWAP, $\kappa_{df}$ should be given as an input by the user. It's value can be measured directly under diffuse sky conditions. The average value is about 0.72 (-) (Goudriaan, 1977).

In many situations, the leaf angle distribution is not spherical. In the model, therefore, the actual leaf angle distribution is accounted for by using a so called cluster factor which is the measured extinction coefficient for diffuse radiation flux, relative to the theoretical one for a spherical leaf area distribution.

On its way through the canopy, part of the direct flux is intercepted and scattered by the leaves; hence, the direct flux segregates into a diffused, scattered component and another component which remains direct. Attenuation of the direct component of the direct flux proceeds equally to the attenuation of light in a hypothetical canopy of black, non scattering leaves. The diffused component is obtained as the difference between the total direct flux and its direct component.

The decline of the radiation flux reflects the amount of absorption. The rate of absorption at a depth $L$ in the canopy, $PAR_{L,a}$ (J $m^{-2}$ leaf $d^{-1}$), is obtained by taking the derivative of Eq. 7.10 with respect to $L$:

$$PAR_{L,a} = \kappa (1 - \rho_{red}) PAR\, e^{-\kappa L} \quad (7.13)$$

Similar expressions can be derived for the separate light components: the diffuse flux, the total direct radiation flux and the direct component of the direct radiation flux. The absorbed diffused component of the direct flux is obtained by subtracting the direct component from the total direct flux.

Two leaf area classes are distinguished: shaded leaf area and sunlit leaf area. The shaded leaf area absorbs the diffuse flux and the diffused component of the direct flux. The sunlit leaf area receives diffuse and direct radiation. At every horizon within the canopy, the intensity of the unobstructed direct beam equals its intensity above the crop.

## 7.5 Instantaneous assimilation rates per leaf layer

The $CO_2$ assimilation rate of a canopy layer is obtained by substituting the absorbed amount of light energy into the assimilation-light response of single leaves. Of the two-parameter response functions, the asymptotic exponential function appears to be the most satisfactory (Peat, 1970):

$$A_L = A_{max} \left(1 - e^{\frac{\varepsilon_{PAR} PAR_{L,a}}{A_{max}}}\right) \quad (7.14)$$

where $A_L$ is the gross assimilation rate (kg $CO_2$ $m^{-2}$ leaf $d^{-1}$), $A_{max}$ the gross assimilation rate at light saturation (kg $CO_2$ $m^{-2}$ leaf $d^{-1}$), and $\varepsilon_{PAR}$ the initial slope or light use efficiency (kg $CO_2$ $J^{-1}$ absorbed).

Substituting into Eq. 7.14 the absorbed amount of radiation by shaded leaves and by sunlit leaves, respectively, yields the assimilation rates of sunlit and shaded leaves. The shaded leaf area receives the diffuse flux and the scattered component of the direct flux. The sunlit leaf area receives both diffuse and direct flux. Illumination intensity of sunlit leaves varies strongly with leaf angle. In the model, the assimilation rate of the sunlit leaf area is therefore integrated over the leaf angle distribution.

The assimilation rate per unit leaf area in a canopy, is the sum of the assimilation rates of sunlit and shaded leaves, taking into account their proportion in each layer. The proportion of sunlit leaf area at depth $L$ in the canopy equals the proportion of the direct component of the direct flux reaching that depth. This proportion is calculated in analogy to Eq. 7.13, using the extinction coefficient of the direct radiation component.

## 7.6 Daily gross assimilation rate of the canopy

The instantaneous rates per leaf layer need to be integrated over the canopy leaf area index and over the day. This is efficiently achieved with the Gaussian integration method (Press et al., 1989). This method specifies the discrete points at which function values have to be calculated, and the weighting factors with which the function values have to be multiplied in order to attain minimum deviation from analytical integration. A three-point algorithm evaluates the function at $0.1127a$, $0.5a$ and $0.8873a$ of the interval $(0,a)$, with weighting coefficients 1.0, 1.6 and 1.0, respectively. The Gaussian integration method is remarkable accurate in case of trigonometric (radiation) and exponential (light absorption) functions. WOFOST computes at three selected moments of the day incoming *PAR* just above the canopy. Using this radiation, assimilation is computed at three selected depths in the canopy (Spitters et al., 1989). Gaussian integration of these values results in the daily rate of potential gross $CO_2$ assimilation, $A_{pgross}$ (kg $CO_2$ $ha^{-1}$ $d^{-1}$).

Until now the assimilation has been treated as a function of the intercepted light and of photosynthetic crop characteristics such as initial light use efficiency and maximum leaf $CO_2$ assimilation at light saturation. Other factors that may reduce the daily assimilation rate are typical crop characteristics, unfavourable temperatures and water stress.

Crop characteristics depend on the phenological crop stage. This is taken into account by specifying the maximum assimilation rate, $A_{max}$ (kg $CO_2$ $ha^{-1}$ $d^{-1}$), as function of development stage.

A reduction factor $f_{tday}$ (-), which is a function of the average daytime temperature $T_{day}$ (°C), accounts for sub-optimum temperatures. $T_{day}$ is calculated by:

$$T_{day} = 0.75\ T_{max} + 0.25\ T_{min} \tag{7.15}$$

where $T_{max}$ and $T_{min}$ (°C) are the daily maximum and minimum temperature, respectively.

The crop characteristics and the day temperature result in a reduction of $A_{pgross}$ to $A_{pgross}^{1}$ (kg $CO_2$ $ha^{-1}$ $d^{-1}$):

$$A_{pgross}^{1} = \max\ (A_{pgross},\ f_{tday}\ A_{max}) \tag{7.16}$$

In addition, low nighttime temperatures affect assimilation. At night, assimilates produced during daytime, are transformed into structural biomass. This process is hampered by low temperature. If these low temperatures prevail for a several days, the assimilates accumulate in the plant and the assimilation rate diminishes and ultimately halts. In the model, this tempera-

ture effect is accounted for by a reduction factor $f_{7min}$, which is a function of the minimum temperature during the last seven days.

Another important factors that may reduce assimilation, is water and/or salinity stress. WOFOST uses the ratio of actual transpiration and potential transpiration, $T_a/T_p$, as reduction coefficient.

Reduction due to low minimum temperatures, water stress, and salinity stress, and taking into account that for each kg $CO_2$ 30/44 kg biomass ($CH_2O$) is formed, results in the following equation for the daily gross assimilation rate $A_{gross}$ (kg ha$^{-1}$ d$^{-1}$):

$$A_{gross} = \frac{30}{44} f_{7min} \frac{T_a}{T_p} A^1_{pgross} \qquad (7.17)$$

## 7.7 Maintenance respiration

Some of the carbohydrates formed are respired to provide energy for maintaining the existing bio structures. This maintenance respiration consumes roughly 15 - 30% of the carbohydrates produced by a crop in a growing season (Penning de Vries et al., 1979). This indicates the importance of accurate quantification of this process in the model.

The maintenance costs may be estimated from the quantities of proteins and minerals present in the biomass and from crop metabolic activity, as presented by De Wit et al. (1978). This method, however, requires information on the vegetation nitrogen and mineral contents. Based on De Wit et al. (1978), typical values for the maintenance coefficients of various plant organs have been derived by Penning de Vries and Van Laar (1982). These coefficients should be specified by the user in WOFOST. According to this approach, the reference maintenance requirements $R_{mref}$ (kg ha$^{-1}$ d$^{-1}$) are proportional to the dry weights of the plant organs to be maintained:

$$R_{mref} = c_{m,leaf} W_{leaf} + c_{m,stem} W_{stem} + c_{m,stor} W_{stor} + c_{m,root} W_{root} \qquad (7.18)$$

where $c_{m,i}$ denotes the maintenance coefficient of organ $i$ (kg kg$^{-1}$ d$^{-1}$) and $W_i$ the organ dry weight (kg ha$^{-1}$).

The maintenance respiration rate still has to be corrected for senescence and temperature. The reduction factor for senescence $f_{senes}$ (-) is crop specific and is defined as a function of development stage. Higher temperatures accelerate the turnover rates in plant tissue and hence the costs of maintenance. An increase in temperature of 10 °C increases maintenance respiration by a factor of about 2 (Kase and Catsky, 1984; Penning de Vries and Van Laar, 1982).

To be more flexible, the user may specify the increase factor of the respiration rate per 10 °C temperature increase, $Q_{10}$ (-):

$$R_m = f_{senes}\, R_{mref}\, Q_{10}^{\frac{T_{avg} - 25}{10}} \qquad (7.19)$$

where $R_m$ is the actual maintenance respiration rate (kg ha$^{-1}$ d$^{-1}$).

Thus, the maintenance respiration rate depends on the amount of dry matter in the various organs, the relative maintenance rate per organ and the temperature. We may assume that the vegetation will not be 'self-consuming' in terms of carbohydrates. Therefore the maintenance respiration rate cannot exceed the gross assimilation rate.

Gross assimilation rate $A_{gross}$ minus maintenance respiration rate $R_m$ results in the net assimilation rate $A_{net}$ (kg ha$^{-1}$ d$^{-1}$), the amount of carbohydrates available for conversion into structural material:

$$A_{net} = A_{gross} - R_m \qquad \text{with} \qquad A_{net} \geq 0 \qquad (7.20)$$

## 7.8 Dry matter partitioning and growth respiration

The primary assimilates in excess of the maintenance costs, are available for conversion into structural plant material. In this conversion process of the glucose molecules, $CO_2$ and $H_2O$ are released. This is a partial combustion of glucose to provide energy required in the various biochemical pathways. Hence, biosynthesis of the various structural compounds can be considered as a process of cut and paste, the scraps representing the weight lost in growth respiration.

The magnitude of growth respiration is determined by the composition of the end product formed (Penning de Vries et al., 1974). Thus the weight efficiency of conversion of primary photosynthates into structural plant material varies with the composition of that material. Fats and lignin are produced at high costs; structural carbohydrates and organic acids are relatively cheap. Proteins and nucleic acids form an intermediate group.

At higher temperatures the conversion processes are accelerated, but the pathways are identical (Spitters et al. 1989). Hence, the assimilate requirements do not vary with temperature.

The increase in total dry weight of the crop is partitioned over the plant organs: roots, leaves, stems and storage organs. This is correct simulation of what occurs during the vegetative phase. Storage organs, however, may not only be formed from current photosynthates but also from carbohydrates and

proteins that have been stored temporarily in vegetative parts and that are redistributed during the reproductive stage. In the model, the latter process is not incorporated: the total growth of the crop is partitioned among the plant organs according to partitioning factors that are introduced as forcing functions; their values only change with the development stage of the crop.

In the model, average (crop specific) conversion factors $C_{e,i}$ (kg kg$^{-1}$) are used for leaf, storage organ, stem and root biomass. A weighted average, $C_e$ (kg kg$^{-1}$), of these organ specific conversion factors is calculated by multiplying the organ specific values with the partitioning factors :

$$C_e = \frac{1}{\left(\frac{\xi_{leaf}}{C_{e,leaf}} + \frac{\xi_{stor}}{C_{e,stor}} + \frac{\xi_{stem}}{C_{e,stem}}\right)(1 - \xi_{root}) + \frac{\xi_{root}}{C_{e,root}}} \qquad (7.21)$$

where $\xi_i$ is the partitioning factor for organ *i*.

The gross dry matter growth rate $w_{gross}$ (kg ha$^{-1}$ d$^{-1}$) is related to the net assimilation rate $A_{net}$ by:

$$w_{gross} = C_e A_{net} \qquad (7.22)$$

Gross dry matter growth is first partitioned between shoots (leafs, stems and storage organs together) and roots:

$$w_{gross,root} = \xi_{root} w_{gross} \quad \text{and} \quad w_{gross,sh} = (1 - \xi_{root}) w_{gross} \qquad (7.23)$$

where $\xi_{root}$ is the partitioning factor for roots (-) and $w_{gross,root}$ and $w_{gross,sh}$ are the gross growing rates (kg ha$^{-1}$ d$^{-1}$) of the roots and the shoots, respectively. The gross growth rate of leaves, stems and storage organs is simply the product of the gross dry matter growth rate of the shoots and the fraction allocated to these organs. The partitioning factors are a function of development stage and are crop specific. Mind that the sum of $\xi_{leaf}$, $\xi_{stem}$ and $\xi_{stor}$ at any development stage should be one!

## 7.9 Senescence

The death rate of storage organs is considered to be zero. The death rate of stem and roots is crop specific and is defined as the daily amount of the living biomass which no longer participates in the plant processes. The death rate of stems and roots is considered to be a function of development stage as specified by the user.

The death rate of leaves is more complicated. Leaf senescence occurs due to water stress, shading (high LAI), and also due to exceedance of the life span.

The potential death rate of leaves due to water stress $\zeta_{leaf,water}$ (kg ha$^{-1}$ d$^{-1}$) is calculated as:

$$\zeta_{leaf,w} = W_{leaf}\left(1 - \frac{T_a}{T_p}\right)\zeta_{leaf,p} \qquad (7.24)$$

where $W_{leaf}$ is the leaf dry matter weight (kg ha$^{-1}$), $T_a$ and $T_p$ are the actual and potential transpiration rates (cm d$^{-1}$), respectively, and $\zeta_{leaf,p}$ is the maximum relative death rate of leaves due to water stress (kg kg$^{-1}$ d$^{-1}$). The latter is crop specific and should be provided by the user.

A potential death rate due to self-shading, $\zeta_{leaf,shade}$ (kg ha$^{-1}$ d$^{-1}$), is defined which increases linearly from zero at a certain critical leaf area index, to its maximum value at twice this critical leaf area index:

$$\zeta_{leaf,shade} = 0.03 W_{leaf}\left(\frac{LAI - LAI_c}{LAI_c}\right) \quad \text{with} \quad 0 < \left(\frac{LAI - LAI_c}{LAI_c}\right) < 1 \qquad (7.25)$$

where $LAI_c$ is the critical leaf area index (-).

$LAI_c$ is set equal to $3.2/\kappa_{df}$, with $\kappa_{df}$ the extinction coefficient (-) for diffuse radiation (Par. 7.4). Typical values for $\zeta_{leaf,p}$ and $LAI_c$ are 0.03 d$^{-1}$ and 4 ha ha$^{-1}$, respectively (Spitters et al., 1989).

WOFOST uses the highest value of $\zeta_{leaf,w}$ and $\zeta_{leaf,shade}$ for the combined effect of water stress and mutual shading.

Leaves that have escaped from premature death due to water stress or mutual shading, inevitably die due to exceedance of the life span for leaves (i.e. physiologic ageing). Life span is defined as the maximum time a leaf can live at a constant temperature of 35 °C. Life span is crop specific. A physiologic ageing factor, $f_{age}$ (-), is calculated each day:

$$f_{age} = \frac{T - T_{b,age}}{35 - T_{b,age}} \quad \text{with} \quad f_{age} \geq 0 \qquad (7.26)$$

with $T_{b,age}$ the lower threshold temperature for physiologic ageing (°C), which is crop specific and should be provided by the user.

The integral of the physiologic ageing factor over time yields the physiologic age, $P_{age}$ (d):

$$P_{age}^{j+1} = P_{age}^{j} + f_{age}\Delta t \qquad (7.27)$$

In order to correct for leaf senescence, the specific leaf area of each day, $S_{la}^{j}$ (ha kg$^{-1}$), the growth of the dry matter weight of leaves per day, $w_{leaf}$, and the

physiological age, $P_{age}$, are stored in three different arrays. The first element of the arrays represents the most recent day and the last element of the arrays represents the oldest day.

The weight of the leaves that have died during a day due to water stress or mutual shading is subtracted from the weight of the oldest leaf class. If there is only one class, the result should be positive. When more leaf classes exist, the oldest leaf class may be emptied completely, and the remainder is subtracted from the next leaf class. Emptying the oldest leaf class continues, until the original amount is dissipated completely or the remaining amount of leaves becomes zero.

Leaves may attain the age defined by the crop specific life span. However, they can not exceed this age. The model checks the leaf classes ages. The first class younger than the defined life span becomes the oldest class.

## 7.10 Net growth

The initial amount of total dry crop weight should be provided by the user. This amount is multiplied by the partitioning factors, $\xi_i$, to yield the dry weight values at emergence.

The net growth rates of the plant organs, $w_{net,i}$ (kg ha$^{-1}$ d$^{-1}$) result from the gross growth rates (Par. 7.8) and the senescence rates, $\zeta_i$ (kg kg$^{-1}$ d$^{-1}$):

$$w_{net,i} = w_{gross,i} - \zeta_i W_i \tag{7.28}$$

By integrating $w_{net,i}$ over time, the dry matter weight of organ *i*, $W_i$ (kg ha$^{-1}$), is calculated.

An exception has to be made for the growth of leaves. In the initial stage, the rate of leaf appearance and final leaf size are constrained by temperature through its effect on cell division and extension, rather than by the supply of assimilates. For a relative wide range of temperatures the growth rate responds more or less linearly to temperature (Hunt et al., 1985; Causton and Venus, 1981; Van Dobben, 1962). The growth rate of the leaf area index, $w_{LAI}$ (ha ha$^{-1}$ d$^{-1}$), in this so-called exponential stage, is described by:

$$w_{LAI} = LAI\ w_{LAI,max}\ T_{eff} \tag{7.29}$$

where $w_{LAI,max}$ is the maximum relative increase of leaf area index (°C$^{-1}$ d$^{-1}$).

WOFOST assumes that the exponential growth rate of leaf area index will continue until it equals the assimilation limited growth rate of the leaf area index. During this second, source limited growth stage, $w_{LAI}$ is described by:

$$w_{LAI} = w_{net,leaf}\ S_{la} \tag{7.30}$$

where $S_{la}$ is the specific leaf area (ha kg$^{-1}$).

The green parts of stems and storage organs, may absorb a substantial amount of radiation. Therefore the so-called green area index $GAI_i$ (ha ha$^{-1}$) should be added to the leaf area index. The green area index of the stems and storage organs, are calculated from the dry matter weights of the organs:

$$GAI_i = S_{ga,i} W_i \tag{7.31}$$

with $S_{ga,i}$ the specific green area (ha kg$^{-1}$) of either stems or storage organ. $S_{ga,i}$ are crop specific and should be provided by the user.

## 7.11 Root growth

Root extension is computed in a straightforward way. The user needs to specify the initial rooting depth, the maximum rooting depth as determined by the crop and by the soil, and the maximum daily increase in rooting depth, $d_{root,max}$ (cm). Daily increase in rooting depth is equal to the maximum daily increase, unless maximum rooting depth is reached or no assimilates are available for root growth:

$$D_{root}^{j+1} = D_{root}^{j} + d_{root,max} \quad \text{if} \quad D_{root}^{j+1} \leq D_{root,max} \quad \text{and} \quad w_{net,root} \geq 0 \tag{7.32}$$

where $D_{root}^{j}$ is the rooting depth (cm) at day $j$.

## 7.12 Simple crop model

This option is useful when crop growth doesn't need to be simulated or when crop growth input data are insufficient. The simple crop growth model represents a green canopy that intercepts precipitation, transpires and shades the ground. The user specifies leaf area index, crop height and rooting depth as function of development stage. In stead of the leaf area index also the soil cover fraction can be provided (see Par. 6.6). The development stage can be controlled either by the temperature sum or can be linear in time.

When the simple crop model is used in combination with the reference evapotranspiration, the crop factor should be given of the particular crop completely covering the soil and with optimal water supply.

The simple model does not calculate the crop potential or actual yield. However, the user may define yield response factors (Doorenbos and Kassam, 1979; Smith, 1992) for various growing stages as function of development stage. Each growing stage $k$ the actual yield $Y_{a,k}$ (kg ha$^{-1}$) relative to the potential yield $Y_{p,k}$ (kg ha$^{-1}$) during this growing stage is calculated by:

$$1 - \frac{Y_{a,k}}{Y_{p,k}} = K_{y,k}\left(1 - \frac{T_{a,k}}{T_{p,k}}\right) \qquad (7.33)$$

where $K_{y,k}$ (-) is the yield response factor of growing stage $k$, and $T_{p,k}$ (cm) and $T_{a,k}$ (cm) are the potential and actual transpiration, respectively, during growing period $k$.

The relative yield of the whole growing season is calculated as product of the relative yields of each growing stage:

$$\frac{Y_a}{Y_p} = \prod_{k=1}^{n}\left(\frac{Y_{a,k}}{Y_{p,k}}\right)^k \qquad (7.34)$$

where $Y_a$ is the cumulative actual yield (kg ha$^{-1}$) of the whole growing season, $Y_p$ is the cumulative potential yield (kg ha$^{-1}$) of the whole growing season, index $k$ is the growing stage and $n$ is the number of defined growing stages.

In case of a linear relation between $Y_a/Y_p$ and $T_a/T_p$ during the whole growing period, or when no information is available of the yield response factors as function of development stage $D_s$ for the particular crop, specify $K_{y,k} = 1$ for $0 < D_s < 2$.

# 8 Field irrigation and drainage

Water balance simulation models are applied for irrigation scheduling in order to develop optimal irrigation schedules by evaluating alternative water application strategies. A common objective at irrigation scheduling is to maximize net return. Other objectives may be: minimize irrigation costs, maximize yield, optimally distribute a limited water supply, minimize groundwater and surface water pollution, or optimize the production from a limited irrigation system capacity. In semi-arid and arid zones irrigation may cause salinity problems. If natural drainage for leaching is not present, artificial drainage has to be installed to create favourable moisture and salinity conditions in the root zone. SWAP can be used to support the design of a combined irrigation and drainage system, including sub-irrigation.

The appropriate management objective depends on the available water amounts and the irrigation costs. In many cases it is optimal to produce near maximum yields on the entire area that can be irrigated. Then the prime objective is to prevent crop water stress throughout the growing season. In case water supplies do not allow irrigation for maximum yield, or irrigation costs are that high, that the economic optimum level of irrigation is below the yield maximizing level, deficit irrigation must be practised. The objective of irrigation management under these conditions is to maximize the economic returns to water and generally three decision criteria are involved:
- how much area to irrigate;
- which crops to plant;
- how to distribute the available supply over the irrigable area during the season.

If land amount is limiting and water is available but expensive, net returns to land are to be optimized: maximum economic efficiency occurs when the cost of an additional unit of water just equals the value of the resulting crop yield increment.

## 8.1 Irrigation scheduling options

In SWAP irrigations may be prescribed at fixed times or scheduled according to a number of criteria. Also a combination of irrigation prescription and scheduling is possible. The scheduling criteria define the time when irrigation should take place, as well as the irrigation depth. A specified combination of timing and depth criteria is valid from a user defined date in the cropping season until the end of crop growth. Both timing and depth criteria may be dynamic i.e. be defined as a function of crop development stage. The reduced growth rate and final yield due to soil moisture stress will depend on the time of occurrence of the stress during the growth cycle. If the stress period occurs

during rapid plant growth and high water demands, or when reproductive processes are critical, the effect of stress will be larger than during stress periods of similar length when growth and development are slow, such as near maturity.

The irrigation scheduling criteria applied in SWAP are similar to the criteria in CROPWAT (Smith, 1992), IRSIS (Raes et al., 1988), and the Hydra Decision Support System for Irrigation Water Management (Jacucci et al., 1994).

## 8.2 Timing criteria

Five different timing criteria can be selected to generate an irrigation schedule:

***Allowable daily stress***
Irrigation is applied whenever the actual transpiration rate $T_a$ drops below a predetermined fraction $f_1$ (-) of the potential transpiration rate $T_p$ :

$$T_a \leq f_1 \, T_p \tag{8.1}$$

This option is relevant for sub-optimal (deficit) irrigation when the water supply is limited.

***Allowable depletion of readily available water in the root zone***
Irrigation is applied whenever the water depletion in the root zone is larger than a fraction $f_2$ (-) of the readily available water amount:

$$U_a - U_{h3} \leq f_2 \, (U_{field} - U_{h3}) \tag{8.2}$$

where $U_a$ (cm) is the actual water storage in the root zone, $U_{field}$ (cm) is the root zone water storage at $h$ = -100 cm (field capacity), and $U_{h3}$ (cm) is the root zone water storage at $h = h_3$, where root water extraction starts being reduced due to drought stress (Fig. 2.2). $U_a$ is calculated by integrating numerically the water content in the rooting layer. This option is useful for optimal scheduling where irrigation is always secured before conditions of soil moisture stress occur. For deficit irrigation purposes, stress can be allowed by specifying $f_2 > 1$.

***Allowable depletion of totally available water in the root zone***
Irrigation is applied whenever the depletion is larger than a fraction $f_3$ (-) of the total available water amount between field capacity and permanent wilting point:

$$U_a - U_{h4} \leq f_3 \, (U_{field} - U_{h4}) \tag{8.3}$$

where $U_{h4}$ is the root zone water storage at $h = h_4$, the pressure head at which root water extraction is reduced to zero (Fig. 2.2).

***Allowable depletion amount of water in the root zone***
Irrigation is applied whenever a predetermined water amount, $\Delta U_{max}$ (cm), is extracted below field capacity:

$$U_a \leq U_{field} - \Delta U_{max} \tag{8.4}$$

This option is useful in case of high frequency irrigation systems (drip).

***Critical pressure head or moisture content at sensor depth***
Irrigation is applied whenever moisture content or pressure head at a certain depth in the root zone drops below a prescribed threshold value $\theta_{min}$ ($cm^3\ cm^{-3}$) or $h_{min}$ (cm):

$$\theta_{sensor} \leq \theta_{min} \qquad \text{or} \qquad h_{sensor} \leq h_{min} \tag{8.5}$$

This option may be used to verify field experiments or to simulate irrigation with automated systems.

The user may also select a combination of two or more of above criteria.

## 8.3 Application depth criteria

Two irrigation depth criteria can be selected:

***Back to Field Capacity (+/- specified amount)***
The soil water content in the root zone is brought back to field capacity. An additional irrigation amount can be defined to leach salts, while the user may define a smaller irrigation amount when rainfall is expected. This option is useful in case of sprinkler and micro irrigation systems, which allow variation of irrigation application depth.

***Fixed irrigation depth***
A specified amount of water is applied. This option applies to most gravity systems, which allow little variation in irrigation application depth.

## 8.4 Field drainage

In Par. 2.4.3 the bottom boundary condition has been described. In addition to the bottom flux, $q_{bot}$ (cm $d^{-1}$), which accounts for regional drainage or seepage fluxes, it is possible in SWAP to define lateral field drainage fluxes, $q_{drain}$ (cm $d^{-1}$), to the local drainage system, see Fig. 2.6. Three methods can be used to calculate $q_{drain}$:
- linear $q_{drain}(\phi_{gwl})$ relation
- tabular $q_{drain}(\phi_{gwl})$ relation
- drainage equations of Hooghoudt and Ernst

where $\phi_{gwl}$ is the phreatic groundwater level midway between the drains or ditches. In SWAP, $z$ (cm) and $\phi$ (cm) are defined positive upward, with zero at the soil surface.

In case of a linear $q_{drain}(\phi_{gwl})$ relation, the drainage resistance, $\gamma_{drain}$ (d), is defined:

$$q_{drain} = \frac{\phi_{gwl} - \phi_{drain}}{\gamma_{drain}} \tag{8.6}$$

with $\phi_{drain}$ the drain hydraulic head (cm). In case of non-linear relations between $q_{drain}$ and $\phi_{gwl}$, tabular values of $q_{drain}$ as function of $\phi_{gwl}$ are input.

The drainage equations of Hooghoudt and Ernst allow the evaluation of drainage design. The theory behind these equations is clearly described in Ritzema (1994) and will not be repeated here. Five typical drainage situations are distinguished, see Fig. 8.1. For each drainage situation the drainage resistance $\gamma_{drain}$ can be defined according to Eq. 8.6.

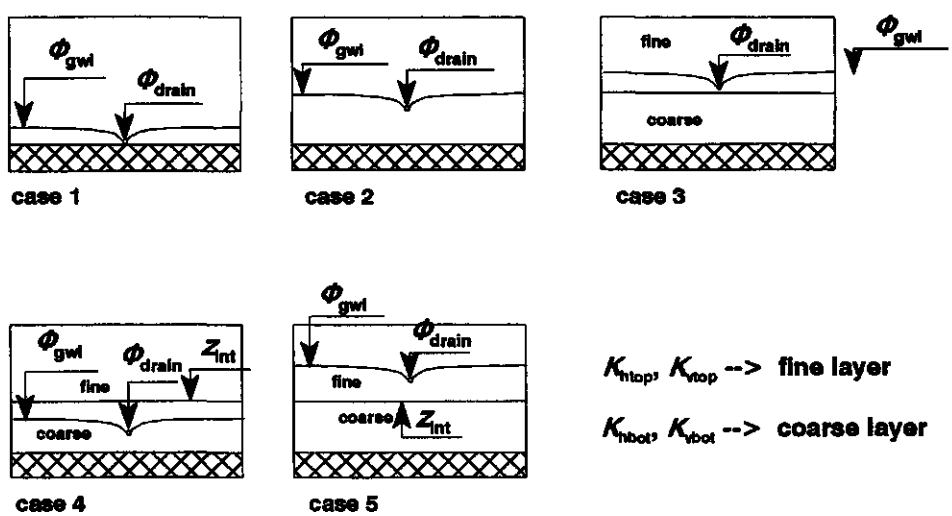


*Fig. 8.1 Five field drainage situations considered in SWAP (after Ritzema, 1994). The hydraulic head $\phi$ is defined positive upward with $\phi$ = 0 at the soil surface*

### *1) Homogeneous profile, drain on top of impervious layer*

The drainage resistance is calculated as:

$$\gamma_{drain} = \frac{L_{drain}^2}{4K_{hprof}(\phi_{gwl} - \phi_{drain})} + \gamma_{entr} \tag{8.7}$$

with $K_{hprof}$ the horizontal saturated hydraulic conductivity above the drainage basis (cm $d^{-1}$), $L_{drain}$ the drain spacing (cm) and $\gamma_{entr}$ the entrance resistance into the drains and/or ditches (d). The value for $\gamma_{entr}$ can be obtained, analogous to the resistance value of an aquitard, by dividing the 'thickness' of the channel walls with the permeability. If this permeability does not differ substantially from the conductivity in the surrounding subsoil, the numerical value of the entry resistance will become relatively minor.

***2) Homogeneous profile, drain above impervious layer***

This drainage situation has been originally described by Hooghoudt (1940). The drainage resistance follows from:

$$\gamma_{drain} = \frac{L_{drain}^2}{8K_{hprof}D_{eq} + 4K_{hprof}(\phi_{gwl} - \phi_{drain})} + \gamma_{entr} \qquad (8.8)$$

where $D_{eq}$ is the equivalent depth (cm).

The equivalent depth was introduced by Hooghoudt to incorporate the extra head loss near the drains caused by converging flow lines. We employ in SWAP a numerical solution of Van der Molen and Wesseling (1991) to calculate $D_{eq}$ (Ritzema, 1994). A typical length variable $x$ is used:

$$x = \frac{2\pi(\phi_{drain} - z_{imp})}{L_{drain}} \qquad (8.9)$$

If $x < 10^{-6}$, then:

$$D_{eq} = \phi_{drain} - z_{imp} \qquad (8.10)$$

with $z_{imp}$ the level of the impervious layer. If $10^{-6} < x < 0.5$, then:

$$F(x) = \frac{\pi^2}{4x} + \ln\frac{x}{2\pi} \qquad (8.11)$$

and the equivalent depth equals:

$$D_{eq} = \frac{\pi L_{drain}}{8\left(\ln\frac{L_{drain}}{\pi r_{drain}} + F(x)\right)} \qquad (8.12)$$

with $r_{drain}$ the radius of the drain or ditch. If $0.5 < x$, then:

$$F(x) = \sum_{j=1,3,5}^{\infty} \frac{4e^{-2jx}}{j(1 - e^{-2jx})} \qquad (8.13)$$

and equivalent depth again follows from Eq. 8.12.

***3) Heterogeneous soil profile, drain at interface between both soil layers***

The equivalent depth $D_{eq}$ is calculated with the procedure of Eq. 8.9 to 8.13.

The drainage resistance follows from:

$$\gamma_{drain} = \frac{L_{drain}^2}{8K_{hbot}D_{eq} + 4K_{htop}(\phi_{gwl} - \phi_{drain})} + \gamma_{entr} \qquad (8.14)$$

with $K_{htop}$ and $K_{hbot}$ the horizontal saturated hydraulic conductivity (cm $d^{-1}$) of upper and lower soil layer, respectively.

***4) Heterogeneous soil profile, drain in bottom layer***

The drainage resistance is calculated according to Ernst (1956) as:

$$\gamma_{drain} = \gamma_{ver} + \gamma_{hor} + \gamma_{rad} + \gamma_{entr} \qquad (8.15)$$

where $\gamma_{ver}$, $\gamma_{hor}$, and $\gamma_{rad}$ are the vertical, horizontal and radial resistance ($d^{-1}$), respectively. The vertical resistance is calculated by:

$$\gamma_{ver} = \frac{\phi_{gwl} - z_{int}}{K_{vtop}} + \frac{z_{int} - \phi_{drain}}{K_{vbot}} \qquad (8.16)$$

with $z_{int}$ the level of the transition (cm) between the upper and lower soil layer, and $K_{vtop}$ and $K_{vbot}$ the vertical saturated hydraulic conductivity (cm $d^{-1}$) of the upper and lower soil layer, respectively. The horizontal resistance is calculated as:

$$\gamma_{hor} = \frac{L_{drain}^2}{8K_{hbot}D_{bot}} \qquad (8.17)$$

with $D_{bot}$ the contributing layer below the drain level (cm), which is calculated as the minimum of ($\phi_{drain}$ - $z_{imp}$) and ¼ $L_{drain}$. The radial resistance is calculated by:

$$\gamma_{rad} = \frac{L_{drain}}{\pi\sqrt{K_{hbot}K_{vbot}}} \ln\frac{D_{bot}}{u_{drain}} \qquad (8.18)$$

with $u_{drain}$ the wet perimeter (cm) of the drain.

***5) Heterogeneous soil profile, drain in top layer***

Again the approach of Ernst (1956) is applied (Eq. 8.15). The resistances are calculated as:

$$\gamma_{ver} = \frac{\phi_{gwl} - \phi_{drain}}{K_{vtop}} \qquad (8.19)$$

$$\gamma_{hor} = \frac{L_{drain}^2}{8K_{htop}D_{top} + 8K_{hbot}D_{bot}} \qquad (8.20)$$

$$\gamma_{rad} = \frac{L_{drain}}{\pi\sqrt{K_{htop}K_{vtop}}} \ln\left( g_{drain} \frac{\phi_{drain} - z_{int}}{u_{drain}} \right) \qquad (8.21)$$

with $D_{top}$ equal to ($\phi_{drain}$ - $z_{int}$) and $g_{drain}$ is the drain geometry factor, which should be specified in the input. The value of $g_{drain}$ depends on the ratio of the hydraulic conductivity of the bottom ($K_{hbot}$) and the top ($K_{htot}$) layer. Using the relaxation method, Ernst (1962) distinguished the following situations:

- $K_{hbot}/K_{htot} < 0.1$: the bottom layer can be considered impervious and the case is reduced to a homogeneous soil profile and $g_{drain} = 1$;
- $0.1 < K_{hbot}/K_{htot} < 50$: $g_{drain}$ depends on the ratios $K_{hbot}/K_{htop}$ and $D_{bot}/D_{top}$, as given in Table 8.1;
- $50 < K_{hbot}/K_{htot}$: $g_{drain} = 4$.

*Table 8.1 The geometry factor $g_{drain}$ (-), as obtained by the relaxation method (after Ernst, 1962)*

| $K_{hbot}/K_{htop}$ | $D_{bot}/D_{top}$ | | | | | |
|---|---|---|---|---|---|---|
| | 1 | 2 | 4 | 8 | 16 | 32 |
| 1 | 2.0 | 3.0 | 5.0 | 9.0 | 15.0 | 30.0 |
| 2 | 2.4 | 3.2 | 4.6 | 6.2 | 8.0 | 10.0 |
| 3 | 2.6 | 3.3 | 4.5 | 5.5 | 6.8 | 8.0 |
| 5 | 2.8 | 3.5 | 4.4 | 4.8 | 5.6 | 6.2 |
| 10 | 3.2 | 3.6 | 4.2 | 4.5 | 4.8 | 5.0 |
| 20 | 3.6 | 3.7 | 4.0 | 4.2 | 4.4 | 4.6 |
| 50 | 3.8 | 4.0 | 4.0 | 4.0 | 4.2 | 4.6 |

# 9 Surface water and multi-level drainage at subregional scale

## 9.1 Introduction

The groundwater-surface water system is modelled in SWAP at the scale of a horizontal subregion. Only a single representative groundwater level is simulated, which is 'stretched' over a scale that in reality involves a variety of groundwater levels. We use the term 'quasi-subregional' for this approach. In the following, due consideration will be given to the schematization of the surface water system, the simulation of drainage/sub-irrigation fluxes (including surface runoff), and the handling of an open surface water level.

## 9.2 Hydrological schematization of the surface water system

The surface water system is divided into a maximum of five channel orders:
- primary water course (1st order);
- secondary water course(s) (2nd order);
- tertiary water courses (3rd order);
- pipe drains (4th order);
- trenches (5th order).

An example of a surface water system with four channel orders is shown in Fig. 9.1.

Each order of channels is defined by its channel bed level, bed width, side-slope, and spacing. For practical cases, the representative spacing $L_i$ (cm) is derived by dividing the area of the subregion $A_{reg}$ (cm$^2$) by the total length of the $i^{th}$ order channels, $l_i$ (cm):

$$L_i = \frac{A_{reg}}{l_i} \tag{9.1}$$

In the surface water model, we assume that the different channels orders are connected in a dendritic manner. Together they form a surface water 'control unit' with a single outlet and, if present, a single inlet. The surface water level at the outlet is assumed to be omnipresent in the subregion. Friction losses are neglected and thus the slope of the surface water level is assumed to be zero. This means that in all parts of the subregion the surface water level has the same depth below soil surface. Its presence, however, is only locally felt in a water course if it is higher than the channel bed level. If it is lower, the water course is free draining, or remains dry if the groundwater level is below the channel bed.

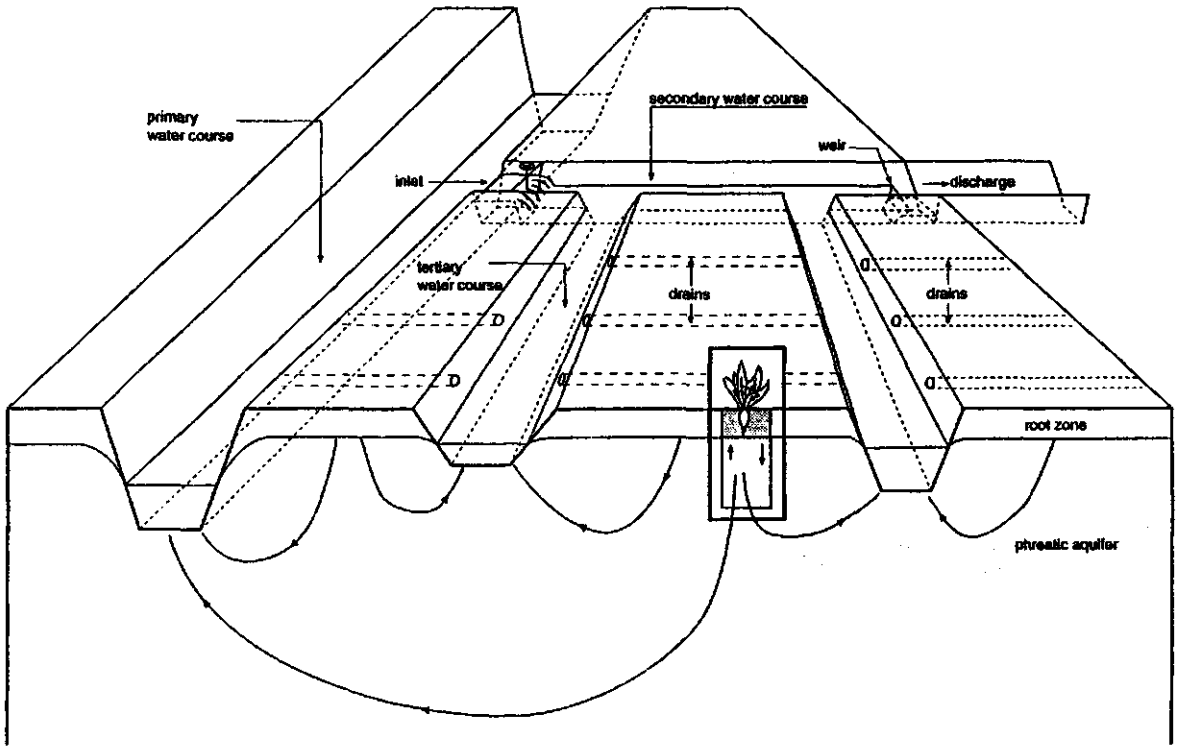


*Fig. 9.1 Schematized surface water system. The primary water course functions separately from the others, but it does interact with the SWAP soil column by the drainage or infiltration flux*

In most applications, the control unit will include the primary watercourse. It is, however, possible to specify that the primary watercourse, e.g. a large river, functions separately from the rest of the subregional surface water system. In that case it has its own surface water level. This level has to be specified in the input, because it is determined by water balances and flows on a much larger scale than that of the modelled subregion. In the real situation there may be some interaction between the primary water course and the control unit: for instance a pumping station for removal of drainage water, and/or an inlet for letting in external surface water supply (Fig. 9.1). The hydraulics of such structures are not included in the model.

The channels do not only act as waterways for surface water transport. Depending on the groundwater level and the open surface water level, the channels will also act as either drainage or sub-irrigation media. In the system modelled by SWAP, it is possible that more than one type of surface water channel becomes active simultaneously. For these situations one can best speak of 'multi-level' drainage or sub-irrigation. In the following, we will refer to channels in terms of their 'order' if their role as part of the surface water system is being considered. When considering their drainage characteristics we will refer to them in terms of their 'level'.

When the groundwater level rises above the soil surface, the soil surface also starts to function as a 'drainage medium' generating surface runoff. The storage of water on the soil surface itself, however, is simulated by SWAP as 'ponding'.

For the water balance of the subregion as a whole, we assume that the soil profile 'occupies' the whole surface area, even though part of the area is covered by surface water. In other words, the water balance terms of the soil profile that are computed per unit area ($cm^3\ cm^{-2}$) have the *same numerical value for the subregion as a whole*. This implies that the evapotranspiration of surface water is set equal to the actual evapotranspiration of land surface. In order to prevent double counting, evapotranspiration and precipitation are not included in the water balance of surface water. We do, however, compute storage characteristics of the surface water based on the lengths of the water courses and the wetted cross sections. There is thus a 'duplicate use' of part of the area, introducing some extra storage in the system, which in reality does not exist. The approach followed here is only valid for subregions with a limited area of surface water, certainly not more than 10%.

## 9.3 Hydrological schematization of drainage and sub-irrigation at subregional scale

The used concepts and methods will first be described for single-level drainage, next for multi-level drainage, and finally for surface runoff.

***Single-level drainage***

Prior to any calculation of the drainage/sub-irrigation rate, we determine whether the flow situation involves drainage, sub-irrigation, or neither. No drainage or sub-irrigation will occur if both the groundwater level and surface water level are below the drainage base. Drainage will only occur if the following two conditions are met:

- the groundwater level is higher than the channel bed level;
- the groundwater level is higher than the surface water level.

Sub-irrigation can only occur if the following two conditions are met:

- the surface water level is higher than the channel bed level;
- the surface water level is higher than the groundwater level.

In both cases we take for the drainage base, $\phi_{drain}$ (cm), either the surface water level, $\phi_{sur}$ (cm), or the channel bed level, $z_{bed}$ (cm), whichever is higher:

$$\phi_{drain} = \max\ (\phi_{sur}, z_{bed}) \qquad (9.2)$$

$\phi$ is defined positive upward, with zero at the soil surface.

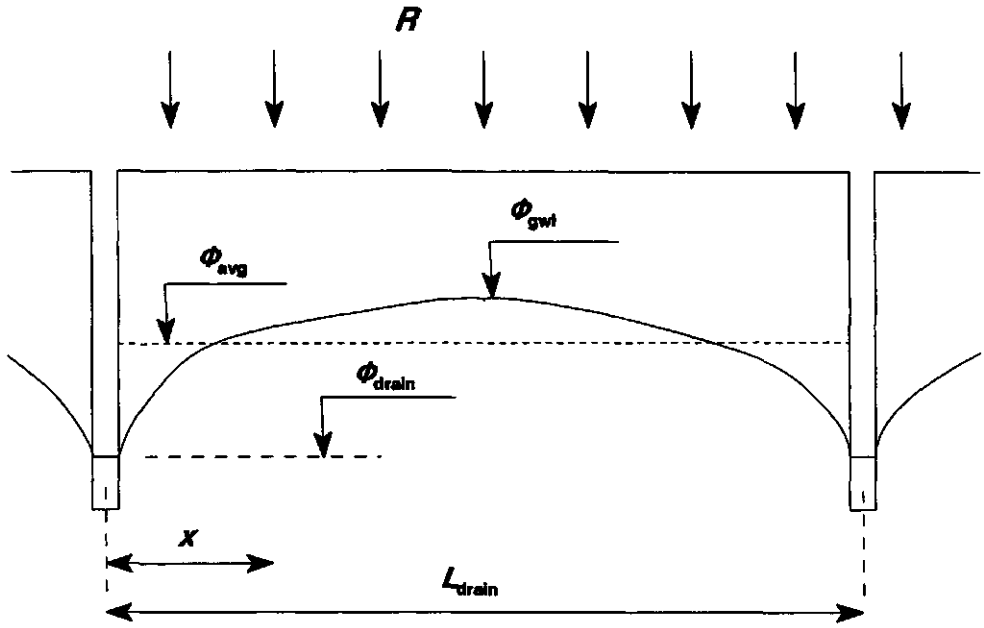


*Fig. 9.2 Cross-section of single-level drainage with $\phi_{gwl}$ the groundwater level midway between the drains and $\phi_{avg}$ the mean groundwater level*

An example of a single-level drainage case is given in Fig. 9.2. In this example we assume that:

- the considered channel is part of a system involving *equidistant* and *parallel* channels, all of the same order;
- the recharge $R$ is evenly distributed and steady-state.

For such situations several drainage formula exist, as described in Par. 8.4. The drainage resistance is for the subregional approach defined as:

$$\gamma_{drain} = \frac{\phi_{avg} - \phi_{drain}}{R} \qquad (9.3)$$

where $\phi_{avg}$ is the mean groundwater level of the whole subregion, and $\phi_{drain}$ the hydraulic head of the drain or ditch (cm), the so-called drainage base. Note that instead of the maximum groundwater level $\phi_{gwl}$ midway between the drains or ditches (Eq. 8.6), the mean groundwater level $\phi_{avg}$ is used. The two definitions of $\gamma_{drain}$ in Eq. 8.6 and 9.3 differ by the so-called shape factor: the shape factor is the ratio between the mean and the maximum groundwater level elevation above the drainage base. The shape factor depends on the vertical, horizontal, radial and entrance resistances of the drainage system (Ernst, 1978). For regional situations, where the 'horizontal' resistance to flow plays an important role, the shape factor is relatively small ($\approx 0.7$). The smaller the horizontal resistance becomes, the more 'rectangular' the water table: in the most extreme case with all the resistance concentrated in the direct vicinity of the channel, the water table is level, except for the abrupt

drop towards the drainage base. In that case the shape factor becomes equal to unity (see Par. 8.4).

In case of sub-irrigation, the entrance resistance (then denoted as $\gamma_{inf}$) can differ from that for drainage ($\gamma_{drain}$): it can either be higher or lower, depending on local conditions. A substantial raising of the surface water level can for instance result in infiltration through a 'bio-active' zone (e.g. involving pores of rain worms) which will reduce the entrance resistance. In most situations with sub-irrigation the radial resistance will be higher than with drainage, because the wetted section of the subsoil is less than in the situation with drainage (the groundwater table becomes concave instead of convex). Especially if the conductivity of the subsoil above the drainage base is larger than in the deeper subsoil, the sub-irrigation resistance $\gamma_{inf}$ will be substantially higher than the drainage resistance $\gamma_{drain}$. In view of these various possible practical situations, the model has the option for using sub-irrigation resistances that differ from the ones for drainage (e.g. $\gamma_{inf} \approx 3/2\ \gamma_{drain}$ in Fig. 9.3).

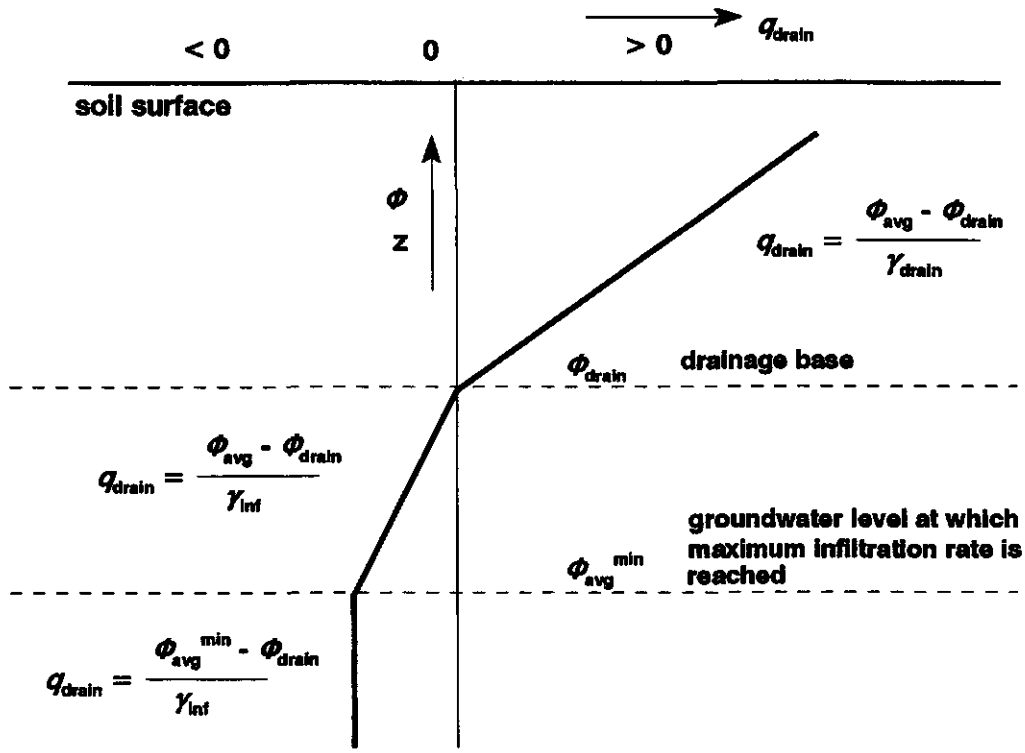


*Fig. 9.3 Linear relationship between drainage ($q_{drain} > 0$) and infiltration ($q_{drain} < 0$) flux and mean groundwater level $\phi_{avg}$*

An additional model option is to limit the simulated sub-irrigation rate. Such a limitation is needed because the sub-irrigation rate does not increase forever when the groundwater level drops: asymptotically a maximum rate is reached.

This maximum rate is determined by the surface water level, the geometry of the wetted channel cross-section and the permeability of the subsoil. For practical reasons we have not set a limit to the sub-irrigation rate itself (Fig. 9.3). Instead, we have limited the simulated sub-irrigation rate by defining the groundwater level $\phi_{avg}^{min}$ at which the maximum sub-irrigation rate is reached. The linearised relationship, given by Eq. 9.3, is not valid at lower groundwater levels.

Because the non-steady groundwater flow is simulated as a sequence of steady-state conditions, we use the linearised relation between $q_{drain}$ and $\phi_{avg}$. This approach is only valid if the drainage resistance is concentrated in the direct vicinity of the channel cross-section, i.e. that the radial resistance is far more important than the horizontal resistance. In such cases the shape factor approaches unity. This contrasts with the case of 'perfect' drains where the shape factor varies with time, depending on the sequence of preceding recharges. After a 'storm recharge' the drainage flow to 'perfect' drains is much higher than the flow predicted by the steady-state relationship. In most situations however, the radial resistance is much higher than the horizontal one, and the use of a steady-state relationship for non-steady simulations will not lead to major errors.

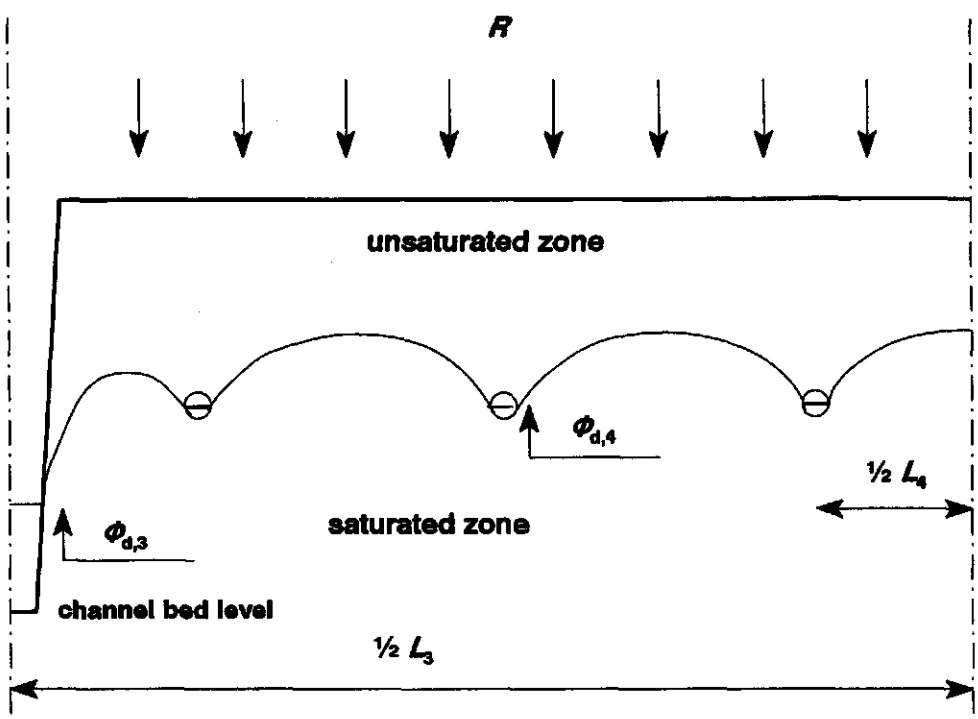


*Fig. 9.4 Cross-section of multi-level drainage, involving a third-order system of ditches and a fourth-order system of pipe drains*

***Multi-level drainage***

For illustration purposes we consider a multi-level drainage involving third and fourth order systems (Fig. 9.4):

- the third-order drainage system consists of ditches;
- the fourth-order system consists of subsurface drains;
- the ditches and drains are assumed to be equidistant and parallel.

In this case of two-level drainage we need to quantify the drainage fluxes to both levels of drainage media. We implicitly assume that nearly all of the flow resistance is concentrated in the vicinity of the drainage media (channels and drains). In the most extreme case with only entrance resistance, the water level is horizontal, as shown in Fig. 9.5. In such a case groundwater behaves as a linear reservoir, with outlets at different levels ('tank with holes', see Fig. 10.1). This approach is valid if the main part of the drainage resistance is concentrated near the drains or ditches. For most soils in the Netherlands this seems a reasonable assumption.

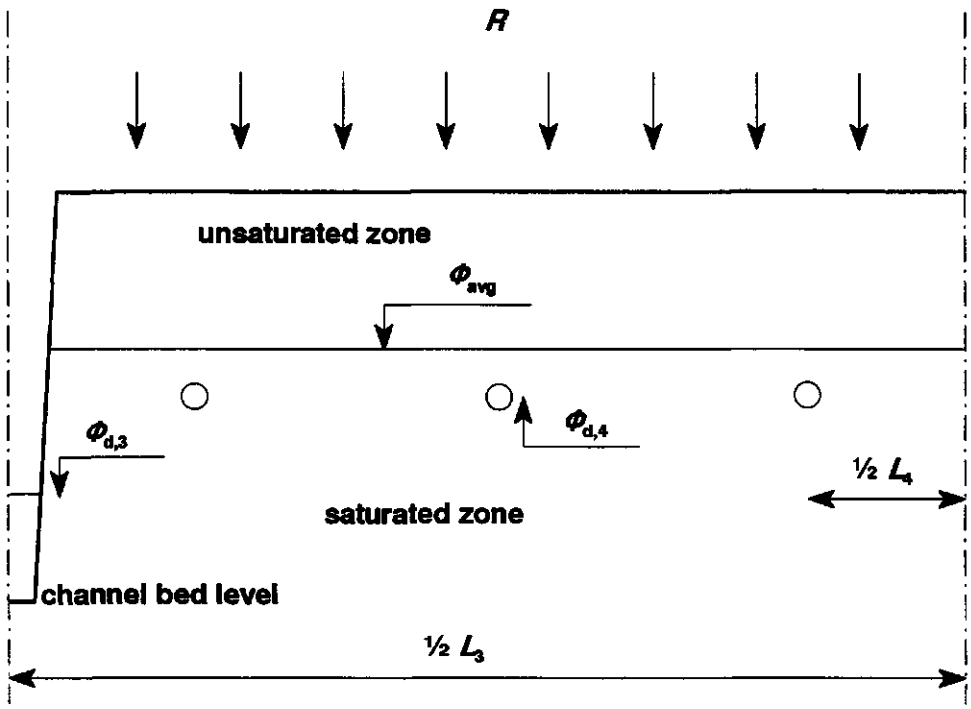


*Fig. 9.5 Cross-section of multi-level drainage. The main part of the flow resistance is assumed to be located near the drains and ditches, which results in a horizontal groundwater table*

Similar to the case of single-level drainage, a drainage level is only 'active' if either the groundwater level or the surface water level is higher than the channel bed level. The drainage base is determined separately for each of the drainage levels, using Eq. 9.2. In computing the total flux to/from surface water, the contributions of the different channel orders are simply added. For

the situation with the groundwater level above the highest bed level and with the surface water level below the lowest one, for instance, the total drainage flux is computed with:

$$q_{drain} = \sum_{i=1}^{n} \frac{\phi_{avg} - \phi_{d,i}}{\gamma_{d,i}} \qquad (9.4)$$

where the drainage base $\phi_{d,i}$ is in this case equal to the channel bed level, $z_{bed,i}$. If the surface water level becomes higher than the channel bed level $z_{bed,i}$, the latter is replaced by the surface water level.

**Surface runoff**

Surface runoff is generally more complicated to handle than drainage and sub-irrigation. In the surface water module of SWAP a simplified approach is followed. Surface runoff $q_{run}$ is simulated using a linear relationship similar to drainage:

$$q_{run} = \frac{h_{pond} - z_{sill}}{\gamma_{sill}} \qquad (9.5)$$

where $h_{pond}$ is the ponding depth of water on the soil surface, $z_{sill}$ the height of the sill which is equal to the maximum ponding height without surface runoff, and $\gamma_{sill}$ the drainage resistance of surface runoff. The maximum ponding height without surface runoff is determined by the irregularities of the soil surface. As surface runoff is a rapid process, the sill resistance $\gamma_{sill}$ will typically have values of less than 1 d. For most SWAP applications, realistic dynamic simulation of surface runoff is not required, but only the effect of surface runoff on the water balance is relevant. Then a rough estimate of $\gamma_{sill}$ is sufficient, e.g. $\gamma_{sill} \approx 0.1$ d. When the dynamics of surface runoff are relevant, the value of $\gamma_{sill}$ might be derived from experimental data or from a hydraulic model of soil surface flow.

The linearised relationship for surface runoff is also used for the simulation of *runon*. The latter occurs when the surface water level rises above the elevation of the sill and above the level of ponded water, if present.

## 9.4 Surface water levels

The surface water level in the primary water course has to be specified in the input, if the primary water course functions separately from the rest of the surface water system (see Par. 9.2). For the surface water in the control unit, the model has two options for obtaining the water level:

- from an external source, using the procedure for 'surface water level as *input*';
- from the water balance simulation of the surface water system, using the procedure for 'surface water level as *output*'.

In case of surface water level as input, the model calculates net discharge or supply on the basis of the surface water balance. In case of surface water level as output, the water level is computed by combining the water balance equation and the hydraulic characteristics of a control section, which can be either a fixed-crest weir or an automatic weir. In the case of an automatic weir, the crest will be lowered or raised in order to maintain a *target level*. With SWAP it is possible to simulate a water management scheme that relates the setting of the target level to the groundwater level. Such a scheme can be an efficient way to conserve as much water as possible, without causing crop damage due to water-logging (Van Walsum & Van Bakel (1983), Van Bakel (1986)). If the groundwater level is low, a high setting of the weir is permitted. If the groundwater level is high, the weir is lowered as much as possible to provide maximum drainage.

In both procedures for obtaining the surface water level (as input or as output) we make a water balance for the water courses within the control unit. In the following we will first explain the terms in this balance, and then continue with explaining the full procedures.

***Water balance of the control unit***

The surface water balance equation for the control unit is formulated as:

$$V_{sur}^{j+1} - V_{sur}^{j} = (q_{sup} - q_{dis} + q_{drain} + q_{c,drain} + q_{run})\ \Delta t^{j} \qquad (9.6)$$

where $V_{sur}$ is the regional surface water storage (cm$^3$ cm$^{-2}$), $q_{sup}$ is the external supply to the control unit (cm$^3$ cm$^{-2}$ d$^{-1}$), $q_{dis}$ is the discharge that leaves the control unit (cm$^3$ cm$^{-2}$ d$^{-1}$), $q_{c,drain}$ is bypass flow (cm$^3$ cm$^{-2}$ d$^{-1}$) through cracks of a dry clay soil to drains or ditches (Par. 5.2), $q_{run}$ is the surface runoff (cm$^3$ cm$^{-2}$ d$^{-1}$), $\Delta t$ is the time increment (d), and superscript $j$ is the time level.

The regional surface water storage $V_{sur}$ (cm$^3$ cm$^{-2}$) is the sum of the surface water storage in each order of the surface water system:

$$V_{sur} = \frac{1}{A_{reg}} \sum_{i=1}^{n} l_i\, A_{d,i} \qquad (9.7)$$

in which $A_{reg}$ is the total area of the subregion (cm$^2$), $l_i$ the total length of channels/drains of order $i$ in the subregion (cm), and $A_{d,i}$ is the wetted area of a channel *vertical* cross-section (cm$^2$). The program calculates $A_{d,i}$ using the surface water level $\phi_{sur}$, the channel bed level, the bottom width, and the side-slope. Substitution of Eq. 9.1 in Eq. 9.7 yields the expression:

$$V_{sur} = \sum_{i=1}^{n} \frac{A_{d,i}}{L_i} \qquad (9.8)$$

Channels of order $i$ only contribute to the storage if $\phi_{sur} > z_{bed,i}$. The storage in

pipe drains is assumed to be zero. Eq. 9.8 is used by the model for computing the storage from the surface water level and vice versa, per time step. Prior to making any dynamic simulations, a table of channel storage as a function of discrete surface water levels is derived.

***Procedure for surface water level as input***

SWAP calculates the net discharge $q_{dis}$- $q_{sup}$ between $t^j$ and $t^{j+1}$ for the given surface water levels $\phi_{sur}{}^j$ and $\phi_{sur}{}^{j+1}$ at the beginning an end of a time step, using Eq. 9.6 in a rearranged form:

$$q_{dis} - q_{sup} = \frac{V_{sur}^{j} - V_{sur}^{j+1}}{\Delta t^{j}} + q_{drain} + q_{c,drain} + q_{run} \qquad (9.9)$$

The terms on the right hand side are known or can be calculated ($V_{sur}$ is a function of the known $\phi_{sur}$). If the sum is positive, discharge has taken place and the supply is equal to zero. If the sum is negative, supply has taken place and the discharge is equal to zero.

***Procedure for surface water level as output***

This procedure calculates the surface water level from the surface water balance of a control unit. For each water management period a fixed or an automatic weir can be simulated. The settings of the weirs can be different for each management period, as can be the other input parameters of water management. One of the most important input parameters is the maximum rate at which water can be supplied from an external source (for sub-irrigation). During each time step, SWAP determines:

- the target level;
- whether the target level is reached, and the amount of external supply that is needed (if any);
- the discharge that takes place (if any) and the surface water level at the end of the time step.

In the case of a fixed weir, the target level coincides with the level of the crest (which is fixed during a certain management period, but can be changed from one period to the next). In the case of an automatic weir, the target level is determined by a water management scheme. This scheme gives the desired setting of the target water level $\phi_{sur,tar}$ in relation to a number of state variables of the system. At present it is possible to relate the target level to:

- the average groundwater level $\phi_{avg}$;
- the soil water pressure head $h$ (cm) at a certain depth in the soil profile;
- total water storage of the unsaturated soil profile $V_{uns}$ (cm).

A high groundwater level will lead to a lower target level, in order to minimize reduction of crop growth due to waterlogging. In nature reserves this criterium does not apply. A soil water pressure head gives a better indication of a threat of waterlogging, than the groundwater level only. The water amount that still can be stored in the soil profile, indicates the buffer capacity in case of

heavy rainfall. Maintaining a certain minimum amount of storage, reduces the risk of flooding and subsequent discharge peaks.

*Table 9.1 Example of a water management scheme, with $\phi_{sur,tar}$ the target level for surface water, the criterium $\phi_{avg,max}$ for the mean groundwater level (maximum), the criterium $h_{max}$ for the pressure head (maximum) and $V_{uns,min}$ for the unsaturated volume (minimum). The program selects the highest target level for which all three criteria are met*

| $\phi_{sur,tar}$ (cm) | $\phi_{avg,max}$ (cm) | $h_{max}$ (cm) | $V_{uns,min}$ (cm) |
|---|---|---|---|
| -180 | 0 | 0 | 0 |
| -160 | -80 | -100 | 1.5 |
| -140 | -90 | -150 | 2.0 |
| -120 | -100 | -200 | 2.5 |
| -100 | -120 | -250 | 3.0 |
| -80 | -130 | -300 | 4.0 |

An example of the water management scheme with target levels and criteria, is shown in Table 9.1. On the first line the minimum target level is specified. The criteria for this level (zeros) are dummies: the minimum target level is chosen whatever the prevailing conditions. The water management scheme selects the highest level for which all three criteria are met.

The water management scheme also has a *maximum drop rate* parameter, which specifies the maximum rate with which the target level of an automatic weir is allowed to drop (cm $d^{-1}$). This is needed to avoid situations in which the target level reacts abruptly to the prevailing groundwater level. An abrupt drop can cause instability of channel walls or wastage of water that could have been infiltrated. Such a situation can occur during a period with surface water supply and a rising groundwater level due to infiltrating water: the rising groundwater level can cause a different target level to be chosen for the surface water system.

After having determined the target level, the next step in the procedure is to determine whether it can be reached within the considered time step. If necessary, surface water supply is used to attain the target level. This supply is not allowed to exceed the maximum supply rate $q_{sup,max}$, which is an input parameter. For situations with supply, it is possible to specify a tolerance for the surface water level in relation to the target level. This tolerance, the *allowed dip* of the surface water level, can for instance be 10 cm. Then the model does not activate the water supply as long as the water level remains within this tolerance limit of the target level. An appropriate setting of this parameter can save a substantial amount of water, because quick switches between supply and discharge are avoided.

The final step in the procedure is to determine the discharge that takes place (if any) and the surface water level at the end of the time step. Discharge takes place if no supply is needed for reaching the target level. In that case the supply rate is set to zero. In the case of an automatic weir, the discharge follows simply from the water balance equation in the form given by Eq. 9.9, with $q_{sup}$ set to zero and the storage $V_{sur}^{j+1}$ set equal to the storage for the target level. The discharge $q_{dis}$ is then the only unknown left, and can be solved directly.

In the case of a fixed weir, the discharge can not be determined so easily. For the 'stage-discharge' relationship $q_{dis}(\phi_{sur})$ of a fixed weir, we use:

$$q_{dis} = \alpha_{weir} (\phi_{sur} - z_{weir})^{\beta_{weir}} \qquad (9.10)$$

in which $z_{weir}$ is the weir crest level (cm), $\alpha_{weir}$ is the discharge coefficient ($cm^{1-\beta} d^{-1}$), and $\beta_{weir}$ is the discharge exponent (-). Also a table can be used to specify this relationship. The relationship should be specified for all the management periods, *including* those with management using an automatic weir. In situations with increasing discharge, at a certain moment the capacity of the automatic weir will be reached. In such situations the crest is lowered to its lowest possible position, and the water level starts to rise above the target level. This type of situation can only be simulated correctly if the lowest possible crest level has been specified, and the discharge relationship has been defined accordingly.

To determine the discharge of a fixed weir, the stage-discharge relationship has to be substituted in the water balance equation of Eq. 9.6. The (unknown) surface water level $\phi_{sur}^{j+1}$ influences both $V_{sur}^{j+1}$ and $q_{dis}$. This equation can not be solved directly because there can be a transition from a no-flow situation at the beginning of the time step to a flow situation at the end of the time step. For this reason an iterative numerical method is used to determine the new surface water level $\phi_{sur}^{j+1}$ and the discharge (see Par. 9.5).

## 9.5 Implementation aspects

***Schematization into subregions***

A simulation at subregional scale will often not stand on its own. A relatively large study area will be divided into several subregions. The boundaries of the subregion(s) should be chosen in a judicious manner. Ideally a subregion is horizontal, has the same type of soil throughout, has a regularly structured dendritic surface water system, and has a groundwater level that does not vary much in depth (a few decimeters). In practice this will hardly ever be the case. By making the subregions very small, the variation of the groundwater depth will be limited, but the number of defined subregions will increase. Another disadvantage can be that the surface water system becomes divided into units that are smaller than the basic control unit which functions in the

field. This makes it hard to translate practical water management strategies into model parameters and vice versa. It may also become difficult to compare measured and simulated water balances with each other, which hampers model calibration. The schematization into subregions is a compromise, affected by these aspects.

***Schematisation of the surface water system***

SWAP uses at most five distinct 'orders' of channels/drains, with exactly defined channel characteristics per order. In reality, the channel characteristics will not be exactly defined. Variations of channel depths by a few decimeters are quite normal. The classification should not involve more classes than necessary, as more classes require more input data and produce more output data. If this extra data load can not be justified by a significantly better simulation result, the extra data will simply be an extra burden and hamper result interpretation.

Obtaining model input data for the smaller channels is relatively straightforward. Each order of channels can be treated as a separate single-level drainage medium, for which data can be derived using formulae given in Par. 8.4. Getting data for the large primary water courses can be more involved, especially if the spacing is at a larger scale than the subregion itself. It will then become less realistic to (for these channels) use the mean groundwater level $\phi_{avg}$. Instead, the position of the subregion with respect to two channels of the primary order should be taken into account. If, for instance, the subregion is roughly midway between two such channels, the drainage resistance for the maximum groundwater level $\phi_{gwl}$ should be used, but only for these large channels, not for the rest of the surface water system. In such a case it is obvious that the surface water level in the primary channel is determined by the water balance on a scale that is much larger than that of the subregion. It is then also appropriate to model the primary channel as being separate from the rest of the surface water system.

An alternative way of making a schematization of the surface water system is by analysis of experimental data. In Fig. 9.6 the results are shown of field measurements by Massop and De Wit (1994) for the Beltrum area. A discharge unit was identified and measurements were made of:

- total surface area;
- discharge at the outlet;
- mean groundwater level.

From Fig. 9.6 one can see that the drainage base of the larger channels is roughly at $z$ = -120 cm, as no discharges were measured below that level.

*Fig. 9.6 Discharge $q_{drain}$ as function of mean phreatic surface $\phi_{avg}$ in the Beltrum area (Massop and de Wit, 1994)*

The schematized $q_{drain}(\phi_{avg})$-relationship is a piece-wise linear function, with

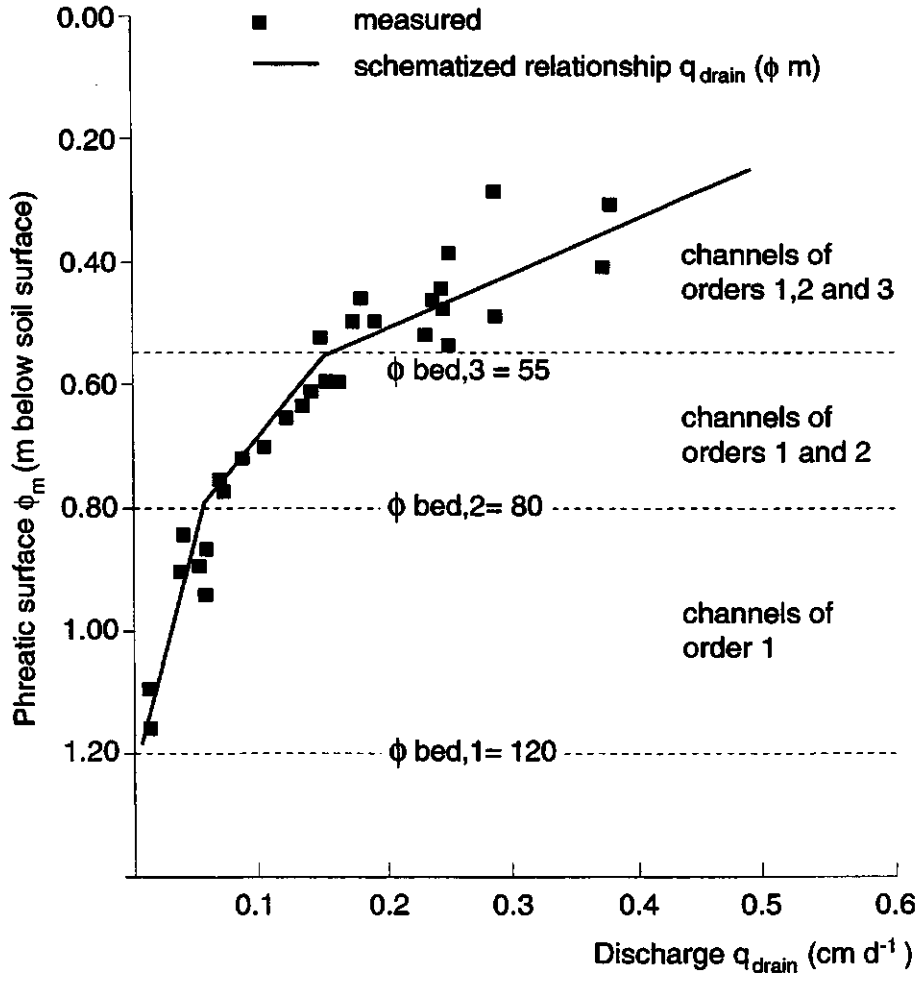


transition points at mean groundwater levels of 80 and 55 cm below soil surface. These transition points correspond to the 'representative' bed levels of the second and third order channels. The drainage resistance of the first order channels can be derived from the transition point at $z$ = -80 cm in the following manner:

$$q(-80) = 0.05 = \frac{\phi_{avg} - \phi_{d,1}}{\gamma_{d,1}} = \frac{-80+120}{\gamma_{d,1}} \qquad (9.11)$$

which gives $\gamma_{d,1}$ = 800 d. The drainage resistance of the second-order channels follows subsequently from:

$$q(-55) = 0.15 = \frac{\phi_{avg} - \phi_{d,1}}{\gamma_{d,1}} + \frac{\phi_{avg} - \phi_{d,2}}{\gamma_{d,2}} = \frac{-55+120}{800} + \frac{-55+80}{\gamma_{d,2}} \qquad (9.12)$$

which results in $\gamma_{d,2}$ = 365 d. Analogously, the drainage resistance of the third-order channels can be derived: $\gamma_{d,3}$ = 135 d.

***Numerical schemes***

The land surface model, in which the Richards' equation is solved, and the surface water model are coupled by means of an *explicit* numerical scheme. In other words, the surface water level update and the calculation of the drainage fluxes do *not* interact with the calculation of the soil water content and the groundwater level *within a time step.* Thus the drainage fluxes are computed using the groundwater level and the surface water level at the *beginning* of a time step. The surface runoff (or runon), however, is computed with Eq. 9.5 using more up-to-date information: the ponding height $h_{pond}$ at the *end* of a time step is used. This is made possible by the sequence of calculations in SWAP for situations with total saturation and ponding at the soil surface:

- first the Richard's equation is solved for the soil profile, with prescribed head $h = h_{pond}$ at the soil surface;
- next the ponding depth $h_{pond}$ is updated from the water balance of the total soil profile, including surface runoff.

Explicit numerical schemes have the disadvantage that the computed levels can become unstable. To reduce the chance of oscillations in the simulated levels, the program reduces the time step automatically as soon as the ponding starts. If the specified 'ponding sill' has been set to zero, however, the first time step with surface runoff may lead to instability, because the time step is reduced from the second time step after ponding onwards. The user can avoid this instability by specifying a non-zero value for the maximum ponding depth, e.g. of 1 cm.

For computing the surface water level in situations with a fixed weir, an equation has to be solved involving a look-up table (storage as a function of surface water level) and an exponential discharge relationship (discharge of weir as a function of the surface water level). We use an implicit iterative procedure for this, involving the surface water level at the *end* of the time step. This scheme has the advantage of being very stable. The disadvantage is that the computed discharge might deviate from the 'average' discharge during the time step. But since the used time steps are relatively small (<0.2 d), the loss of accuracy is not significant.

It can nevertheless be possible, even without surface runoff, that the simulated surface water and groundwater levels become unstable. SWAP warns the user if large oscillations of surface or groundwater levels occur. In such a case the user should reduce the maximum time step. In general, a time step of 1/50 of the smallest drainage resistance (Par. 9.3) should lead to a stable simulation. If, however, the surface water system is highly reactive to drainage flows, an even smaller time step may be required.

# 10 Fate of discharge water in a regional system

Following the discussion in Chapter 9, the drain densities of a three level drainage system are defined as:

$$M_1 = \frac{\Sigma l_1}{A_{reg}}; \qquad M_2 = \frac{\Sigma l_2}{A_{reg}}; \qquad M_3 = \frac{\Sigma l_3}{A_{reg}} \tag{10.1}$$

where $A_{reg}$ ($cm^2$) is the area of the subregion, $\Sigma l_1$, $\Sigma l_2$ and $\Sigma l_3$ are the total lengths (cm) of respectively the first, second and third order drains and $M_1$, $M_2$, $M_3$ are the drainage densities ($cm^{-1}$) of respectively the first order, the second order and the third order drainage system. The drainage fluxes $q_{d,1}$, $q_{d,2}$ and $q_{d,3}$ (cm $d^{-1}$) are calculated by linearized flux-head relationships (see Eq. 9.3):

$$q_{d,1} = \frac{\phi_{avg} - \phi_{d,1}}{\gamma_1}; \qquad q_{d,2} = \frac{\phi_{avg} - \phi_{d,2}}{\gamma_2}; \qquad q_{d,3} = \frac{\phi_{avg} - \phi_{d,3}}{\gamma_3} \tag{10.2}$$

where $\phi_{avg}$ is the regional averaged groundwater level (cm), $\phi_{d,i}$ the drainage hydraulic head (cm) of drainage system order $i$, and $\gamma_i$ the drainage resistance (d) of drainage system order $i$. This drainage concept is schematically illustrated in Fig. 10.1, depicting a linear reservoir model with outlets at different heights.

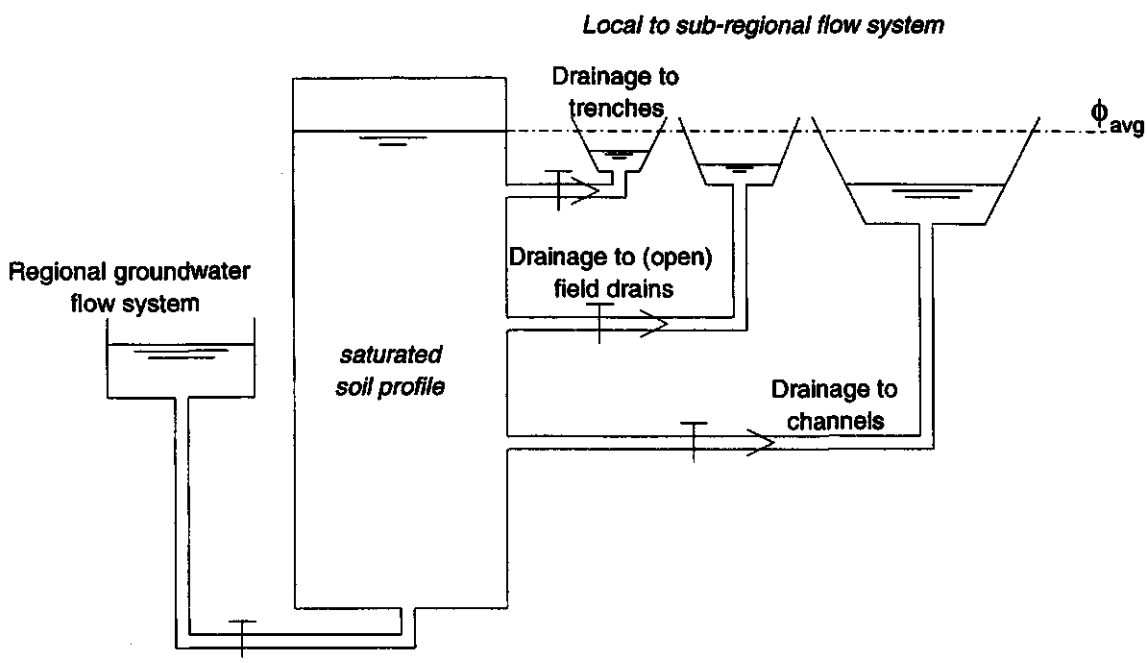


*Fig. 10.1 Illustration of regional drainage concept. The resistance mainly consists of radial and entrance resistance near the drainage devices*

## 10.1 The horizontal groundwater flux

One-dimensional leaching models generally represent a vertical soil column. Within the unsaturated zone, chemical substances are transported by vertical water flows, whereas in the saturated zone the drainage discharge leaves the vertical column side-ways. For example in the ANIMO model (Rijtema et al., 1997), the distribution of lateral drainage fluxes with depth has been used to simulate the response of the load of chemicals on the surface water system to the inputs in the groundwater system. In this section, the concept for a distribution of lateral drainage fluxes with depth in an one-dimensional hydrological simulation model will be described. The following assumptions are made:

- steady groundwater flow and homogeneous distribution of recharge rates by rainfall;
- the aquifer has a constant thickness.

For convenience, only three levels of drains are considered, although the concept discussed here is valid for a system having any number of drainage levels.

Van Ommen (1986) has shown that for simple single level drainage systems, the travel time distribution is independent from the size and the shape of the recharge area. Under these assumptions, the average concentration of an inert solute in drainage water to a well or a watercourse, can mathematically be described by the linear behaviour of a single reservoir. This behaviour depends only on the groundwater recharge rate, the aquifer thickness and its porosity.

The non-homogeneous distribution of exfiltration points as well as the influence of chemical reactions on the concentration behaviour necessitates to distinguish between the hydraulic and chemical properties of different soil layers. In the drainage model, which describes the drainage discharge to parallel equidistant water courses, the discharge flow of system $i$, $Q_{d,i}$ is calculated as:

$$Q_{d,i} = L_i \, q_{d,i} \tag{10.3}$$

where $L_i$ is the spacing of drainage system $i$. According to the Dupuit-Forcheimer assumption, the head loss due to radial flow and vertical flow can be ignored in the largest part of the flow domain. Following this rule, the ratio between occupied flow volumes $V_i$ can be derived from the proportionality between flow volumes and discharge rates:

$$\frac{V_i}{V_{i-1}} = \frac{Q_{d,i}}{Q_{d,i-1}} \tag{10.4}$$

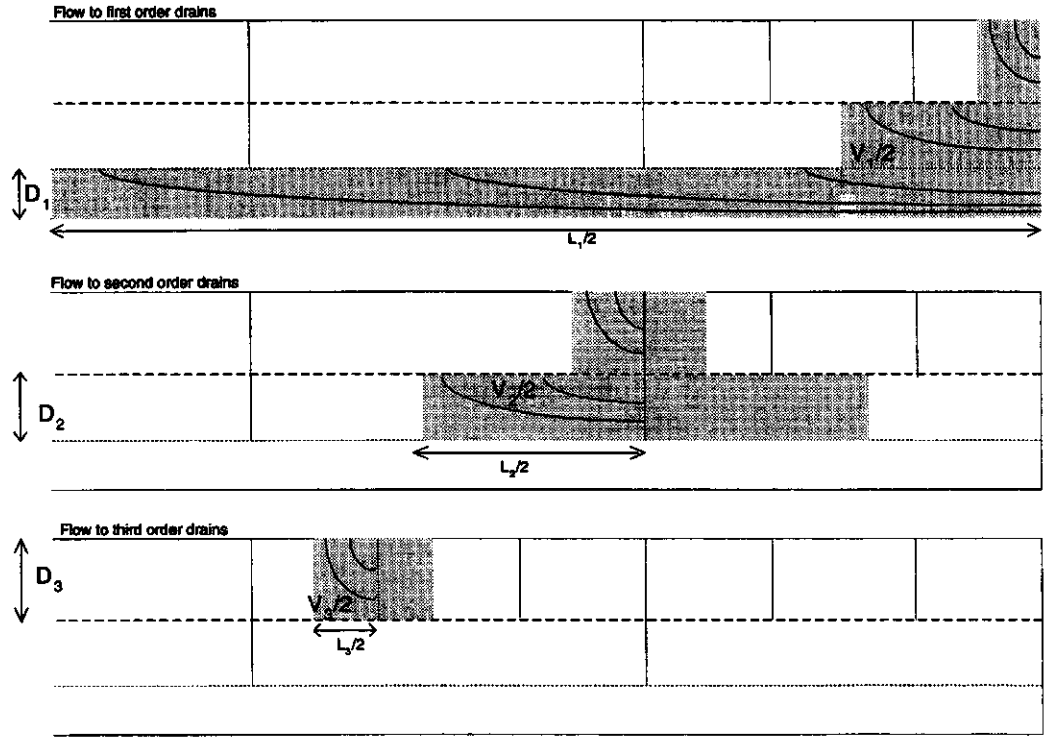


*Fig. 10.2 Schematization of regional groundwater flow to drains of three different orders*

First order drains act also as field ditches and trenches and next higher drains act partly as third order drains. In the SWAP-model the lumped discharge flux per drainage system is computed from the relation between groundwater elevation and drainage resistance. Figure 10.2 shows the schematization of the regional groundwater flow, including the occupied flow volumes for the nested drain systems. The volume $V_i$ consists of summed rectangles $L_iD_i$ of superposed drains, where $D_i$ is the thickness (cm) of discharge layer *i*.

The flow volume $V_i$ assigned to drains of order 1, 2 and 3 is related to drain distances $L_i$ and thickness $D_i$ of discharge layers as follows:

$$V_1 = L_1 D_1 + L_2 D_2 + L_3 D_3 \tag{10.5}$$

$$V_2 = L_2 D_2 + L_3 D_3 \tag{10.6}$$

$$V_3 = L_3 D_3 \tag{10.7}$$

Rewriting Eq. 10.5 to 10.7 and substituting Eq. 10.3 and Eq. 10.4 yields an expression which relates the proportions of the discharge layer to the discharge flow rates:

$$L_1 D_1 : L_2 D_2 : L_3 D_3 = (q_{d,1} L_1 - q_{d,2} L_2) : (q_{d,2} L_2 - q_{d,3} L_3) : (q_{d,3} L_3) \tag{10.8}$$

In theory, the terms $q_{d,1} L_1 - q_{d,2} L_2$ and $q_{d,2} L_2 - q_{d,3} L_3$ can take negative values for specific combinations of $q_{d,1} L_1$, $q_{d,2} L_2$ and $q_{d,3} L_3$. When $q_{d,1} L_1 - q_{d,2} L_2 < 0$ it is assumed that $D_1$ will be zero and the nesting of superposed flows systems on top of the flow region assigned to drainage class 1 will not occur. Likewise, a separate nested flow region related to a drainage class will not show up when $q_{d,2} L_2 - q_{d,3} L_3 < 0$. These cases are depicted schematically in Fig. 10.3.

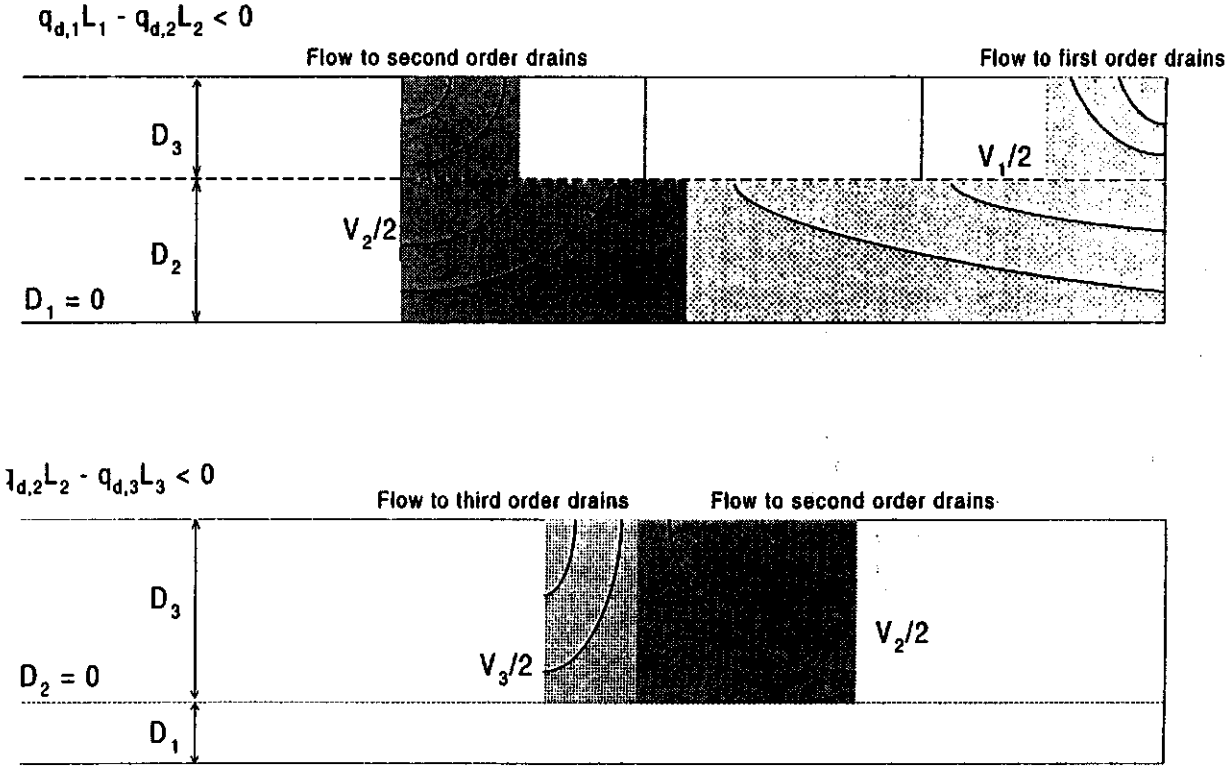


*Fig. 10.3 Schematization of regional groundwater flow to drains of three orders when either $q_{d,1}L_1 - q_{d,2}L_2 < 0$ or $q_{d,2}L_2 - q_{d,3}L_3 < 0$*

If the soil profile is heterogeneous with respect to horizontal permeabilities, the heterogeneity can be taken into account by substituting transmissivities $kD$ for layer thicknesses in Eq. 10.8:

$$(kD)_1 : (kD)_2 : (kD)_3 = \left(\frac{q_1 L_1 - q_2 L_2}{L_1}\right) : \left(\frac{q_2 L_2 - q_3 L_3}{L_2}\right) : \left(\frac{q_3 L_3}{L_3}\right) \qquad (10.9)$$

The thickness of a certain layer can be derived by considering the vertical cumulative transmissivity relation with depth as shown in Fig. 10.4.

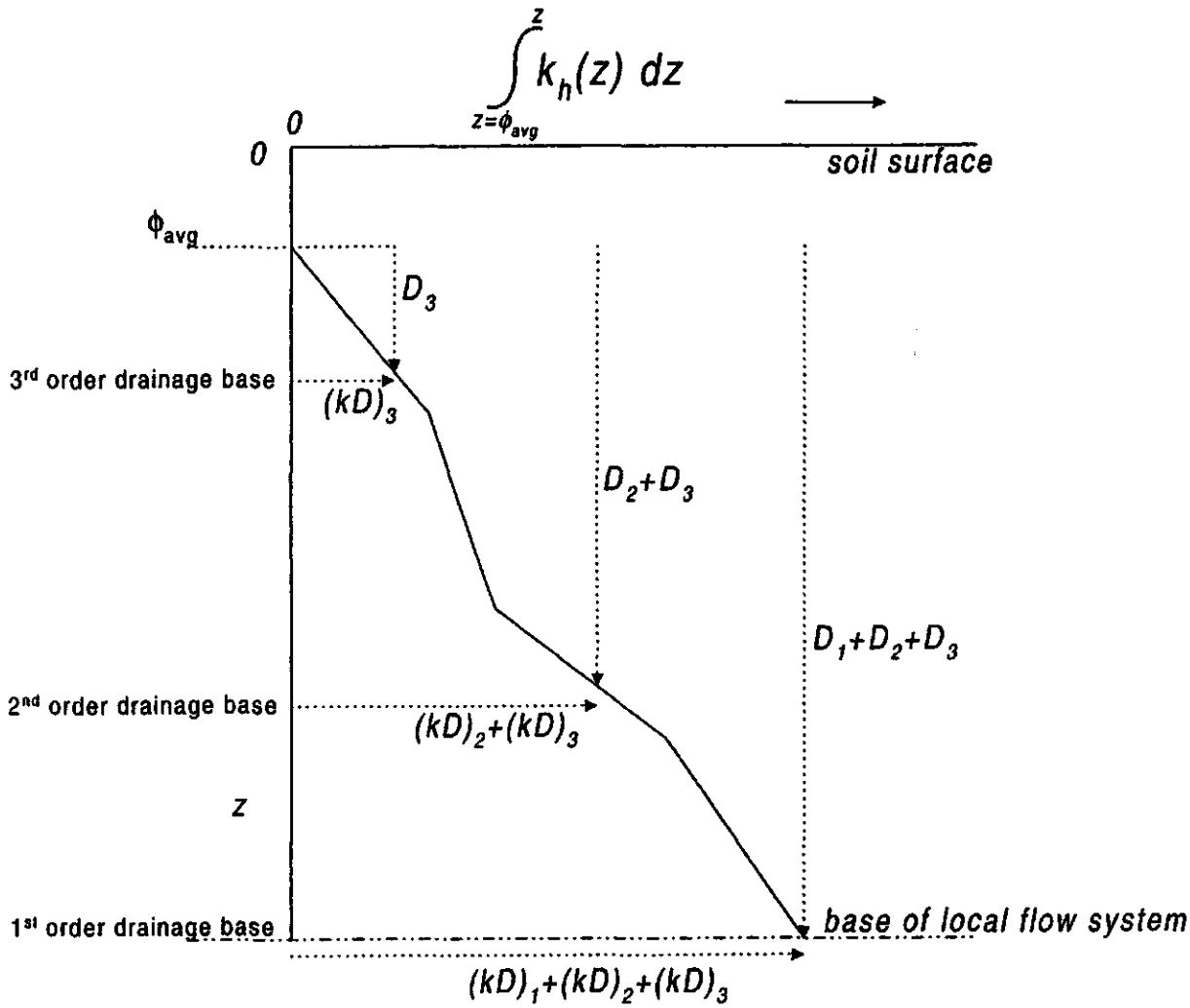


*Fig. 10.4 Discharge layer thickness $D_i$ as function of cumulative transmissivity $kD_i$ in a heterogeneous soil profile*

The lateral flux relation per unit soil depth shows a uniform distribution. Lateral drainage fluxes $q_{d,k,i}$ to drainage system $k$ for each nodal compartment $i$ of the simulation model are calculated by:

$$q_{d,1,i} = q_{d,1} \frac{k_{h,i}\Delta z_i}{\sum_{I_{z=-D_1-D_2-D_3}}^{I_{z=\phi_{avg}}} k_{h,i}\Delta z_i} \quad \text{for} \quad -D_1 - D_2 - D_3 < z < \phi_{avg} \tag{10.10}$$

$$q_{d,2,i} = q_{d,2} \frac{k_{h,i}\Delta z_i}{\sum_{I_{z=-D_2-D_3}}^{I_{z=\phi_{avg}}} k_{h,i}\Delta z_i} \quad \text{for} \quad -D_2 - D_3 < z < \phi_{avg} \tag{10.11}$$

$$q_{d,3,i} = q_{d,3} \frac{k_{h,i} \Delta z_i}{\sum_{i_{z=-D_3}}^{i_{z=\phi_{avg}}} k_{h,i} \Delta z_i} \quad \text{for} \quad -D_3 < z < \phi_{avg} \tag{10.12}$$

where $k_{h,i}$ is the horizontal conductivity (cm $d^{-1}$) of compartment $i$, $\Delta z_i$ is the thickness (cm) of compartment $i$, and $i_{z=-D1-D2-D3}$ and $i_{z=\phi avg}$ are resp. the numbers of the bottom compartment and the compartment in which the regional groundwater level is situated. Water quality models such as ANIMO (Rijtema et al., 1997) compute the average concentration of discharge water which flows to a certain order drainage system on the basis of these lateral fluxes. The avering rules are:

$$\bar{c}_1 = \frac{\sum_{i=n_{z=\phi_{avg}}}^{n_{z=-D_1-D_2-D_3}} q_{d,1,i}\, c_i}{q_{d,1}} \tag{10.13}$$

$$\bar{c}_2 = \frac{\sum_{i=n_{z=\phi_{avg}}}^{n_{z=-D_2-D_3}} q_{d,2,i}\, c_i}{q_{d,2}} \tag{10.14}$$

$$\bar{c}_3 = \frac{\sum_{i=n_{z=\phi_{avg}}}^{n_{z=-D_3}} q_{d,3,i}\, c_i}{q_{d,3}} \tag{10.15}$$

Using these average concentrations computed by a leaching model, the average concentration $c_R$ at the scale of a sub-region is calculated as:

$$\bar{c}_R = \frac{q_{d,1}\,\bar{c}_1 + q_{d,2}\,\bar{c}_2 + q_{d,3}\,\bar{c}_3}{q_{d,1} + q_{d,2} + q_{d,3}} \tag{10.16}$$

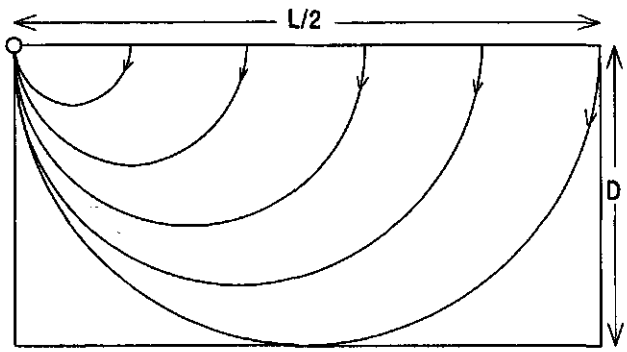


*Fig. 10.5 Flow field to a drain with half circular shaped stream lines*

## 10.2 Maximum depth of a discharge layer

For the purpose of water quality simulations, the thickness of a model discharge layer has to be limited to a certain depth. In the water quality model, the maximum thickness $D$ of a discharge layer has been set at:

$$D \leq \frac{L}{4} \tag{10.17}$$

This rule of thumb is based on the assumption of a half-circular shape of streamlines in a flow field (Fig. 10.5). The deepest streamline which arrives in the drain, originates from a point at distance *L/2*. It can be seen that following to the circular shape, the horizontal distance *L/2* corresponds to the length *2D*.

### *Homogeneous anisotropic soil profile*

In the saturated zone, the horizontal permeability is often larger than the vertical permeability. General assumptions to deal with the transformation of the anisotropic conditions of a two-dimensional flow field are:

- hydraulic heads and flow rates are the same as in an isotropic situation
- x-coordinate: $x' = x\sqrt{(k_v/k_h)}$
- z-coordinate: $z' = z$
- permeability: $k' = \sqrt{(k_v\, k_h)}$

where the primes denote the transformed values of an anisotropic condition. Applying these assumptions to the relation between thickness of the discharge layer $D$ and the horizontal drain distance $L$ yields:

$$D' \leq \frac{L'}{4} \qquad \Rightarrow \qquad D \leq \frac{L}{4}\sqrt{\frac{k_v}{k_h}} \tag{10.18}$$

At first sight, this condition does not agree with the 'penetration depth' derived by Zijl and Nawalany (1993) for the estimation of the order of magnitude of the characteristic depth of the flow problem in case of a single layer model. However, these authors consider the wave length of an assumed sinusoidal shaped phreatic head. This assumption does not hold for most of the flow systems where only 1 or 2% of the area shows an upward discharge flux at the phreatic level. Transforming the wave length variable given by Zijl and Nawalany (1993) to the characteristic distance relevant for drainage systems (L/2) and taking into account the sinusoidal function can fully explain the difference between Eq. 10.18 and the 'penetration depth'.

***Heterogeneous anisotropic soil profile***

For heterogeneous soil profiles, an average value for the anisotropic factor $\sqrt{(k_v/k_h)}$ has to be considered. The average horizontal and vertical conductivity is calculated as:

$$\bar{k}_h = \frac{\sum_{l_{z=\phi_{avg}}}^{l_{z=-D_1-D_2-D_3}} k_{h,i}\Delta z_i}{\sum_{l_{z=\phi_{avg}}}^{l_{z=-D_1-D_2-D_3}} \Delta z_i} \qquad (10.19)$$

$$\bar{k}_v = \frac{\sum_{l_{z=\phi_{avg}}}^{l_{z=-D_1-D_2-D_3}} \Delta z_i}{\sum_{l_{z=\phi_{avg}}}^{l_{z=-D_1-D_2-D_3}} \frac{\Delta z_i}{k_{v,i}}} \qquad (10.20)$$

and the maximum depth of the discharge layer bottom:

$$D \leq \frac{L}{4}\sqrt{\frac{\bar{k}_v}{\bar{k}_h}} \qquad (10.21)$$

The assumption of cylindrical shaped streamlines is an abstraction of the actual streamline pattern. The condition ($D \leq L/4$) based on this model assumption is most relevant at large $D/L$ ratios. Ernst (1973) provides a mathematical formulation of a streamline pattern in a saturated soil profile of infinite thickness. Such a hydrological situation can be seen as the most extreme situation for evaluating the influence of the $D/L$-ratio. In reality, the drainage flow will occupy less space in the saturated groundwater body and the flow paths will be less deep. The streamlines can be described as:

$$\Psi(x,z) = \frac{q_0}{\pi} \arctan\left(\frac{e^{2\pi\frac{-z}{L}}\sin(2\pi\frac{x}{L})}{e^{2\pi\frac{-z}{L}}\cos(2\pi\frac{x}{L})-1}\right) \qquad (10.22)$$

where $\psi(x,z)$ is the stream function and $q_0$ is the discharge flow rate which originates from the area between $x = 0$ en $x = L/2$. The streamline pattern is shown graphically in Fig. 10.6, where the water enters the groundwater body along the line $z = 0$ and the water is discharged by a drain at (0,0).

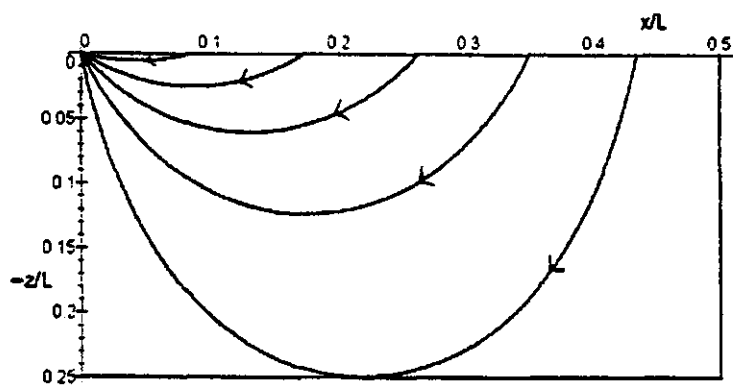


*Fig. 10.6 Stream line pattern in a groundwater system of infinite thickness*

The majority of the precipitation surplus does not reach the line at depth -z/D = 0.25. In this soil column, imaginary horizontal planes at $z = -D$ can be considered. The streamline with its deepest point at $-z/D = 1$, but not intersecting the line $z = -D$, bounds the stream zone which will never be found below $z = -D$. The following condition holds for the streamline with its tangent-line at $z = -D$:

$$\frac{\partial \Psi(x,D)}{\partial x} = 0 \qquad (10.23)$$

Evaluation of this expression yields a value for the horizontal coordinate of the point of contact between the streamline and the line $z = -D$. Together with the value $z = -D$, the horizontal distance can be substituted into the general stream function equation. This action yields a flow fraction $\psi/q_0$ of the total drainage discharge which will never be found below the line $z = -D$. This flow fraction is graphically depicted as a function of depth in Fig. 10.7. The depth has been transformed to a fraction of the drain distance to summarize all possible relations into one graph.

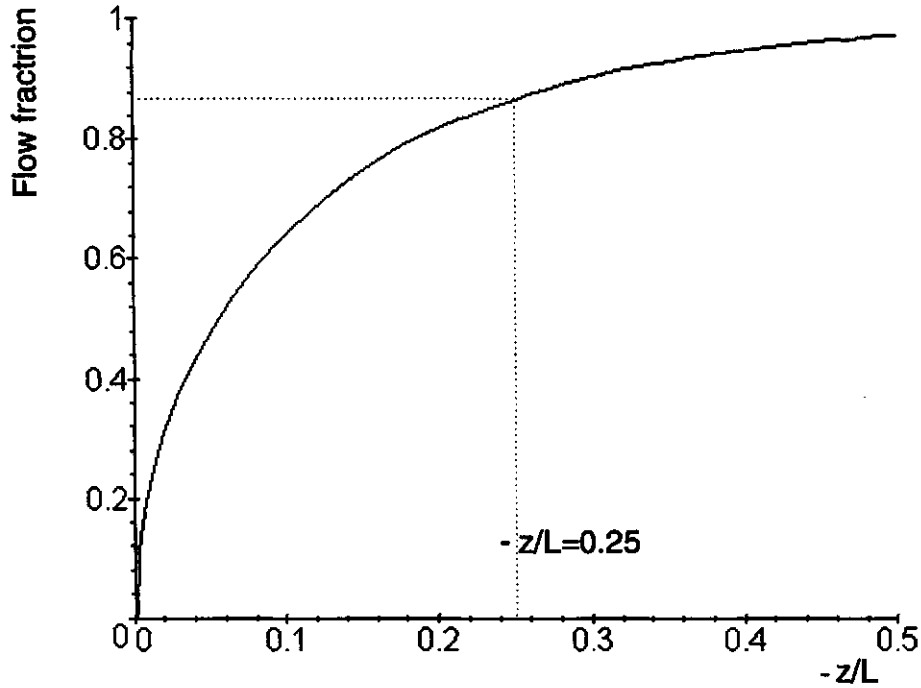


*Fig. 10.7 Fraction of total drain discharge flowing above level -z/l, where L is the drain spacing*

In a soil profile with infinite thickness, about 87% of the total drain discharge is conveyed above the plane at $z = -L/4$. In a deep soil profile with finite thickness, more than 87% of the total drain discharge will be transported above this plane.

## 10.3 Concentration of solutes in drainage water

The discharge layer approach assumes a uniform function of the lateral flux intensity with depth. Therefore, the vertical flux as a function of depth for a single drainage system can be described by a linear relation:

$$q(z) = \epsilon \frac{dz}{dt} = (1 + \frac{z}{D})\, q_{drain} + q_{bot} \qquad (10.24)$$

where $\varepsilon$ is the soil porosity (-), $q$ the vertical flux (cm $d^{-1}$) and $q_{bot}$ the vertical flux across the lower boundary of the soil profile. The relations hold between the phreatic level at $z = \phi_{avg}$ and the lower boundary at $z = -D$ (m). This equation can be used to derive the residence time $T$ (d) as a function of depth, provided $t = T_0$ at $z = \phi_{avg}$:

$$T = T_0 + \frac{\epsilon D}{q_{drain}} \ln \frac{q(\phi_{avg})}{q(z)} \qquad (10.25)$$

Streamlines can be described mathematically by a stream function. For a two-dimensional transect between parallel drains, assuming a zero flux at the bottom of the aquifer and a negligible radial flow in the vicinity of the drains, the stream function $\psi(x,z)$ can be given as a function of depth $z$ and distance $x$ relative to the origin at the bottom of the aquifer, as depicted in Fig. 10.8:

$$\psi(x,z) = -\frac{R}{D} x(D+z) \qquad (10.26)$$

where $R$ is the net recharge and $D$ is the thickness of the homogeneous layer.

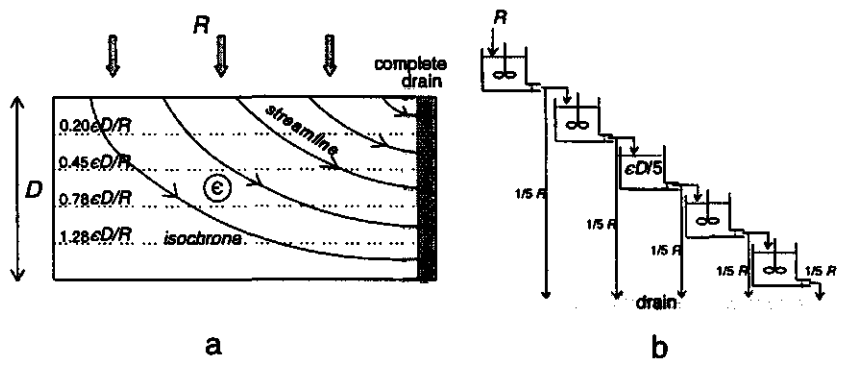


*Fig. 10.8 (a) Streamlines and isochrones of a soil profile with complete drains and (b) schematization of the flow pattern by a cascade of perfectly mixed reservoirs*

Construction of isochrones for solute displacement after uniform infiltration at the phreatic level yields horizontal lines, because the vertical fluxes do not depend on the horizontal distance relative to the origin. In the model, the isochrones are regarded as imaginary boundaries between soil layers.

Each of the soil layers may be regarded as a perfectly mixed reservoir. Part of the inflow is conveyed to underlying soil layers, the remainder flows horizontally to the water course or drainage tube. Assuming a steady state situation and equal distances between the soil layers, the displacement of a non-reactive solute through this system may be described by a set of linear differential equations. For the first reservoir, the following equation applies:

$$\frac{\varepsilon D}{N}\frac{dc_1}{dt} = Rc_{inp} - Rc_1 \qquad (10.27)$$

where $N$ is the number of soil layers and $c_{inp}$ is the input concentration. For an arbitrary reservoir $i$, the change in concentration is described by:

$$\frac{\varepsilon D}{N}\frac{dc_i}{dt} = \frac{N-i+1}{N} R\, c_{i-1} - \frac{N-i+1}{N} R\, c_i \qquad (10.28)$$

Assuming an initial concentration $c_0$ uniform over the entire depth, the solution to the differential equations yields the concentration course over time in reservoir $j$:

$$\frac{c_j(t) - c_{inp}}{c_0 - c_{inp}} = \sum_{i=1}^{j} \binom{N}{i-1} \binom{N-j}{j-i} (-1)^{j+1}\, e^{-(N-i+1)\frac{R}{\varepsilon D}t} \qquad (10.29)$$

Since the outflows of all reservoirs are assumed to be equal, the resulting concentration in drainage discharge can be found as the average of all reservoirs. Lengthy, but straight forward algebraic summation of the binomial series in Eq. 10.29 yields a simple relation for the concentration in drainage water:

$$\frac{c_d(t) - c_{inp}}{c_0 - c_{inp}} = \frac{1}{N} \sum_{j=1}^{N} \frac{c_j(t) - c_{inp}}{c_0 - c_{inp}} = e^{-\frac{R}{\varepsilon D} t} \qquad (10.30)$$

This relation is also found if the concentration in the drainage water is modelled by describing the groundwater system as one perfectly stirred reservoir. Breakthrough curves of the individual reservoirs as denoted in Fig. 10.8 are presented in Fig. 10.9. The flow averaged concentration (indicated by circles) fits to the concentration relation as has been given in Par. 3.5 for the single reservoir approach. Overall effects of vertical dispersion which are introduced by defining distinct soils layers can thus be described by using one single reservoir. For the single drainage system, the simulation of solute migration by describing a vertical column with uniform lateral outflow agrees with the solutions found by Gelhar and Wilson (1974), Raats (1978) and Van Ommen (1986).

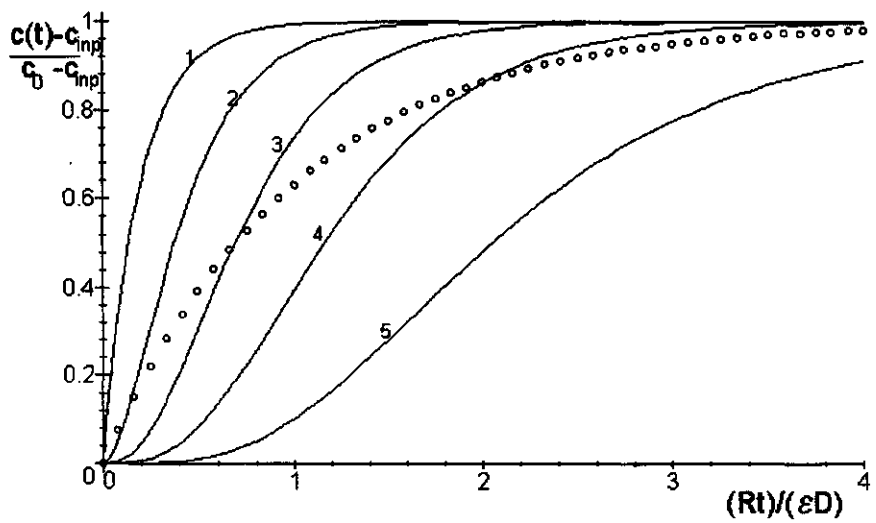


*Fig. 10.9 Step response of outflow concentrations per soil layer (numbered lines) and step response of the averaged concentration which enters the drains (circles)*

## 10.4 Discussion

As a consequence of a number assumptions and schematization of the flow pattern, the model user should be aware of the following limitations:

- assumption of steady state during the time increment;
- constant depth of the drainage base;
- assumption of perfect drains;
- uniform thickness of the hydrological profile.

In most of the applications of the regional water quality model, the time step is set at 1 day up to 10 days. During an interval of 10 days, the drainage flux may vary as a result of variation of the meteorological conditions. For chemical substances which are bounded in the upper soil layers, the assessment of the solute discharge to the surface water may lead to considerable inaccuracies.

The boundary between the groundwater flow affected by the 'local' drainage system and the regional flow can be defined as the depth in the soil profile below which no direct discharge to surface water occurs (Fig. 10.2). Above this depth, the larger part of the precipitation surplus flows to water courses and other drainage systems. This boundary depends on the deepest streamline discharging water to the drainage systems. It can be expected that the size of the subregion influences the depth of the boundary surface. With larger schematized areas, discharge water can originate from greater distances, having deeper streamlines. The influence of the seasonal variation of trans-boundary fluxes at the lower boundary of the modelled soil profile is not considered.

The uniform distribution of the lateral flux pattern is based on the assumption of perfect drains. In reality, the flow pattern converges in the surrounding area of the drain. The soil profile has a uniform depth. When the height difference between maximum groundwater level and drainage level is larger than a certain fraction of the depth of the saturated profile, this assumption may not be valid. In theory, these effects can be simulated by defining a correction function for the lateral flux relation with depth. From the point of view of data acquisition and validation of hydro-geological parameters, refinement of this relationship is questionable.

The Dupuit-assumption has been applied implicitly by assuming horizontal discharge layers. The discharge layer which corresponds to the channel system has been defined as a horizontal layer at the bottom of the local flow system. In reality, the water discharging to canals at larger distances infiltrates into the saturated zone. This water takes up some space in the upper zone of the groundwater system. A way to validate the 'discharge layer' approach presented above is by comparing a set of simulation results with the outcome of three dimensional streamline models at regional scale.

## References


Allen, R.G., M.E. Wright and R.D. Burman, 1989. Operational estimates of evapotranspiration. Agron. J., 81, 650-662.

Allen, R.G., 1991. REF-ET Reference evapotranspiration calculator, version 2.1. Utah State University, Logan, 39 pp.

Angus, J.F., R.B. Cunningham, M.W. Moncur and D.H. Mackenzie, 1981. Phasic development in field crops. I. Thermal response in seedling phase. Field Crops Research 3, 365-378.

Ashby, M., A.J. Dolman, P. Kabat, E.J. Moors and M.J. Ogink-Hendriks, 1996. SWAPS version 1.0. Technical reference manual. Technical document 42, Winand Staring Centre, Wageningen.

Bear, J., 1972. Dynamics of fluids in porous media. Elsevier, Amsterdam.

Belmans, C., J.G. Wesseling and R.A. Feddes, 1983. Simulation of the water balance of a cropped soil: SWATRE. J. Hydrol., 63, 271-286.

Beltman, W.H.J., J.J.T.I. Boesten and S.E.A.T.M. van der Zee, 1995. Analytical modelling of pesticide transport from the soil surface to a drinking water well. J. Hydrol., 169, 209-228.

Biggar, J.W. and D.R. Nielsen, 1976. The spatial varability of the leaching characteristics of a field soil. Water Resour. Res., 12, 78-84.

Black, T.A., W.R. Gardner and G.W. Thurtell, 1969. The prediction of evaporation, drainage, and soil water storage for a bare soil. Soil Sci. Soc. Am. J., 33, 655-660.

Boesten, J.J.T.I., 1986. Behaviour of herbicides in soil : Simulation and experimental assessment. Ph.D. thesis Winand Staring Centre, Wageningen.

Boesten, J.J.T.I. and L. Stroosnijder, 1986. Simple model for daily evaporation from fallow tilled soil under spring conditions in a temperate climate. Neth. J. Agric. Sci., 34, 75-90.

Boesten, J.J.T.I. and A.M.A. van der Linden, 1991. Modeling the influence of sorption and transformation on pesticide leaching and persistence. J. Environ. Qual., 20, 425-435.

Bolt, G.H., 1979. Movement of solutes in soils: principles of adsorption/exchange chromatography. In: G.H. Bolt (Ed.), Soil Chemistry B, Physico-Chemical Models. Elsevier, Amsterdam. p. 285-348.

Boons-Prins, E.R., G.H.J. de Koning, C.A. van Diepen and F.W.T. Penning de Vries, 1993. Crop specific simulation parameters for yield forecasting across the European Community. Simulation Rep. 32, CABO-DLO and SC-DLO, Wageningen, The Netherlands.

Bos, M.G., J. Vos and R.A. Feddes, 1996. CRIWAR 2.0. A simulation model on crop irrigation water requirements. ILRI publ. 46, Wageningen, The Netherlands.

Bouma, J., C. Belmans, L.W. Dekker and W.J.M. Jeurissen, 1983. Assessing the suitability of soils with macropores for subsurface liquid waste disposal. J. Environ. Qual. 12, 305-311.

Bouten, W., 1992. Monitoring and modelling forest hydrological processes in support of acidification research. Diss. Univ. A'dam. 218 pp.

Braden, H., 1985. Ein Energiehaushalts- und Verdunstungsmodell for Wasser und Stoffhaushaltsuntersuchungen landwirtschaftlich genutzer Einzugsgebiete. Mittelungen Deutsche Bodenkundliche Geselschaft, 42, 294-299.

Bresler, E., B.L. McNeal and D.L. Carter, 1982. Saline and sodic soils: principles, dynamics modelling. Adv. in Agr. Sciences 10, Springer Verlag. 236 pp.

Bronswijk, J.J.B. and J.J. Evers-Vermeer, 1990. Shrinkage of Dutch clay soil aggregates. Neth. J. of Agric. Sci., 38, 175-194.

Bronswijk, J.J.B., 1991. Magnitude, modeling and significance of swelling and shrinkage processes in clay soils. PhD thesis, Wageningen Agricultural University.

Bronswijk, J.J.B., W. Hamminga and K. Oostindie, 1995. Field-scale solute transport in a heavy clay soil. Water Resour. Res., 31, 517-526.

Brooks, R.H. and A.T. Corey, 1964. Hydraulic properties of porous media. Colorado State Univ., Hydrology paper no. 3, p. 27.

Brunt, D., 1952. Physical and dynamical meteorology. Second edition, University Press, Cambridge, 428 pp.

Burman, R.D., M.E. Jensen and R.G. Allen, 1987. Thermodynamic factors in evapotranspiration. In 'Proc. Irrig. and Drain. Spec. Conf.', L.G. James and M.J. English (Eds.), ASCE, Portland, Ore., July, p. 28-30.

Carrera, J. and S.P. Neuman, 1986. Estimation of aquifer parameters under transient and steady state conditions. 2. Uniqueness, stability, and solution algorithms. Water Resour. Res. 22, 211-227.

Carsel, R.F. and R.S. Parrish, 1988. Developing joint probability distributions of soil water characteristics. Water Resour. Res., 24, 755-769.

Causton, D.R. and J.C. Venus, 1981. The biometry of plant growth. Edward Arnold, London. 307 pp.

Celia, M.A., E.T. Bouloutas and R.L. Zarba, 1990. A general mass-conservative numerical solution for the unsaturated flow equation. Water Resour. Res., 26, 1483-1496.

Clausnitzer, V., J.W. Hopmans and D.R. Nielsen, 1992. Simultaneous scaling of soil water retention and hydraulic conductivity curves. Water Resour. Res., 28, 19-31.

Clothier, B.E., M.B. Kirkham and J.E. McLean, 1992. In situ measurement of the effective transport volume for solute moving through soil. Soil Sci. Soc. Am. J., 56, 733-736.

Deardorff, J.W., 1977. Efficient prediction of ground surface temperature and moisture, with inclusion of a layer of vegetation. J. Atmos. Sci., 16, 1182-1185.

Dekker, L.W. and P.D. Jungerius, 1990. Water repellency in the dunes with special reference to the Netherlands. In 'Dunes of the European Coasts', Catena Suppl., 18, 173-183.

Dekker, L.W. and C.J. Ritsema, 1994. How water moves in a water repellent sandy soil. 1. Potential and actual water repellency. Water Resour. Res., 30, 2507-2517.

De Koning, G.H.J., M.J.W. Jansen, E.R. Boons-Prins, C.A. van Diepen, F.W.T. Penning de Vries, 1993. Crop growth simulation and statistical validation for regional yield forecasting across the European Communities. Joint Research Centre of the European Communities (JRC), Ispra, Italy. Commission of the European Communities.

De Rooij, G.H., 1996. Preferential flow in water-repellent sandy soils. Model development and lysimeter experiments. Ph.D. thesis, Wageningen Agricultural University, The Netherlands, 229 p.

Desbarats, A.J., 1995. An interblock conductivity scheme for finite difference models of steady unsaturated flow in heterogeneous media. Water Resour. Res., 31, 2883-2889.

De Smedt, F. and P.J. Wierenga, 1979. A generalized solution for solute flow in soils with mobile and immobile water. Water Resour. Res., 1137-1141.

De Vries, D.A., 1975. Heat transfer in soils. In 'Heat and mass transfer in the biosphere. I. Transfer processes in plant environment', De Vries, D.A. and N.H. Afgan (eds.), Scripts Book Company, Washington D.C., p. 5-28.

De Wit, C.T. et al., 1978. Simulation of assimilation and transpiration of crops. Simulation Monographs, Pudoc, Wageningen, The Netherlands. 100 pp.

Dirksen, C., 1979. Flux-controlled sorptivity measurements to determine soil hydraulic property functions. Soil Sci. Soc. Am. J., 43, 827-834.

Dirksen, C., 1991. Unsaturated hydraulic conductivity. In 'Soil analysis, physical methods', K.A. Smith and C.E. Mullins (eds), Marcel Dekker, New York, p. 209-269.

Dirksen, C., J.B. Kool, P. Koorevaar and M.Th. van Genuchten, 1993. Hyswasor: simulation model of hysteretic water and solute transport in the root zone. In: D. Russo and G. Dagan (Eds.), Water flow and solute transport in soils. Springer-Verlag, Adv. Series in Agric. Sci., 20, 99-122.

Dirksen, C. and S. Matula, 1994. Automatic atomized water spray system for soil hydraulic conductivity measurements. Soil Sci. Soc. Am. J., 58, 319-325.

Doorenbos, J. and W.O. Pruitt, 1977. Guidelines for predicting crop water requirements. Irrigation and Drainage Paper 24, FAO, Rome, Italy.

Doorenbos, J. and A.H. Kassam, 1979. Yield response to water. FAO Irrigation and Drainage Paper 33, FAO, Rome, Italy.

Duffy, C.J. and D.H. Lee, 1992. Base flow response from nonpoint source contamination: simulated spatial variability in source, structure and initial condition. Water Resour. Res., 28, 905-914.

Dumm, L.D. 1954. Drain spacing formula. Agric. Engin. 35, 726-730.

Elrick, D.E. and W.D. Reynolds, 1992. Infiltration from constant-head well permeameters and infiltrometers. In 'Advances in measurement of soil physical properties: bringing theory into practice', G.C. Topp, W.D. Reynolds and R.E. Green (eds.), SSSA special publication no. 30, p. 1-24.

Ernst, L.F., 1956. Calculation of the steady flow of groundwater in vertical cross-sections. Netherlands Journal of Agricultural Science 4, 126-131.

Ernst, L.F. 1962. Groundwater flow in the saturated zone and its calculation when parallel open conduits are present. Thesis (Dutch with English summary), University of Utrecht, 189 pp.

Ernst, L.F., 1973. The determination of residence times in case of groundwater flow. Nota 755 I.C.W., now Winand Staring Centre, Wageningen (in Dutch).

Ernst, L.F. 1978. Drainage of undulating sandy soils with high groundwater tables. I en II. Journal of Hydrology 39, 1-50.

Ernst, L.F. and R.A. Feddes, 1979. Invloed van grondwateronttrekking voor beregening en drinkwater op de grondwaterstand. Report 1116, ICW (currently Winand Staring Centre), Wageningen, The Netherlands.

Feddes, R.A., 1971. Water, heat and crop growth. Ph.D. thesis, Wageningen Agricultural University, The Netherlands.

Feddes, R.A., P.J. Kowalik and H. Zaradny, 1978. Simulation of field water use and crop yield. Simulation Monographs. Pudoc. Wageningen. 189 pp.

Feddes, R.A., 1987. Crop factors in relation to Makking reference crop evapotranspiration. In 'Evaporation and weather', TNO Committee on Hydrological Research, Proceedings and information no 39, p. 33-46.

Feddes, R.A., P. Kabat, P.J.T. van Bakel, J.J.B. Bronswijk and J. Halbertsma, 1988. Modelling soil water dynamics in the unsaturated zone - state of the art. J. Hydrol., 100, 69-111.

Feddes, R.A., G.H. de Rooij, J.C van Dam, P. Kabat, P. Droogers and J.N.M. Stricker, 1993. Estimation of regional effective soil hydraulic parameters by inverse modeling. In 'Water flow and solute transport in soils: modeling and application', D. Russo and G. Dagan (eds.), Adv. Series in Agric. Sciences 20, Springer Verlag, Berlin, p. 211-231.

Feddes, R.A. and K.J. Lenselink, 1994. Evapotranspiration. In 'Drainage priciples and applications', H.P. Ritzema (ed.), ILRI publication 16, second ed., Wageningen, p. 145-174.

Flury, M. and H. Flühler, 1995. Tracer characteristics of Brilliant Blue FCF. Soil Sci. Soc. Am. J., 59, 22-27.

Francois, L.E., E.V. Maas, T.J. Donovan and V.L. Youngs, 1986. Effect of salinity on grain yield and quality, vegetative growth, and germination of semi-dwarf and durum wheat. Agron. J., 78, 1053-1058.

Gelhar, L.W. and J.L. Wilson, 1974. Groundwater quality modeling. Ground Water, 12, 399-408.

Gerke, H.H. and M.Th van Genuchten, 1993. A dual-porosity model for preferential movement of water and solutes in structured porous media. Water Resour. Res., 29, 305-319.

Goudriaan, J., 1977. Crop meteorology: a simulation study. Simulation monographs, Pudoc, Wageningen.

Goudriaan, J., 1982. Some techniques in dynamic simulation. In 'Simulation of plant growth and crop production', F.W.T. Penning de Vries and H.H. van Laar (Eds.), Simulation Monographs, Pudoc, Wageningen, p. 66-84.

Groen, K.P., 1997. Pesticide leaching in polders. Field and model studies on cracked clays and loamy sand. PhD thesis, Wageningen Agricultural University, Wageningen, The Netherlands, 296 pp.

Groenendijk, P. and J.G. Kroes, 1997. Modelling the nitrogen and phosphorus leaching to groundwater and surface water; ANIMO 3.5. Report 144, DLO Winand Staring Centre, Wageningen.

Hadley, P., E.H. Roberts, R.J. Summerfield and F.R. Minchin, 1984. Effects of temperature and photoperiod on flowering in soya bean: a quantitative model. Annals of Botany, 53, 669-681.

Harrison, L.P., 1963. Fundamental concepts and definitions relating to humidity. In 'Humidity and moisture', A. Wexler (Ed.), Vol. 3, Reinhold Publishing Company, New York.

Haverkamp, R., M. Vauclin, J. Touma, P.J. Wierenga and G. Vachaud, 1977. A comparison of numerical simulation models for one-dimensional infiltration. Soil Sci. Soc. Am. J., 41, 285-294.

Haverkamp, R., and M. Vauclin, 1979. A note on estimating finite difference interblock hydraulic conductivity values for transient unsaturated flow problems. Water Resour. Res., 15, 181-187.

Hijmans, R.J., I.M. Guiking-Lens and C.A. van Diepen, 1994. User's guide for the WOFOST 6.0 crop growth simulation model. Technical Document 12, Winand Staring Centre, Wageningen, The Netherlands, 144 p.

Hillel, D., 1980. Fundamentals of soil physics. Academic Press, San Diego, CA, 412 p.

Hooghoudt, S.B., 1940. Algemene beschouwing van het probleem van de detailontwatering en de infiltratie door middel van parallel lopende drains, greppels, sloten en kanalen. Versl. Landbouwk. Onderz., 46, B, 193 pp.

Hopmans., J.W., and J.H. Dane, 1986. Combined effects of hysteresis and temperature on soil-water movement. J. Hydrol., 83, 161-171.

Hopmans, J.W., and J.N.M. Stricker, 1989. Stochastic analysis of soil water regime in a watershed. J. Hydrol., 105, 57-84.

Hopmans, J.W., J.C. van Dam, S.O. Eching and J.N.M. Stricker, 1994. Parameter estimation of soil hydraulic functions using inverse modeling of transient outflow experiments. Trends in Hydrology, 1, 217-242.

Hornung, U., and W. Messing, 1983. Truncation errors in the numerical solution of horizontal diffusion in saturated/unsaturated media. Adv. Water Resour., 6, 165-168.

Huang, K., B.P Mohanty and M.Th. van Genuchten, 1996. A new convergence criterion for the modified Picard iteration method to solve the variably saturated flow equation. J. Hydrol., 178, 69-91.

Hunt, E.R., J.A. Weber and D.M. Gates, 1985. Effects of nitrate application on Amaranthuspowellii Wats. I. Changes in photosynthesis, growth rates, and leaf area. Plant Physiology 79, 609-613.

Jacucci, G., P. Kabat, L. Pereira, P. Verrier, P. Steduto, C. Uhrik, G. Bertanzon, J.Huygen, B. van den Broek, J. Teixeira, R. Fernando, G. Giannerini, F. Carboni, M. Todorovic, G. Toller, G. Tziallas, E. Fragaki, J. Vera Munoz, D. Carreira, P. Yovchev, D. Calza, E. Valle and M. Douroukis, 1994. The Hydra Project: a Decision Support System for Irrigation Water Management. Proceedings of the International Conference on Land and Water Resources Management in the Mediterranean Region. 4-8 September 1994, Valenzano (Bari), Italy.

Jaynes, D.B., 1984. Comparison of soil water hysteresis models. J. Hydrol., 75, 287-299.

Jensen, M.E., R.D. Burman and R.G. Allen, 1990. Evapotranspiration and irrigation water requirements. ASCE manuals and reports on enigineering practice 70, ASCE, New York. 332 pp.

Jury, W.A., 1982. Simulation of solute transport using a transfer function mode. Water Resour. Res., 18, 363-368.

Jury, W.A., D. Russo and G. Sposito, 1987. The spatial variability of water and solute transport properties in unsaturated soil, II Scaling of water transport. Hilgardia, 55, 33-56.

Jury, W.A., W.R. Gardner and W.H. Gardner, 1991. Soil Physics. Fifth edition. Wiley, New York. 330 pp.

Kabat, P., B.J. Broek, van den and R.A. Feddes, 1992. SWACROP: A water management and crop production simulation model. ICID Bulletin 92, vol. 41 No. 2, 61-84.

Kase, M. and J. Catský, 1984. Maintenance and growth components of dark respiration rate in leaves of $C_3$ and $C_4$ plants as affected by leaf temperature. Biologia Plantarum 26, 461-470.

Kim, D.J., 1992. Characterization of swelling and shrinkage behaviour, hydraulic properties and modelling of water movement in a physically ripening marine clay soil. PhD thesis, Catholic University Leuven.

Kim, R., 1995. The water budget of heterogeneous areas. Doctoral thesis. Wageningen Agricultural University, Wageningen, The Netherlands, 182 pp.

Kool, J.B., J.C. Parker and M.Th. van Genuchten, 1985. Determining soil hydraulic properties from One-step outflow experiments by parameter estimation: I. Theory and numerical studies. Soil Sci. Soc. Am. J.,49, 1348-1354.

Kool, J.B., and J.C. Parker, 1987. Development and evaluation of closed form expressions for hysteretic soil hydraulic properties. Water Resour. Res., 23, 105-114.

Kool, J.B., J.C. Parker and M.Th. van Genuchten, 1987. Parameter estimation for unsaturated flow and transport models - a review. J. Hydrol., 91, 255-293.

Kool, J.B., and M.Th. van Genuchten, 1991. HYDRUS, One-dimensional variably saturated flow and transport model including hysteresis and root water uptake. Research Report 124, U.S. Salinity Laboratory, USDA, ARS, Riverside, CA.

Koorevaar, P., G. Menelik and C. Dirksen, 1983. Elements of soil physics. Developments in Soil Science 13, Elsevier, Amsterdam, p. 223.

Klute, A., 1986. Water retention: laboratory methods. In 'Methods of soil analysis; Part 1; Physical and Mineralogical methods', A. Klute (Ed.), Agronomy series n. 9, ASA and SSSA, Madison, Wisconsin, p. 635-662.

Klute, A., and C. Dirksen, 1986. Hydraulic conductivity and diffusivity: laboratory methods. In 'Methods of soil analysis; Part 1; Physical and Mineralogical methods', A. Klute (Ed.), Agronomy series n. 9, ASA and SSSA, Madison, Wisconsin, p. 687-734.

Krammes, J.S., and L.F. DeBano, 1965. Soil wettability: a neglected factor in watershed management. Water Resour. Res., 1, 283-288.

Kroes, J.G., and J. Roelsma, 1997. User's Guide ANIMO 3.5; input instructions and technical programme description. Technical Document 46, DLO Winand Staring Centre, Wageningen.

Kropff, M.J., H.H. van Laar and H.F.M. ten Berge (Eds.), 1993. ORYZA1 A basic model for irrigated lowland rice production. IRRI, Los Banos, The Philippines.

Leij, F.J., W.J. Alves, M. Th. van Genuchten and J.R. Williams, 1996. The UNSODA Unsaturated Soil Hydraulic Database. User's manual Version 1.0, Soil Salinity Laboratory, Riverside, California.

Maas, E.V., and G.J. Hoffman, 1977. Crop salt tolerance-current assessment. J. Irrig. and Drainage Div., ASCE 103, 115-134.

Maas, E.V., 1990. Crop salt tolerance. In 'Agricultural salinity assessment and management', K.K. Tanji (Ed.), ASCE Manuals and Reports on Engineering practice, No 71, New York.

Massop, H.Th.L., and P.A.J.W. de Wit, 1994. Hydrologisch onderzoek naar de gewasweerstanden van het tertiair ontwateringsstelsel in Oost-Gelderland. Report 373, Winand Staring Centre, Wageningen, The Netherlands, 132 p.

Miller, E.E., and R.D. Miller, 1956. Physical theory for capillary flow phenomena. J. Appl. Phys., 27, 324-332.

Millington, R.J., and J.P. Quirk., 1961. Permeability of porous solids. Trans. Faraday Soc., 57, 1200-1207.

Milly, P.C.D., 1985. A mass conservative procedure for time-stepping in models of unsaturated flow. Adv. Water Resour., 8, 32-36.

Mishra, S., J.L. Zhu and J.C. Parker, 1990. How effective are effective medium properties ? In 'ModelCARE 90: Calibration and reliability in groundwater modeling', Proc. Conf. The Hague, Sept. 1990, IAHS Publ. 195.

Monteith, J.L., 1965. Evaporation and the Environment. In: G.E. Fogg (ed.), The state and movement of water in living organisms. Cambridge University Press, p. 205-234.

Monteith, J.L., 1981. Evaporation and surface temperature. Quarterly J. Royal Soc., 107, 1-27.

Mualem, Y., 1976. A new model for predicting the hydraulic conductivity of unsaturated porous media. Water Resour. Res., 12, 513-522.

Murray, F.W., 1967. On the computation of saturation vapor pressure. J. Appl. Meteor., 6, 203-204.

Nielsen, D.R., M.Th. van Genuchten and J.W. Biggar, 1986. Water flow and solute transport in the unsaturated zone. Water Resour. Res., 22, supplement, 89S-108S.

Nimmo, J.R., J. Rubin and D.P. Hammermeister, 1987. Unsaturated flow in a centrifugal field: Measurement of hydraulic conductivity and testing of Darcy's law. Water Resour. Res., 32, 124-134.

Peat, W.E., 1970. Relationships between photosynthesis and light intensity in the tomato. Annal Bot., 34, 319-328.

Peck, A.J., R.J. Luxmoore and J.L. Stolzy, 1977. Effects of spatial variability of soil hydraulic properties in water budget modeling. Water Resour. Res., 13, 348-354.

Penning de Vries, F.W.T., A.H.M. Brunsting and H.H. van Laar, 1974. Products requirements and efficiency of biosynthesis: a quantitative approach. Journal of Theoretical Biology 45, 339-377.

Penning de Vries, F.W.T., 1975. The cost of maintenance processes in plant cells. Annals of Botany 39, 77-92.

Penning de Vries, F.W.T., J.M. Witlage and D. Kremer, 1979. Rates of respiration and of increase in structural dry matter in young wheat, ryegrass and maize plants in relation to temperature, to water stress and to their sugar content. Annals of Botany (London) 44, 595-609.

Penning de Vries, F.W.T. and H.H. van Laar, 1982. Simulation of growth processes and the model BACROS. In Penning de Vries, F.W.T. and H.H. van Laar (Eds.) Simulation of plant growth and crop production. Simulation Monographs, Pudoc, Wageningen, The Netherlands. p. 114-135.

Penning de Vries, F.W.T., D.M. Jansen, H.F.M. ten Berge and A. Bakema, 1989. Simulation of ecophysiological processes of growth in several annual crops. Pudoc, Wageningen, the Netherlands, 271 pp.

Penman, H.L., 1948. Natural evaporation from open water, bare soil, and grass. Proc. Royal Society, London 193, 120-146.

Press, W.H., B.P. Flannery, S.A. Teukolsky and W.T. Vetterling, 1989. Numerical Recipes. The art of scientific computing. Cambridge University Press. 702 pp.

Raats, P.A.C., 1973. Unstable wetting fronts in uniform and nonuniform soils. Soil Sci. Soc. Am. J., 37, 681-685.

Raats, P.A.C., 1978. Convective transport of solutes by steady flows. I. General theory. Agric. Water Manag., 1, 201-218.

Raes, D., H. Lemmens, P. van Aelst, M. van der Bulcke and M. Smith, 1988. IRSIS (Irrigation Scheduling Information System), reference manual. Laboratory of Land Management, K.U. Leuven, Belgium.

Reinink, K., I. Jorritsma and A. Darwinkel, 1986. Adaption of the AFRC wheat phenology model for Dutch conditions. Neth. J. Agric. Science, 34, 1-13.

Rijniersce, K., 1983. A simulation model for physical ripening in the IJsselmeerpolders. Rijksdienst voor IJsselmeerpolders. Lelystad, The Netherlands, 216 pp.

Rijtema, P.E., P. Groenendijk and J.G. Kroes, 1997. ANIMO, a dynamic simulation model for transport and transformation of nutrients and organic materials in soils. Report 30, DLO Winand Staring Centre, Wageningen, in press.

Ritchie, J.T., 1972. A model for predicting evaporation from a row crop with incomplete cover. Water Resour. Res., 8, 1204-1213.

Ritsema, C.J., L.W. Dekker, J.M.H. Hendrickx and W. Hamminga, 1993. Preferential flow mechanism in a water repellent sandy soil. Water Resour. Res., 29, 2183-2193.

Ritsema, C.J., and L.W. Dekker, 1994. How water moves in a water repellent sandy soil. 2. Dynamics of fingered flow. Water Resour. Res., 30, 2519-2531.

Ritzema, H.P., 1994. Subsurface flow to drains. In 'Drainage principles and applications', H.P. Ritzema (Ed. in Chief), ILRI publication 16, second edition, Wageningen, p. 263-304.

Ross, P.J., 1990. Efficient numerical methods for infiltration using Richards' equation. Water Resour. Res., 26, 279-290.

Russo, D., E. Bresler, U. Shani and J. Parker, 1991. Analysis of infiltration events in relation to determining soil hydraulic properties by inverse problem methodology. Water Resour. Res., 27, 1361-1373.

Saxena, R.K., N.J. Jarvis and L. Bergström, 1994. Interpreting non-steady state tracer breakthrough experiments in sand and clay soils using a dual-porosity model. J. Hydrol., 162, 279-298.

Scott, P.S., G.J. Farquhar and N. Kouwen, 1983. Hysteretic effects on net infiltration. In 'Advances in infiltration', American Society of Agricultural Engineers, St. Joseph, Mich, p. 163-170.

Shalhevet, J., 1994. Using water of marginal quality for crop production: major issues. Agric. Water Man., 25, 233-269.

Šimůnek, J., T. Vogel and M.Th. van Genuchten, 1992. The SWMS-2D code for simulating water flow and solute transport in two-dimensional variably saturated media. Version 1.1. Res. Rep. 126, U.S. Salinity Lab., Agric. Res. Ser., U.S. Dept. of Agric., Riverside, Calif.

Šimůnek, J., and D.L. Suarez, 1994. Two-dimensional transport model for variably saturated porous media with major ion chemistry. Water Resour. Res., 30, 1115-1133.

Smith, M., 1991. Expert consultation on revision of FAO methodologies for crop water requirements. FAO, Rome, 60 p.

Smith, M., 1992. CROPWAT, a computer program for irrigation planning and management. FAO Irrigation and Drainage Paper 46. Rome, Italy.

Spitters, C.J.T., 1986. Separating the diffuse and direct component of global radi-ation and its implications for modelling canopy photosynthesis. Part II: Calculation of canopy photosynthesis. Agricultural and Forest Meteorology 38, 231-242.

Spitters, C.J.T., H.A.J.M. Toussaint, J. Goudriaan, 1986. Separating the diffuse and direct component of global radiation and its implications for model-ling canopy photosynthesis. Part I: components of incoming radiation. Agricultural and Forest Meteorology 38, 217-229.

Spitters, C.J.T., H. van Keulen and D.W.G. van Kraalingen, 1989. A simple and universal crop growth simulator: SUCROS87. In: R. Rabbinge, S.A. Ward and H.H. van Laar (Eds.) Simulation and systems management in crop protection. Simulation Monographs, Pudoc, Wageningen, The Netherlands. p. 147-181.

Stolte, J., J.I. Freijer, W. Bouten, C. Dirksen, J.M. Halbertsma, J.C. van Dam, J.A. van den Berg, G.J. Veerman and J.H.M. Wösten, 1994. Comparison of six methods to determine unsaturated soil hydraulic conductivity. Soil Sci. Soc. Am. J., 58, 1596-1603.

Supit, I., A.A. Hooyer and C.A. van Diepen (Eds.), 1994. System description of the WOFOST 6.0 crop simulation model implemented in CGMS. Vol. 1: Theory and algorithms. EUR publication 15956, Agricultural series, Luxembourg, 146 p.

Taylor, S.A., and G.M. Ashcroft, 1972. Physical Edaphology. Freeman and Co., San Francisco, California, p. 434-435.

ten Berge, H.F.M., 1986. Heat and water transfer at the bare soil surface: aspects affecting thermal images. PhD thesis, Wageningen Agricultural University, Wageningen, The Netherlands.

Tetens, O., 1930. Uber einige meteorologische Begriffe. Z. Geophys, 6, 297-309.

Van Bakel, P.J.T., 1986. Planning, design and operation of surface water management systems; a case study. PhD thesis, Wageningen Agricultural University.

Van Dam, J.C., J.M.H. Hendrickx, H.C. van Ommen, M.H. Bannink, M.Th. van Genuchten and L.W. Dekker, 1990. Water and solute movement in a coarse-textured water-repellent field soil. J. Hydrol., 120, 359-379.

Van Dam, J.C., J.N.M. Stricker and P. Droogers, 1994. Inverse method to determine soil hydraulic functions from multi-step outflow experiments. Soil Sci. Soc. Am. J., 58, 647-652.

Van Dam, J.C., J.H.M. Wösten and A. Nemes, 1996. Unsaturated soil water movement in hysteretic and water repellent soils. J. Hydrol., 184, 153-173.

Van Dam, J.C., and R.A. Feddes, 1997. Simulation of infiltration, evaporation and shallow groundwater levels with the Richards' equation, in preparation.

Van de Pol, R.M., P.J. Wierenga and D.R. Nielsen, 1977. Solute movement in a field soil. Soil Sci. Soc. Am. J., 41, 10-13.

Van den Berg, F., 1997. Users manual and technical description of PESTLA version 3. Report DLO Winand Staring Centre, Wageningen, in preparation.

Van den Broek, B.J., J.C. van Dam, J.A. Elbers, R.A. Feddes, J. Huygen, P. Kabat and J.G. Wesseling, 1994. SWAP 1993, input instructions manual. Report 45, Dep. Water Resources, Wageningen Agricultural University.

Van der Molen, W.H., and J. Wesseling, 1991. A solution in closed form and a series solution to replace the tables for the thickness of the equivalent layer in Hooghoudt's drain spacing formula. Agricultural Water Management 19, p. 1-16.

Van der Zee, S.E.A.T.M., and W.H. van Riemsdijk, 1987. Transport of reactive solute in spatially variable soil systems. Water Resour. Res., 23, 2059-2069.

Van Dobben, W.H., 1962. Influence of temperature and light conditions on dry matter distribution, development rate and yield in arable crops. Netherlands Journal of Agricultural Science 10, 377-389.

Van Genuchten, M.Th., and P.J. Wieringa, 1974. Simulation of one-dimensional solute transfer in porous media. New Mexico State University Agric. Exp. Stn. Bull. 628, New Mexico.

Van Genuchten, M.Th., and R.W. Cleary, 1979. Movement of solutes in soil : computer simulated and laboratory results. In: G.H. Bolt (Ed.), Soil Chemistry B, Physico-Chemical Models. Elsevier, Amsterdam, pp. 349-386.

Van Genuchten, M.Th., 1980. A closed form equation for predicting the hydraulic conductivity of unsaturated soils. Soil Sci. Soc. Am. J., 44, 892-898.

Van Genuchten, M.Th., 1982. A comparison of numerical solutions of the one-dimensional unsaturated-saturated flow and transport equations. Adv. Water Resour., 5, 47-55.

Van Genuchten, M.Th., 1987. A numerical model for water and solute movement in and below the root zone. Res. Report, US Salinity Laboratory, Riverside, CA.

Van Genuchten, M.Th., and R.J. Wagenet, 1989. Two-site/two-region models for pesticide transport and degradation: Theoretical development and analytical solutions. Soil Sci. Soc. Am. J., 53, 1303-1310.

Van Genuchten, M.Th., F.J. Leij and S.R. Yates, 1991. The RETC code for quantifying the hydraulic functions for unsaturated soils. U.S. Salinity Laboratory, Riverside, California.

Van Genuchten, M.Th., and F.J. Leij, 1992. On estimating the hydraulic properties of unsaturated soils. In 'Indirect methods for estimating hydraulic properties of unsaturated soils', M.Th. van Genuchten and F.J. Leij (eds.), Proc. Int. Workshop, Riverside, California, p. 1-14.

Van Grinsven, J.J.M., C. Dirksen and W. Bouten, 1985. Evaluation of hot air method for measuring soil water diffusivity. Soil Sci. Soc. Am. J., 49, 1093-1099.

Van Heemst, H.D.J., 1986a. The distribution of dry matter during growth of a potato crop. Potato Research 29, 55-66.

Van Heemst, H.D.J., 1986b. Crop phenology and dry matter distribution. In: H. van Keulen and J. Wolf (Eds.). Modelling of agricultural production: soil, weather and crops. p. 13-60.

Van Laar, H.H., J. Goudriaan and H. van Keulen (Eds.), 1992. Simulation of crop growth for potential and water-limited production situations (as applied to spring wheat). Simulation reports CABO-TT 27. CABO-DLO, WAU-TPE, Wageningen. 72 pp.

Van Keulen, H., 1975. Simulation of water use and herbage growth in arid regions. Simulation Monographs. Pudoc, Wageningen, the Netherlands. 184 pp.

Van Keulen, H., N.G. Seligman and R.W.Benjamin, 1981. Simulation of water use and herbage growth in arid regions - A re-evaluation and further development of the model 'Arid Crop'. Agricultural systems 6, 159-193.

Van Keulen, H., and N.G. Seligman, 1987. Simulation of water use, nitrogen nutrition and growth of a spring wheat crop. Simulation Monographs. Pudoc, Wageningen, The Netherlands. 310 pp.

Van Ommen, H.C., 1985. Systems approach to an unsaturated-saturated groundwater quality model, including adsorption, decomposition and bypass. Agric. Water. Man., 10, 193-203.

Van Ommen, H.C., 1986. Influence of diffuse sources of contamination on the quality of outflowing groundwater including non-equilibrium adsorption and decomposition. J. Hydrol., 88, 79-95.

Van Ommen, H.C., M.Th. van Genuchten, W.H. van der Molen, R. Dijksma and J. Hulshof, 1989. Experimental assessment of preferential flow paths in a field soil. J. Hydrol., 105, 253-262.

Van Walsum, P.E.V. and P.J.T van Bakel, 1983. Berekening van de effecten van infiltratie op de gewasverdamping in het herinrichtings-gebied, met een aangepaste versie van het model SWATRE. Wageningen, DLO-Staring Centrum, ICW Nota 1434. 135 pp.

Van Wijk, W.R. (Ed.), 1966. Physics of plant environment. North Holland Publ. Comp., Amsterdam, The Netherlands, 2nd edition. 382 pp.

Verhoef, A. and R.A. Feddes, 1991. Preliminary review of revised FAO radiation and temperature methods. Department of Water Resources, Report 16. Wag. Agric. Univ. 116 pp.

Vogel, T., K. Huang, R. Zhang and M.Th. van Genuchten, 1996. The HYDRUS code for simulating one-dimensional water flow, solute transport,

and heat movement in variably saturated media. Research Rep. 140, U.S. Salinity Laboratory, ARS-USDA, Riverside, California, 130 p.

Von Hoyningen-Hüne, J., 1983. Die Interception des Niederschlags in landwirtschaftlichen Beständen. Schriftenreihe des DVWK 57, 1-53.

Walker, A., 1974. A simulation model for prediction of herbicide persistence. J. Environ. Qual., 3, 396-401.

Warrick, A.W., 1991. Numerical approximations of darcian flow through unsaturated soil. Water Resour. Res., 27, 1215-1222.

Weir, A.H., P.L. Bragg, J.R. Porter and J.H. Rayner, 1984. A winter wheat crop simulation model without water and nutrient limitations. Journal of Agricultural Science 102, 371-382.

Wendroth, O., W. Ehlers, J.W. Hopmans, H. Kage, J. Halbertsma and J.H.M. Wösten, 1993. Reevaluation of the evaporation method for determining hydraulic functions in unsaturated soils. Soil Sci. Soc. Am. J., 57, 1436-1443.

Wesseling, J.G., 1987. Invloed van bodemsoort en vochtgehalte op de bodemtemperatuur. Een theoretische beschouwing. Cultuurtechnisch tijdschrift, 27(2), 117-128.

Wesseling, J.G., 1991. Meerjarige simulaties van grondwateronttrekking voor verschillende bodemprofielen, grondwatertrappen en gewassen met het model SWATRE. Report 152, Winand Staring Centre, Wageningen.

Wesseling, J.G., J.A. Elbers, P. Kabat and B.J. van den Broek, 1991. SWATRE; instructions for input. Internal note, Winand Staring Centre, Wageningen.

Wesseling, J.G., 1998. The mechanism of heat flow in soils. In 'SWAP: Simulation of water flow, solute and heat transport, and crop growth', R.A. Feddes and P. Kabat, (eds.), Wageningen, The Netherlands (in preparation).

West, D.W. and L.E. Francois, 1982. Effects of salinity on germination, growth and yield of cowpea. Irrig. Sci., 3, 169-175.

Wolfe, N.L., U. Mingelgrin, G.C. Miller, 1990. Abiotic transformations in water, sediments and soil. In: H.H. Cheng (Ed.), Pesticides in the soil environment: processes, impacts and modeling. SSSA Book Series no. 2, Madison, Wisconsin, USA.

Wösten, J.H.M., 1990. Use of soil survey data to improve simulation of water movement in soils. Doctoral thesis. Wageningen Agricultural University, Wageningen, The Netherlands, 103 pp.

Wösten, J.H.M., C.H.J.E. Schuren, J. Bouma and A. Stein, 1990. Functional sensitivity analysis of four methods to generate soil hydraulic functions. Soil Sci. Soc. Am. J., 54, 832-836.

Wösten, J.H.M., G.H. Veerman and J. Stolte, 1994. Water retention and hydraulic conductivity functions of top- and subsoils in The Netherlands: The Staring series. Technical Document 18, Winand Staring Centre, Wageningen, The Netherlands, 66 p. (in Dutch).

Yates, S.R., M.Th. van Genuchten, A.W. Warrick and F.J. Leij, 1992. Analysis of measured, predicted and estimated hydraulic conductivity using the RETC computer program. Soil Sci. Soc. Am. J., 56, 347-354.

Youngs, E.G., and R.I. Price, 1981. Scaling of infiltration behaviour in dissimilar porous materials. Water Resour. Res., 17, 1065-1070.

Zaidel, J., and D. Russo, 1992. Estimation of finite difference interblock conductivities for simulation of infiltration into initially dry soils. Water Resour. Res., 28, 2285-2295.

Zijl, W., and M. Nawalany, 1993. Natural groundwater flow. Lewis Publishers, Boca Raton, USA.

## Annex A: Data set of soil hydraulic functions (Wösten et al., 1994), based on Dutch texture classes. The functions are described with the analytical model of Mualem - van Genuchten

| TOP-SOILS | Dutch nomenclature | Clay-Silt (50µm) (%) | Clay (<2µm) (%) | Organic matter (%) | M50 (µm) | Number of curves (-) |
|---|---|---|---|---|---|---|
| *Sand* | *Zand* | | | | | |
| B1 | Leemarm, zeer fijn tot matig fijn zand | 0-10 | | 0-15 | 105-210 | 10 |
| B2 | Sterk lemig, zeer fijn tot matig fijn zand | 10-18 | | 0-15 | 105-210 | 20 |
| B3 | Sterk lemig, zeer fijn tot matig fijn zand | 18-33 | | 0-15 | 105-210 | 9 |
| B4 | Zeer sterk lemig, zeer fijn tot matig fijn zand | 35-50 | | 0-15 | 105-210 | 5 |
| *Loam* | *Zavel* | | | | | |
| B7 | Zeer lichte zavel | | 8-12 | 0-15 | | 6 |
| B8 | Matig lichte zavel | | 12-18 | 0-15 | | 41 |
| B9 | Zware zavel | | 18-25 | 0-15 | | 29 |
| *Clay* | *Klei* | | | | | |
| B10 | Lichte klei | | 25-35 | 0-15 | | 9 |
| B11 | Matig zware klei | | 35-50 | 0-15 | | 11 |
| B12 | Zeer zware klei | | 50-100 | 0-15 | | 7 |
| *Silt* | *Leem* | | | | | |
| B14 | Siltige leem | 85-100 | | 0-15 | | 67 |
| *Peat* | *Moerig* | | | | | |
| B16 | Zandig veen en veen | | 0-8 | 23-100 | | 4 |
| B17 | Venige klei | | 8-100 | 16-45 | | 25 |
| B18 | Kleiig veen | | 8-100 | 25-70 | | 20 |

| SUB-SOILS | Dutch nomenclature | Clay-Silt (50µm) (%) | Clay (<2µm) (%) | Organic matter (%) | M50 (µm) | Num-ber of curves (-) |
|---|---|---|---|---|---|---|
| *Sand* | *Zand* | | | | | |
| O1 | Leemarm, zeer fijn tot matig fijn zand | 0-10 | | 0-3 | 105-210 | 79 |
| O2 | Zwak lemig, zeer fijn tot matig fijn zand | 10-18 | | 0-3 | 105-210 | 12 |
| O3 | Sterk lemig, zeer fijn tot matig fijn zand | 18-33 | | 0-3 | 105-210 | 18 |
| O4 | Zeer sterk lemig, zeer fijn tot matig fijn zand | 35-50 | | 0-3 | 105-210 | 5 |
| O5 | Grof zand | | | 0-3 | 210-2000 | 11 |
| O6 | Keileem | 0-50 | | 0-3 | 50-2000 | 4 |
| *Loam* | *Zavel* | | | | | |
| O8 | Zeer lichte zavel | | 8-12 | 0-3 | | 14 |
| O9 | Matig lichte zavel | | 12-18 | 0-3 | | 30 |
| O10 | Zware zavel | | 18-25 | 0-3 | | 20 |
| *Clay* | *Klei* | | | | | |
| O11 | Lichte klei | | 25-35 | 0-3 | | 11 |
| O12 | Matig zware klei | | 35-50 | 0-3 | | 24 |
| O13 | Zeer zware klei | | 50-100 | 0-3 | | 16 |
| *Silt* | *Leem* | | | | | |
| O14 | Zandige leem | 50-85 | | 0-3 | | 5 |
| O15 | Siltige leem | 85-100 | | 0-3 | | 53 |
| *Peat* | *Veen* | | | | | |
| O16 | Oligotroof veen | | | 35-100 | | 16 |
| O17 | Mesotroof en eutroof veen | | | 35-100 | | 34 |

| TOP-SOILS | $\theta_{res}$ ($cm^3\ cm^{-3}$) | $\theta_{sat}$ ($cm^3\ cm^{-3}$) | $K_{sat}$ ($cm\ d^{-1}$) | $\alpha$ ($cm^{-1}$) | $\lambda$ (-) | $n^{(1)}$ (-) |
|---|---|---|---|---|---|---|
| *Sand* | | | | | | |
| B1 | 0.01 | 0.43 | 17.46 | 0.0249 | -0.140 | 1.507 |
| B2 | 0.02 | 0.43 | 9.65 | 0.0227 | -0.983 | 1.548 |
| B3 | 0.01 | 0.45 | 17.81 | 0.0152 | -0.213 | 1.412 |
| B4 | 0.01 | 0.42 | 54.80 | 0.0163 | 0.177 | 1.559 |
| *Loam* | | | | | | |
| B7 | 0.00 | 0.40 | 14.07 | 0.0194 | -0.802 | 1.250 |
| B8 | 0.00 | 0.43 | 2.25 | 0.0096 | -2.733 | 1.284 |
| B9 | 0.00 | 0.43 | 1.54 | 0.0065 | -2.161 | 1.325 |
| *Clay* | | | | | | |
| B10 | 0.01 | 0.42 | 1.17 | 0.0118 | -4.795 | 1.224 |
| B11 | 0.00 | 0.60 | 5.26 | 0.0243 | -5.395 | 1.111 |
| B12 | 0.00 | 0.55 | 15.46 | 0.0532 | -8.823 | 1.081 |
| *Silt* | | | | | | |
| B14 | 0.01 | 0.42 | 0.80 | 0.0051 | 0.000 | 1.305 |
| *Peat* | | | | | | |
| B16 | 0.00 | 0.73 | 13.44 | 0.0134 | 0.534 | 1.320 |
| B17 | 0.00 | 0.72 | 4.46 | 0.0180 | -0.350 | 1.140 |
| B18 | 0.00 | 0.77 | 6.67 | 0.0197 | -1.845 | 1.154 |

| SUB-SOILS | $\theta_{res}$ ($cm^3\ cm^{-3}$) | $\theta_{sat}$ ($cm^3\ cm^{-3}$) | $K_{sat}$ ($cm\ d^{-1}$) | $\alpha$ ($cm^{-1}$) | $\lambda$ (-) | $n$ (-) |
|---|---|---|---|---|---|---|
| *Sand* | | | | | | |
| O1 | 0.01 | 0.36 | 13.21 | 0.0224 | 0.000 | 2.167 |
| O2 | 0.02 | 0.38 | 15.56 | 0.0214 | 0.039 | 2.075 |
| O3 | 0.01 | 0.34 | 18.30 | 0.0211 | -0.522 | 1.564 |
| O4 | 0.00 | 0.36 | 53.10 | 0.0216 | -0.520 | 1.540 |
| O5 | 0.01 | 0.32 | 43.55 | 0.0597 | 0.343 | 2.059 |
| O6 | 0.00 | 0.41 | 5.48 | 0.0291 | -6.864 | 1.152 |
| *Loam* | | | | | | |
| O8 | 0.00 | 0.47 | 9.08 | 0.0136 | -0.803 | 1.342 |
| O9 | 0.00 | 0.46 | 2.23 | 0.0094 | -1.382 | 1.400 |
| O10 | 0.00 | 0.49 | 2.22 | 0.0107 | -2.123 | 1.280 |
| *Clay* | | | | | | |
| O11 | 0.00 | 0.42 | 13.79 | 0.0191 | -1.384 | 1.152 |
| O12 | 0.00 | 0.56 | 1.14 | 0.0095 | -4.171 | 1.159 |
| O13 | 0.00 | 0.57 | 3.32 | 0.0171 | -4.645 | 1.110 |
| *Silt* | | | | | | |
| O14 | 0.00 | 0.38 | 0.36 | 0.0025 | 0.057 | 1.686 |
| O15 | 0.01 | 0.41 | 3.70 | 0.0071 | 0.912 | 1.298 |
| *Peat* | | | | | | |
| O16 | 0.00 | 0.89 | 1.07 | 0.0103 | -1.411 | 1.376 |
| O17 | 0.00 | 0.86 | 2.75 | 0.0127 | -1.832 | 1.274 |

(1) The parameters of the Mualem - van Genuchten model are explained in Par. 2.2.2.

## Annex B: Data set of soil hydraulic functions (Carsel and Parrish, 1988), based on USDA texture classes. The functions are described with the analytical model of Mualem - van Genuchten

| Texture | $\theta_{res}$ ($cm^3\ cm^{-3}$) | $\theta_{sat}$ ($cm^3\ cm^{-3}$) | $\alpha$ ($cm^{-1}$) | $n$ $K_{sat}$ (-)($cm\ d^{-1}$) |
|---|---|---|---|---|
| Sand | 0.045 | 0.43 | 0.145 | 2.68712.8 |
| Loamy sand | 0.057 | 0.41 | 0.124 | 2.28350.2 |
| Sandy loam | 0.065 | 0.41 | 0.075 | 1.89106.1 |
| Loam | 0.078 | 0.43 | 0.036 | 1.5625.0 |
| Silt | 0.034 | 0.46 | 0.016 | 1.376.0 |
| Silt loam | 0.067 | 0.45 | 0.020 | 1.4110.8 |
| Sandy clay loam | 0.100 | 0.39 | 0.059 | 1.4831.4 |
| Clay loam | 0.095 | 0.41 | 0.019 | 1.316.2 |
| Silty clay loam | 0.089 | 0.43 | 0.010 | 1.231.7 |
| Sandy clay | 0.100 | 0.38 | 0.027 | 1.232.9 |
| Silty clay | 0.070 | 0.36 | 0.005 | 1.090.5 |
| Clay | 0.068 | 0.38 | 0.008 | 1.094.8 |

**Annex C: Critical pressure head values (cm) of the sink term function (Fig. 2.2) for some main crops (Wesseling, 1991).**

| Crop | $h^1$ | $h_2$ | $h_{3h}$ | $h_{3l}$ | $h_4$ |
|---|---|---|---|---|---|
| Potatoes | -10 | -25 | -320 | -600 | -16000 |
| Sugar beet | -10 | -25 | -320 | -600 | -16000 |
| Wheat | 0 | -1 | -500 | -900 | -16000 |
| Pasture | -10 | -25 | -200 | -800 | -8000 |
| Corn | -15 | -30 | -325 | -600 | -8000 |

## Annex D: Critical pressure head values (cm) of the sink term function (Fig. 2.2) for various crops (Taylor and Ashcroft, 1972)

| Crop | $h_{3h}$ | $h_{3l}$ | Crop | $h_{3h}$ | $h_{3l}$ |
|---|---|---|---|---|---|
| *Vegetative crops* | | | Deciduous fruit | -500 | -800 |
| Alfalfa | -1500 | -1500 | Avocadoes | -500 | -500 |
| Beans (snap and lima) | -750 | -2000 | Grapes | | |
| Cabbage | -600 | -700 | early season | -400 | -500 |
| Canning peas | -300 | -500 | during maturity | -1000 | -1000 |
| Celery | -200 | -300 | Strawberries | -200 | -300 |
| Grass | -300 | -1000 | Cantaloupe | -350 | -450 |
| Lettuce | -400 | -600 | Tomatoes | -800 | -1500 |
| Tobacco | -300 | -800 | Bananas | -300 | -1500 |
| Sugar cane | | | | | |
| tensiometer | -150 | -500 | *Grain crops* | | |
| blocks | -1000 | -2000 | Corn | | |
| Sweet corn | -500 | -1000 | vegetative period | -500 | -500 |
| Turfgrass | -240 | -360 | during ripening | -8000 | -12000 |
| | | | Small grains | | |
| *Root crops* | | | vegetative period | -400 | -500 |
| Onions | | | during ripening | -8000 | -12000 |
| early growth | -450 | -550 | | | |
| bulbing time | -550 | -650 | *Seed crops* | | |
| Sugar beets | -400 | -600 | Alfalfa | | |
| Potatoes | -300 | -500 | prior to bloom | -2000 | -2000 |
| Carrots | -550 | -650 | during bloom | -4000 | -8000 |
| Broccoli | | | during ripening | -8000 | -15000 |
| early | -450 | -550 | Carrots | | |
| after budding | -600 | -700 | at 60 cm depth | -4000 | -6000 |
| Cauliflower | -600 | -700 | Onions | | |
| | | | at 7 cm depth | -4000 | -6000 |
| *Fruit crops* | | | at 15 cm depth | -1500 | -1500 |
| Lemons | -400 | -400 | Lettuce | | |
| Oranges | -200 | -1000 | during productive phase | -3000 | -3000 |

## Annex E: Salt tolerance data (Fig. 2.3) of various crops (Maas, 1990)[a]

| Crop common name | Crop botanical name | $EC_{max}$[b] (dS $m^{-1}$) | $EC_{slope}$ (% per dS $m^{-1}$) | Rating[c] | Ref.[d] |
|---|---|---|---|---|---|
| *Fiber and grain crops* | | | | | |
| Barley[e] | Hordeum vulgare | 8.0 | 5.0 | T | 1 |
| Bean | Phaseolus vulgaris | 1.0 | 19.0 | S | 1 |
| Corn | Zea mays | 1.7 | 12.0 | MS | 1 |
| Cotton | Gossypium hirsutum | 7.7 | 5.2 | T | 1 |
| Peanut | Arachis hypogaea | 3.2 | 29.0 | MS | 1 |
| Rice (paddy) | Oryza sativa | 3.0 | 12.0 | S | 1 |
| Rye | Secale cereale | 11.4 | 10.8 | T | 2 |
| Sorghum | Sorghum bicolor | 6.8 | 16.0 | MT | 2 |
| Soybean | Glycine max | 5.0 | 20.0 | MT | 1 |
| Sugar beet[f] | Beta vulgaris | 7.0 | 5.9 | T | 1 |
| Sugar cane | Sacharum officinarum | 1.7 | 5.9 | MS | 1 |
| Wheat | Triticum aestivum | 6.0 | 7.1 | MT | 1 |
| Wheat, durum | Triticum turgidum | 5.9 | 3.8 | T | 2 |
| *Grasses and forage crops* | | | | | |
| Alfalfa | Medicago sativa | 2.0 | 7.3 | MS | 1 |
| Barley (forage)[e] | Hordeum vulgare | 6.0 | 7.1 | MT | 1 |
| Bermuda grass[g] | Cynodon dactylon | 6.9 | 6.4 | T | 1 |
| Clover, ladino | Trifolium repens | 1.5 | 12.0 | MS | 1 |
| Corn (forage) | Zea mays | 1.8 | 7.4 | MS | 1 |
| Cowpea (forage) | Vigna unguiculata | 2.5 | 11.0 | MS | 3 |
| Ryegrass, perennial | Lolium perenne | 5.6 | 7.6 | MT | 1 |
| Sundan grass | Sorghum sudanese | 2.8 | 4.3 | MT | 1 |
| Wheat (forage)[h] | Triticum aestivum | 4.5 | 2.6 | MT | 2 |
| Wheat, durum (forage) | Triticum turgidum | 2.1 | 2.5 | MT | 2 |
| *Vegetables and fruit crops* | | | | | |
| Bean | Phaseolus vulgaris | 1.0 | 19.0 | S | 1 |
| Beet, red[f] | Beta vulgaris | 4.0 | 9.0 | MT | 1 |
| Broccoli | Brassica oleracea botrytis | 2.8 | 9.2 | MS | 1 |
| Cabbage | Brassica oleracea capitata | 1.8 | 9.7 | MS | 1 |
| Carrot | Daucus carota | 1.0 | 14.0 | S | 1 |
| Corn, sweet | Zea mays | 1.7 | 12.0 | MS | 1 |
| Cucumber | Cucumis sativus | 2.5 | 13.0 | MS | 1 |
| Lettuce | Lactuca sativa | 1.3 | 13.0 | MS | 1 |
| Onion | Allium cepa | 1.2 | 16.0 | S | 1 |
| Potato | Solanum tuberosum | 1.7 | 12.0 | MS | 1 |
| Spinach | Spinacia oleracea | 2.0 | 7.6 | MS | 1 |
| Tomato | Lycopersicon lycopersicum | 2.5 | 9.9 | MS | 1 |

(a) These data serve only as a guideline to relative tolerances among crops. Absolute tolerances vary, depending on climate, soil conditions and cultural practices.

(b) In gypsiferous soils, plants will tolerate $EC_e$ values about 2 dS/m higher than indicated.

(c) Ratings according to Maas (1990): S sensitive, MS moderately sensitive, MT moderately tolerant, and T tolerant.

(d) References: 1 Maas and Hoffman (1977), 2 Francois et al. (1986), 3 West and Francois (1982).

(e) Less tolerant during seedling stage, $EC_e$ at this stage should not exceed 4 dS/m or 5 dS/m.

(f) Sensitive during germination and emergence, $EC_e$ should not exceed 3 dS/m.

(g) Average of several varieties. Suwannee and Coastal are about 20% more tolerant, and common and Greenfield are about 20% less tolerant than the average.

(h) Data from one cultivar, 'Pobred'.

## Annex F: Numerical solution of Richards' equation as applied in SWAP

The discrete form of Richards' equation, Eq. 2.3, as given in Eq. 2.16, is:

$$C_i^{j+1,p-1}\left(h_i^{j+1,p} - h_i^{j+1,p-1}\right) + \left(\theta_i^{j+1,p-1} - \theta_i^j\right) =$$

$$\frac{\Delta t^j}{\Delta z_i}\left[K_{i-\frac{1}{2}}^j\left(\frac{h_{i-1}^{j+1,p} - h_i^{j+1,p}}{\Delta z_u}\right) + K_{i-\frac{1}{2}}^j - K_{i+\frac{1}{2}}^j\left(\frac{h_i^{j+1,p} - h_{i+1}^{j+1,p}}{\Delta z_\ell}\right) - K_{i+\frac{1}{2}}^j\right] - \Delta t^j S_i^j \qquad \text{(F1)}$$

Application of Eq. F1 to each node results in a tridiagonal matrix:

$$\begin{bmatrix} \beta_1 & \gamma_1 & & & & \\ \alpha_2 & \beta_2 & \gamma_2 & & & \\ & \alpha_3 & \beta_3 & \gamma_3 & & \\ & & & & & \\ & & & \alpha_{n-1} & \beta_{n-1} & \gamma_{n-1} \\ & & & & \alpha_n & \beta_n \end{bmatrix} \begin{bmatrix} h_1^{j+1,p} \\ h_2^{j+1,p} \\ h_3^{j+1,p} \\ \\ h_{n-1}^{j+1,p} \\ h_n^{j+1,p} \end{bmatrix} = \begin{bmatrix} f_1 \\ f_2 \\ f_3 \\ \\ f_{n-1} \\ f_n \end{bmatrix} \qquad \text{(F2)}$$

### *Intermediate nodes*

Rearrangement of Eq. F1 results in the coefficients:

$$\alpha_i = -\frac{\Delta t^j}{\Delta z_i\, \Delta z_u} K_{i-\frac{1}{2}}^j \qquad \text{(F3)}$$

$$\beta_i = C_i^{j+1,p-1} + \frac{\Delta t^j}{\Delta z_i\, \Delta z_u} K_{i-\frac{1}{2}}^j + \frac{\Delta t^j}{\Delta z_i\, \Delta z_\ell} K_{i+\frac{1}{2}}^j \qquad \text{(F4)}$$

$$\gamma_i = -\frac{\Delta t^j}{\Delta z_i\, \Delta z_\ell} K_{i+\frac{1}{2}}^j \qquad \text{(F5)}$$

$$f_i = C_i^{j+1,p-1}\, h_i^{j+1,p-1} + \theta_i^j - \theta_j^{j+1,p-1} + \frac{\Delta t^j}{\Delta z_i}\left(K_{i-\frac{1}{2}}^j - K_{i+\frac{1}{2}}^j\right) - \Delta t^j\, S_i^j \qquad \text{(F6)}$$

***Top node***
*Flux boundary condition*

The right hand side of Eq. F1 transforms to:

$$\frac{\Delta t^j}{\Delta z_1}\left[ - q_{sur} - K^j_{1½}\left(\frac{h_1^{j+1,p} - h_2^{j+1,p}}{\Delta z_\ell}\right) - K^j_{1½}\right] - \Delta t^j S_1^j \qquad \text{(F7)}$$

Rearrangement gives the coefficients:

$$\beta_1 = C_1^{j+1,p-1} + \frac{\Delta t^j}{\Delta z_1\ \Delta z_\ell} K^j_{1½} \qquad \text{(F8)}$$

$$\gamma_1 = - \frac{\Delta t^j}{\Delta z_1\ \Delta z_\ell} K^j_{1½} \qquad \text{(F9)}$$

$$f_1 = C_1^{j+1,p-1}\ h_1^{j+1,p-1} + \theta_1^j - \theta_1^{j+1,p-1} - \frac{\Delta t^j}{\Delta z_1}(q_{surf} + K^j_{1½}) - \Delta t^j\ S_1^j \qquad \text{(F10)}$$

*Head boundary condition*

The right hand side of Eq. F1 transforms to:

$$\frac{\Delta t^j}{\Delta z_1}\left[ K^j_{½}\left(\frac{h_{sur} - h_1^{j+1,p}}{\Delta z_u}\right) + K^j_{½} - K^j_{1½}\left(\frac{h_1^{j+1,p} - h_2^{j+1,p}}{\Delta z_\ell}\right) - K^j_{1½}\right] - \Delta t^j S_1^j \qquad \text{(F11)}$$

Rearrangement gives the coefficients:

$$\beta_1 = C_1^{j+1,p-1} + \frac{\Delta t^j}{\Delta z_1\ \Delta z_u} K^j_{½} + \frac{\Delta t^j}{\Delta z_1\ \Delta z_\ell} K^j_{1½} \qquad \text{(F12)}$$

$$\gamma_1 = - \frac{\Delta t}{\Delta z_1\ \Delta z_\ell} K^j_{1½} \qquad \text{(F13)}$$

$$f_1 = C_1^{j+1,p-1}\ h_1^{j+1,p-1} + \theta_1^j - \theta_1^{j+1,p-1} + \frac{\Delta t^j}{\Delta z_1}(K^j_{½} - K^j_{1½}) + \frac{\Delta t^j}{\Delta z_1\ \Delta z_u} K^j_{½}\ h_{sur} - \Delta t^j\ S_1^j \qquad \text{(F14)}$$

***Bottom node***
*Flux boundary condition*

The right hand side of Eq. F1 transforms to:

$$\frac{\Delta t^j}{\Delta z_n}\left[K^j_{n-½}\left(\frac{h^{j+1,p}_{n-1} - h^{j+1,p}_n}{\Delta z_u}\right) + K^j_{n-½} + q_{bot}\right] - \Delta t^j S^j_n \qquad \text{(F15)}$$

Rearrangement gives the coefficients:

$$\alpha_n = -\frac{\Delta t^j}{\Delta z_n\,\Delta z_u} K^j_{n-½} \qquad \text{(F16)}$$

$$\beta_n = C^{j+1,p-1}_n + \frac{\Delta t^j}{\Delta z_n\,\Delta z_u} K^j_{n-½} \qquad \text{(F17)}$$

$$f_n = C^{j+1,p-1}_n\, h^{j+1,p-1}_n + \theta^j_n - \theta^{j+1,p-1}_n + \frac{\Delta t_j}{\Delta z_n}(K^j_{n-½} + q_{bot}) - \Delta t^j\, S^j_n \qquad \text{(F18)}$$

*Head boundary condition*

The right hand side of Eq. F1 transforms to:

$$\frac{\Delta t^j}{\Delta z_n}\left[K^j_{n-½}\left(\frac{h^{j+1,p}_{n-1} - h^{j+1,p}_n}{\Delta z_u}\right) + K^j_{n-½} - K^j_{n+½}\left(\frac{h^{j+1,p}_n - h_{bot}}{\Delta z_\ell}\right) - K^j_{n+½}\right] - \Delta t^j S^j_n \qquad \text{(F19)}$$

Rearrangement gives the coefficients:

$$\alpha_n = -\frac{\Delta t^j}{\Delta z_n\,\Delta z_u} K^j_{n-½} \qquad \text{(F20)}$$

$$\beta_n = C^{j+1,p-1}_n + \frac{\Delta t^j}{\Delta z_n\,\Delta z_u} K^j_{n-½} + \frac{\Delta t^j}{\Delta z_n\,\Delta z_\ell} K^j_{n+½} \qquad \text{(F21)}$$

$$f_n = C^{j+1,p-1}_n\, h^{j+1,p-1}_n + \theta^j_n - \theta^{j+1,p-1}_n + \frac{\Delta t^j}{\Delta z_n}(K^j_{n-½} - K^j_{n+½}) + \frac{\Delta t^j}{\Delta z_n\,\Delta z_\ell} K^j_{n+½} h_{bot} - \Delta t^j\, S^j_n$$

## Annex G: Numerical solution of the heat flow equation as applied in SWAP

The discretized form of the heat flow equation, Eq. 4.3, as given in Eq. 4.9, is:

$$C_i^{j+½}(T_i^{j+1} - T_i^j) = \frac{\Delta t^j}{\Delta z_i}\left[\lambda_{i-½}^{j+½}\frac{T_{i-1}^{j+1} - T_i^{j+1}}{\Delta z_u} - \lambda_{i+½}^{j+½}\frac{T_i^{j+1} - T_{i+1}^{j+1}}{\Delta z_l}\right] \quad \text{(G1)}$$

where for notational convencience the subscript *heat* of thermal conductivity $\lambda$ and soil heat capacity $C$ is omitted. Equation G1 can be rewritten as:

$$-\frac{\Delta t^j}{\Delta z_i \Delta z_u}\lambda_{i-½}^{j+½}T_{i-1}^{j+1} + \left[C_i^{j+½} + \frac{\Delta t^j}{\Delta z_i \Delta z_u}\lambda_{i-½}^{j+½} + \frac{\Delta t^j}{\Delta z_i \Delta z_l}\lambda_{i+½}^{j+½}\right]T_i^{j+1} - \frac{\Delta t^j}{\Delta z_i \Delta z_l}\lambda_{i+½}^{j+½}T_{i+1}^{j+1} = C_i^{j+½}T_i^j \quad \text{(G2)}$$

Application of Eq. G2 to each node results in a tri-diagonal matrix:

$$\begin{bmatrix} \beta_1 & \gamma_1 & & & & \\ \alpha_2 & \beta_2 & \gamma_2 & & & \\ & \alpha_3 & \beta_3 & \gamma_3 & & \\ & & & & & \\ & & & \alpha_{n-1} & \beta_{n-1} & \gamma_{n-1} \\ & & & & \alpha_n & \beta_n \end{bmatrix} \begin{bmatrix} T_1^{j+1} \\ T_2^{j+1} \\ T_3^{j+1} \\ \\ T_{n-1}^{j+1} \\ T_n^{j+1} \end{bmatrix} = \begin{bmatrix} f_1 \\ f_2 \\ f_3 \\ \\ f_{n-1} \\ f_n \end{bmatrix} \quad \text{(G3)}$$

where $n$ is the number of nodal points. Next the coefficients $\alpha_i$, $\beta_i$, $\gamma_i$, and $f_i$ are explained for the intermediate nodes and for the top and bottom node.

### *Intermediate nodes*

By comparing Eq. G2 and Eq. G3 it will be clear that the coefficients are:

$$\alpha_i = - \frac{\Delta t^j}{\Delta z_i \Delta z_u} \lambda_{i-\frac{1}{2}}^{j+\frac{1}{2}} \tag{G4}$$

$$\beta_i = C_i^{j+\frac{1}{2}} + \frac{\Delta t^j}{\Delta z_i \Delta z_u} \lambda_{i-\frac{1}{2}}^{j+\frac{1}{2}} + \frac{\Delta t^j}{\Delta z_i \Delta z_\ell} \lambda_{i+\frac{1}{2}}^{j+\frac{1}{2}} \tag{G5}$$

$$\gamma_i = - \frac{\Delta t^j}{\Delta z_i \Delta z_\ell} \lambda_{i+\frac{1}{2}}^{j+\frac{1}{2}} \tag{G6}$$

$$f_i = C_i^{j+\frac{1}{2}} T_i^j \tag{G7}$$

### *Top node*

The temperature at soil surface is set equal to the daily average air temperature, $T_{avg}$. Therefore, in case of the top node, Eq. G2 transforms to:

$$C_1^{j+\frac{1}{2}} (T_1^{j+1} - T_1^j) = \frac{\Delta t^j}{\Delta z_1} \left[ \lambda_{\frac{1}{2}}^{j+\frac{1}{2}} \frac{T_{avg} - T_1^{j+1}}{\Delta z_u} - \lambda_{1\frac{1}{2}}^{j+\frac{1}{2}} \frac{T_1^{j+1} - T_2^{j+1}}{\Delta z_\ell} \right] \tag{G8}$$

which can be written as:

$$\left[ C_1^{j+\frac{1}{2}} + \frac{\Delta t^j}{\Delta z_1 \Delta z_u} \lambda_{\frac{1}{2}}^{j+\frac{1}{2}} + \frac{\Delta t^j}{\Delta z_1 \Delta z_\ell} \lambda_{1\frac{1}{2}}^{j+\frac{1}{2}} \right] T_1^{j+1} - \frac{\Delta t^j}{\Delta z_1 \Delta z_\ell} \lambda_{1\frac{1}{2}}^{j+\frac{1}{2}} T_2^{j+1} = C_1^{j+\frac{1}{2}} T_1^j + \frac{\Delta t^j}{\Delta z_1 \Delta z_u} \lambda_{\frac{1}{2}}^{j+\frac{1}{2}} T_{avg} \tag{G9}$$

Combination of Eq. G3 and G9 gives the following coefficients:

$$\beta_1 = C_1^{j+\frac{1}{2}} + \frac{\Delta t^j}{\Delta z_1 \Delta z_u} \lambda_{\frac{1}{2}}^{j+\frac{1}{2}} + \frac{\Delta t^j}{\Delta z_1 \Delta z_\ell} \lambda_{1\frac{1}{2}}^{j+\frac{1}{2}} \tag{G10}$$

$$\gamma_1 = - \frac{\Delta t^j}{\Delta z_1 \Delta z_\ell} \lambda_{1\frac{1}{2}}^{j+\frac{1}{2}} \tag{G11}$$

$$f_1 = C_1^{j+\frac{1}{2}} T_1^j + \frac{\Delta t^j}{\Delta z_1 \Delta z_u} \lambda_{\frac{1}{2}}^{j+\frac{1}{2}} T_{avg} \tag{G12}$$

### *Bottom node*

SWAP adopts a heat flow rate $q_{heat,bot}$ (J cm$^{-2}$ d$^{-1}$) at the bottom of the soil profile. At the bottom node, the general heat flow equation, Eq. G2, transforms to:

$$C_n^{j+½}(T_n^{j+1} - T_n^j) = \frac{\Delta t^j}{\Delta z_n}\left[\lambda_{n-½}^{j+½}\frac{T_{n-1}^{j+1} - T_n^{j+1}}{\Delta z_u} - q_{heat,bot}\right] \quad \text{(G13)}$$

which can be written as:

$$-\frac{\Delta t^j}{\Delta z_n \Delta z_u}\lambda_{n-½}^{j+½}T_{n-1}^{j+1} + \left[C_n^{j+½} + \frac{\Delta t^j}{\Delta z_n \Delta z_u}\lambda_{n-½}^{j+½}\right]T_n^{j+1} = C_n^{j+½}T_n^j - \frac{\Delta t^j}{\Delta z_n}q_{heat,bot} \quad \text{(G14)}$$

Combination of Eq. G3 and G14 gives the following coefficients:

$$\alpha_n = -\frac{\Delta t^j}{\Delta z_n \Delta z_u}\lambda_{n-½}^{j+½} \quad \text{(G15)}$$

$$\beta_n = C_n^{j+½} + \frac{\Delta t^j}{\Delta z_n \Delta z_u}\lambda_{n-½}^{j+½} \quad \text{(G16)}$$

$$f_n = C_n^{j+½}T_n^j - \frac{\Delta t^j}{\Delta z_n}q_{heat,bot} \quad \text{(G17)}$$

## Annex H: Soil physical data of seven selected clay soils, including the parameters $e_0$, $\nu_1$ and $\nu_s$ which describe the shrinkage characteristic, as derived from Bronswijk and Vermeer (1990)

| Place | Depth | Horizon | $\rho_s$ [2] | Composition | | | | | | Shrinkage par. | | |
|---|---|---|---|---|---|---|---|---|---|---|---|---|
| | | | | in weight % of soil | | in weight % of mineral parts | | | | $e_0$ | $\nu_1$ | $\nu_s$ |
| [1] | cm | - | g cm$^{-3}$ | $CaCO_3$ | H [3] | <2 | 2-16 | 16-50 | >50$\mu$m | - | - | - |
| 1 | 0- 22 | A11 | 2.52 | 0.0 | 10.3 | 39.9 | 20.9 | 33.4 | 5.8 | 0.45 | 1.0 | 0.0 |
| | 22-42 | ACg | 2.60 | 0.0 | 6.9 | 40.7 | 25.9 | 28.3 | 5.1 | 0.37 | 0.6 | 0.0 |
| | 42-78 | C1g | 2.66 | 2.5 | 4.5 | 58.1 | 24.7 | 16.2 | 1.1 | 0.43 | 0.7 | 0.0 |
| | 78-120 | C2g | 2.68 | 6.9 | 2.2 | 24.1 | 14.3 | 53.5 | 8.1 | 0.56 | 0.7 | 0.0 |
| 2 | 0- 26 | Ap | 2.64 | 1.4 | 4.8 | 45.4 | 27.8 | 16.6 | 10.2 | 0.52 | 0.8 | 0.2 |
| | 26-34 | A12 | 2.61 | 0.8 | 3.9 | 45.9 | 27.4 | 18.9 | 6.8 | 0.46 | 0.9 | 0.0 |
| | 34-56 | C11g | 2.62 | 1.7 | 2.2 | 51.6 | 29.2 | 15.4 | 3.8 | 0.48 | 0.9 | 0.1 |
| | 56-75 | C12g | 2.68 | 3.3 | 1.9 | 39.1 | 24.1 | 32.8 | 4.0 | 0.50 | 0.9 | 0.1 |
| | 75-107 | C13g | 2.69 | 0.3 | 3.0 | 59.3 | 31.7 | 6.9 | 2.1 | 0.50 | 0.9 | 0.05 |
| 3 | 0- 29 | Ap | 2.65 | 9.0 | 3.3 | 52.0 | 24.2 | 20.4 | 3.4 | 0.49 | 0.7 | 0.2 |
| | 29-40 | AC | 2.67 | 10.6 | 2.9 | 62.9 | 17.0 | 17.7 | 2.4 | 0.50 | 0.8 | 0.2 |
| | 40-63 | C21 | 2.69 | 11.3 | 2.7 | 52.4 | 25.3 | 18.3 | 4.0 | 0.55 | 0.8 | 0.1 |
| | 63-80 | C22g | 2.66 | 9.8 | 2.8 | 55.8 | 24.1 | 16.7 | 3.4 | 0.58 | 1.0 | 0.1 |
| | 80-100 | C23g | 2.69 | 11.6 | 2.2 | 59.6 | 26.4 | 12.2 | 1.8 | 0.57 | 1.0 | 0.1 |
| 4 | 0- 21 | A11 | 2.59 | 11.7 | 5.9 | 34.8 | 17.9 | 27.9 | 19.5 | 0.52 | 1.0 | 0.0 |
| | 21-52 | A12 | 2.61 | 11.1 | 6.2 | 42.9 | 22.1 | 26.5 | 8.5 | 0.53 | 0.9 | 0.0 |
| | 52-77 | C21g | 2.62 | 17.6 | 3.7 | 32.1 | 20.4 | 33.2 | 14.2 | 0.82 | 1.2 | 0.0 |
| | 77-100 | C22g | 2.63 | 18.8 | 3.1 | 16.2 | 10.1 | 37.8 | 36.0 | 0.79 | 1.0 | 0.0 |
| 5 | 0- 22 | Ap1 | 2.66 | 9.9 | 2.6 | 36.8 | 22.2 | 27.5 | 13.5 | 0.48 | 0.8 | 0.0 |
| | 22-38 | A12 | 2.66 | 8.1 | 2.2 | 45.6 | 27.2 | 22.9 | 4.3 | 0.56 | 0.8 | 0.0 |
| | 38-60 | C22g | 2.63 | 6.6 | 7.6 | 35.3 | 43.9 | 19.7 | 1.1 | 0.68 | 1.2 | 0.1 |
| | 60-90 | C23g | 2.59 | 5.8 | 7.0 | 15.9 | 23.9 | 58.2 | 2.0 | 1.10 | 2.0 | 0.0 |
| | 90-110 | C24g | 2.57 | 4.6 | 10.5 | 20.2 | 27.2 | 51.2 | 1.4 | 1.10 | 2.1 | 0.0 |
| 6 | 0- 18 | A11 | 2.52 | 0.0 | 9.9 | 58.1 | 30.7 | 10.2 | 1.0 | 0.30 | 0.9 | 0.0 |
| | 18-30 | A12 | 2.60 | 0.0 | 7.5 | 55.8 | 35.5 | 8.1 | 0.6 | 0.34 | 0.9 | 0.0 |
| | 30-58 | C11g | 2.64 | 0.0 | 3.7 | 59.6 | 29.5 | 10.1 | 0.8 | 0.37 | 0.5 | 0.0 |
| | 58-85 | C12g | 2.59 | 0.0 | 3.8 | 51.7 | 37.0 | 9.6 | 1.7 | 0.40 | 0.8 | 0.05 |
| 7 | 0- 35 | Ap | 2.67 | 10.2 | 2.1 | 30.8 | 15.7 | 30.2 | 23.3 | 0.43 | 1.0 | 0.0 |
| | 35-60 | C21g | 2.67 | 13.6 | 1.6 | 46.4 | 20.5 | 21.2 | 11.9 | 0.45 | 0.8 | 0.0 |
| | 60-80 | C22g | 2.70 | 15.7 | 1.3 | 41.9 | 18.3 | 23.3 | 15.5 | 0.40 | 1.3 | 0.0 |
| | 80-95 | C23g | 2.69 | 9.5 | 0.3 | 16.2 | 6.7 | 21.0 | 56.1 | 0.40 | 1.3 | 0.0 |

(1) Locations: 1-Oosterend, 2-Nieuw Beerta, 3-Nieuw Statenzijl, 4-Schermerhorn, 5-Dronten, 6-Bruchem and 7-Kats.
(2) Density of the solid phase
(3) Organic matter